University of Alberta

Inclusion of Geomechanics in Streamline Simulation

by

Rhamid Hortensia Rodríguez de la Torre

A thesis submitted to the Faculty of Graduate Studies and Research
in partial fulfillment of the requirements for the degree of

Master of Science
in
Petroleum Engineering

Department of Civil and Environmental Engineering

Spring 2010
Edmonton, Alberta

Examining Committee

Japan Trivedi, Civil and Environmental Engineering

Richard J. Chalaturnyk, Civil and Environmental Engineering

Rajender Gupta, Chemical and Materials Engineering

Abstract

Since oil and gas production from conventional fields is decreasing, the production of unconventional hydrocarbon reservoirs is becoming imperative, where geomechanical responses play an important role.

This research presents a methodology that starts exploring the inclusion of geomechanics in streamline simulations using a two-way explicit coupling approach between a reservoir and geomechanical simulators. This was done in an effort of conducting field-scale simulations considering the impact of geomechanical parameters on reservoir "static" properties, which affect ultimate recovery.

Porosity, permeability, and porosity and permeability were used as the coupling parameters; the influence that they have on the process is problem-dependant as well.

The results obtained from the two study cases presented, reveal that the performance of the approach is problem-dependent; the more complex the models are, the larger the geomechanical response is.

One of the main aspects of this study was the limitations of the simulators. When software and hardware capacities improve, so will the results of the coupling approach. Until then, more complex models should be tested, as well as more rigorous techniques, to improve the results presented here.

Acknowledgement

The realization of this thesis could not have been possible without the contribution of so many people, that I would like to express my endless gratitude to each and every one of them.

First of all, I would like to thank God and my lovely family for their unconditional love and support. Without their inspiration and example, I would have renounced to my dreams a long time ago.

I would also like to make a special recognition to Dmitry, who became my lighthouse during the stormy and darkest nights, and helped me find my way back.

Many thanks to my supervisors and Dr. Luis Rodrigues for their valuable assistance; this work is a reality because them.

Last but not least, I would like to acknowledge my dear friends, new and old, who have been there for me.

Table of Contents

1 Introduction 1

1.1 Statement of the problem 2

1.2 Objectives 4

1.2.1 Main Objective 4

1.2.2 Secondary Objective 4

1.3 Methodology 4

1.4 Overview of Chapters 5

2 Literature Review 6

2.1 Streamline Simulation 7

2.1.1 General Description 7

2.1.2 Streamline-Based Simulations in Coupled Approach 14

2.2 Basics of Geomechanics 15

2.2.1 Elasticity 15

2.2.1.1 Young's Modulus and Poisson's Ratio 16

2.2.2 Stress, σ 16

2.2.2.1 Effective Stress, σ' 16

2.2.3 Volumetric strain, ε_v 17

2.3 Coupled Geomechanics-Reservoir Flow Simulation 17

2.3.1 Background and Historical Review 19

2.3.2 Governing Equations 20

2.3.2.1 Basic Flow Equations 20

2.3.2.2 Basic Equations for a Deformable Porous Medium 21
2.3.2.3 Coupled Equations 22
2.3.3 Solutions for the Coupled Approach 23
2.3.3.1 Fully Coupled Solution 23
2.3.3.2 Partially Coupled Solution 24
2.3.3.3 Pseudo-Coupling 27
2.3.4 Parameters of Coupling 27
2.3.4.1 Volume Coupling 28
2.3.4.2 Coupling Through Flow Properties (or Stress-Permeability Coupling) 28
2.3.5 Upscaling 30
2.3.6 Other Challenges for Reservoir-Geomechanics Coupling 30

3 Methodology 31

3.1 Proposed Two-Way Coupling Approach 31
3.1.1 Porosity Equation 33
3.1.2 Permeability Equation 34
3.1.3 Motivation and Justification 34
3.2 General Cases 35
3.2.1 Uncoupled Case (Base Case) 35
3.2.2 Coupled Cases 35
3.3 Description of Simulators 36
3.3.1 FrontSim 36
3.3.1.1 Limitations 36
3.3.2 FLAC^{3D} 37
3.3.2.1 Constitutive models 38
3.3.2.2 Boundary conditions 38
3.3.2.3 Equilibrium 39
3.3.2.4 Limitations 39

4 Study Cases: Description 41

4.1 Study Case 1: Single-Phase 41

4.1.1 FrontSim™ 43

4.1.2 FLAC3D 45

4.2 Study Case 2: Two-Phase Flow 47

4.2.1 FrontSim™ 48

4.2.2 FLAC3D 50

5 Results, Discussion, and Analysis 52

5.1 Study Case 1 52

5.1.1 Geomechanical Equilibrium (Preliminary Phase) 53

5.1.2 Volumetric Strains 54

5.1.3 Average Porosity and Permeability Multipliers 57

5.1.4 Pore Pressure Profiles 61

5.1.4.1 Pore Pressure Profiles at Monitored Cells 61

5.1.4.2 Average Reservoir Pressure Profiles 63

5.1.5 Geomechanical Parameters 66

5.1.6 Smaller Timesteps 67

5.1.7 Increment in Number of Gridblocks 67

5.1.8 Simulation Time 69

5.2 Study Case 2 70

5.2.1 Geomechanical Equilibrium (Preliminary Phase) 71

5.2.2 Volumetric Strains 75

5.2.3 Porosity and Permeability Multipliers 76

5.2.4 Pore Pressure Profiles 79

5.2.4.1 Pore Pressure Profiles at Monitored Cells 79

5.2.4.2 Average Reservoir Pressure Profiles 79

5.2.5 Production Data 82

5.2.5.1 Oil Production 82
5.2.5.2 Water Production Rate 85
5.2.6 Simulation Time 87

6 Conclusions 88

6.1 Accomplishments 89
6.2 Future work 93

7 References 95

Appendix A Matlab File (Main Program) 102

Appendix B Study Case 1. FrontSim File 115

Appendix C Study Case 1. FLAC^{3D} File 119

Appendix D Study Case 2. FrontSim File 121

Appendix E Study Case 2. FLAC^{3D} File 124

Appendix F Study Case 2. Pore Pressure Profiles 126

List of Tables

Table 4.1: Summary of reservoir parameters, Study Case 1 44

Table 4.2: Summary of geomodel characteristics, Study Case 1 45

Table 4.3: Summary of reservoir parameters, Study Case 2 48

Table 4.4: Summary of descriptive statistics for horizontal permeability, Study Case 2 49

Table 5.1: Average porosity and permeability multipliers, Study Case 1 60

Table 5.2: Comparison of total elapsed time runs among different simulations, Study Case 1 70

Table 5.3: Average porosity and permeability multipliers, Study Case 2 78

Table 5.4: Comparison of total elapsed time runs among different simulations, Study Case 2 87

List of Figures

Fig. 2.1: Relationship between streamline and velocity in 2D 8

Fig. 2.2: Schematic transformation of velocity into streamlines 8

Fig. 2.3: Relation between streamlines and time of flight 9

Fig. 2.4: Permeability, streamline geometry and time of flight 11

Fig. 2.5: Streamline simulation flowchart 13

Fig. 3.1: Proposed two-way coupling workflow 33

Fig. 4.1: FrontSim grid showing the well location, Study Case 1 44

Fig. 4.2: Geomodel for Study Case 1, built in FLAC^{3D} 46

Fig. 4.3: Boundary conditions of the FLAC^{3D} model 47

Fig. 4.4: Histogram of horizontal permeability, Study Case 2 49

Fig. 4.5: Geomodel for Study Case 2 50

Fig. 5.1: FLAC^{3D} results showing no shear stresses, Study Case 1 53

Fig. 5.2: Initial vertical stresses after equilibrium run, Study Case 1 54

Fig. 5.3: Volumetric strain profile, Study Case 1 56

Fig. 5.4: Porosity multipliers profile, Study Case 1 58

Fig. 5.5: Permeability multipliers profile, Study Case 1 58

Fig. 5.6: Relative difference of porosity, in percentage, Study Case 1 59

Fig. 5.7: Relative difference of permeability, in percentage, Study Case 1 60

Fig. 5.8: Pore pressure profile for monitored cells, Study Case 1 62

Fig. 5.9: Average reservoir pressure profile for all cases, Study Case 1 64

Fig. 5.10: Relative difference in pressure profile when compared with Un-coupled Case, Study Case 1 66
Fig. 5.11: Reservoir pressure profile for all cases, using one-day timesteps, Study Case 1 67
Fig. 5.12: Study Case 1 with more gridblocks 68
Fig. 5.13: Reservoir pressure profile for all cases, using more gridblocks, Study Case 1 69
Fig. 5.14: Maximum balanced force, Study Case 2 72
Fig. 5.15: Z-displacements after equilibrium run, Study Case2 73
Fig. 5.16: Initial vertical stresses after equilibrium run, Study Case 2 74
Fig. 5.17: Initial vertical stresses after equilibrium run, Study Case 2 75
Fig. 5.18: Volumetric strain profile, Study Case 2 76
Fig. 5.19: Porosity multipliers profile, Study Case 2 77
Fig. 5.20: Permeability multipliers profile, Study Case 2 78
Fig. 5.21: Average reservoir pressure profile for all cases, Study Case 2 80
Fig. 5.22: Relative difference in pressure profile when compared with Un-coupled Case, Study Case 2 82
Fig. 5.23: Field oil production rate and cumulative oil production, Study Case 2 83
Fig. 5.24: Relative difference in oil production rate, Study Case 2 84
Fig. 5.25: Relative difference in cumulative oil production, Study Case 2 85
Fig. 5.26: Field water production rate, Study Case 2 86
Fig. 5.27: Relative difference in water production rate, Study Case 2 87

Nomenclature

B_g	Gas formation volume factor, RB/Mscf
B_o	Oil formation volume factor, RB/STB
B_w	Water formation volume factor, RB/STB
c_p	Pore compressibility, psi^{-1}
c_r	Rock compressibility, psi-1
dV_p	Change of pore volume, ft^3
dp	Change of pressure, psi
E	Young's modulus, psi
f	Body force per unit mass, ft/s^2
G	Shear modulus, psi
k	Permeability, md
K	Bulk modulus, psi
k_0	Initial permeability, md
k_r	Relative permeability, dimensionless
L	Length of the rock sample, ft
p	Pore pressure, psi
p_0	Initial pore pressure, psi
p_{cwo}	Capillary pressure between oil and water, psi
p_{cgo}	Capillary pressure between gas and oil, psi
p_g	Gas pressure, psi
p_o	Oil pressure, psi
p_w	Water pressure, psi
q_g	Gas rate, Mscf/D

q_o	Oil rate, STB/D
q_w	Water rate, STB/D
r_s	Solution gas/oil ratio into gas phase, STB oil/scf gas
R_s	Solution gas/oil ratio into oil phase, scf gas/STB oil
S_g	Gas saturation, dimensionless
S_o	Oil saturation, dimensionless
S_w	Water saturation, dimensionless
u	Displacement, ft
$\vec{v}$	Velocity, ft/s
V_b	Current bulk volume, ft^3
V_b^o	Initial bulk volume, ft^3
V_p	Current pore volume, ft^3
V_p^o	Initial pore volume, ft^3
α	Biot coefficient, dimensionless
γ_g	Gas specific weight, lb_f/ft^3
γ_o	Oil specific weight, lb_f/ft^3
γ_w	Water specific weight, lb_f/ft^3
ΔL	Difference in length of the rock sample, ft
ε	Strain, dimensionless
ε_{long}	Longitudinal strain, dimensionless
ε_{trans}	Transversal strain, dimensionless
ε_v	Volumetric strain, dimensionless
ε_x	Strain in x-direction, dimensionless
ε_y	Strain in y-direction, dimensionless
ε_z	Strain in z-direction, dimensionless
λ_g	Gas mobility, md/cp

λ_o	Oil mobility, md/cp
λ_w	Water mobility, md/cp
μ	Viscosity, cp
ν	Poisson's ratio, dimensionless
ρ	Density, lb_m/ft^3
σ	Total stress, psi
σ'	Effective stress, psi
σ_1	Maximum principal stress, psi
σ_3	Minimum principal stress, psi
σ_x	Component of normal stress in x-direction, psi
σ_y	Component of normal stress in y-direction, psi
σ_z	Component of normal stress in z-direction, psi
τ_{xy}	Component of shear stress related to a force in x-direction ($\tau_{xy}=\tau_{yx}$), psi
τ_{yz}	Component of shear stress related to a force in y-direction ($\tau_{yz}=\tau_{zy}$), psi
τ_{zx}	Component of shear stress related to a force in z-direction ($\tau_{zx}=\tau_{xz}$), psi
ϕ	True porosity, dimensionless
ϕ^*	Reservoir porosity, dimensionless
ϕ_0	Initial porosity, dimensionless
∇p_g	Gas pressure gradient, psi/ft
∇p_o	Oil pressure gradient, psi/ft
∇p_w	Water pressure gradient, psi/ft

1
Introduction

Demand for hydrocarbons is increasingly outstripping reserves. Most of today's producing fields are considered mature, and the number of oil and gas fields discovered annually is declining (Nwaozo 2006). Meeting global demand requires not only the more efficient production of mature reservoirs, but also a focus on unconventional hydrocarbons.

Unconventional sources of oil and gas (heavy oil and bitumen reservoirs, shales, coal beds, etc.) require "sophisticated technology", high energy input, and a high level of reservoir characterization to be produced. This translates into more complex mechanisms affecting reservoir performance, which "must be thoroughly studied and accounted for when designing any field operation" (Bogatkov 2008).

The geomechanical response plays an important role in the recovery process for this class of reservoirs, which also includes naturally fractured, stress sensitive reservoirs and those undergoing thermal recovery processes. Geomechanical models allow the prediction of reservoir compaction, the description of *in situ* stresses, and the determination of rock mechanical parameters, all of which can lead to optimized production strategies.

Thus, coupling reservoir flow simulators with geomechanical codes becomes a useful technique that can contribute to the reaching of this objective, especially for unconventional reservoirs.

1.1 Statement of the problem

Treating geomechanics and multiphase fluid flow in a reservoir as coupled processes represents a complex challenge. It is still common practice to consider them separately: stress/strain behavior is modeled by a geomechanical simulator, while the multiphase fluid flow and heat transfer in porous media is modeled by a reservoir flow simulator.

Most commercial reservoir simulators neglect or simplify stress changes and rock deformation (Gutierrez and Lewis 1996; Koutsabeloulis and Hope 1996; Settari and Mourits 1998; Stone et al. 2000; Rodrigues et al. 2007). Mechanical and/or temperature changes in the rock are taken into account only by a constant "single scalar", that of rock compressibility (Gutierrez and Lewis 1996; Koutsabeloulis and Hope 1996; Stone et al. 2000) while reservoir properties, like porosity and permeability, remain constant (Koutsabeloulis and Hope 1996). It is sometimes possible to modify permeability and porosity through lookup tables by using empirical relationships between permeability and porosity, and pressure (Stone et al. 2000; Samier et al. 2006). These relationships are usually obtained by measuring permeability and porosity at different pressures during depletion tests (Samier et al. 2006). It may be possible to obtain results comparable to those from a coupled formulation without considering stresses and rock deformation, but this is not always the case (Stone et al. 2000; Samier et al. 2006; Tran et al. 2005a).

Changes in pore pressure and temperature affect the stress state in a reservoir, causing changes in the volume of both reservoir fluids and rock (i.e., rock deformation). This in turn modifies the reservoir's "static" properties, such as porosity and permeability (Gutierrez and Lewis 1996; Rodrigues et al. 2007; Wan et al. 2003; Samier et al. 2006; Vidal-Gilbert and Tisseau 2006). These parameters, along with their modifications, affect the flow pattern in the reservoir and ultimately, the recovery (Settari 2002; Rodrigues et al. 2007).

When considering geomechanical problems, a much larger domain (i.e., sideburden, overburden, and sometimes underburden), should also be addressed, as should faults and other relevant geological features (Settari 2002; Yale 2002).

Numerous researchers have studied the interactions of solid mechanics and fluid flow for the past several years (Tran et al. 2000). They have acknowledged that geomechanical response and multiphase fluid flow are coupled and simultaneous processes that occur while a reservoir is producing. Moreover, these interactions between fluid pressure, rock stresses, and flow parameters produce oil and gas (Stone et al. 2000).

Different methods of coupling such as full and iterative coupling have been used. However their (extremely) high computational costs prevent their application in full-field studies. (Tran et al. 2004)

On the other hand, oil and gas industry is considering using streamline technique, which allows a "fast" flow simulation, in full-field studies. Due to its special characteristics, this technique allows the direct use of geological models (some of which consist of multimillion cells) in reservoir simulations, without the high computational costs this kind of models involve.

In this sense, streamline-geomechanical simulations may be the solution for conducting full-field studies, considering the complex processes of geomechanical response, without too many computational resources. However, the limited application of geomechanics to streamline techniques makes it difficult to establish the relative importance of geomechanics in this context. This research begins to explore the possibility of including geomechanical behavior in a commercial streamline simulator, using an explicit coupling approach.

1.2 Objectives

1.2.1 Main Objective

The main objective of this research is to implement streamline-geomechanical simulations to examine the potential influence that changes in the rock structure may have on a reservoir's "static" properties, which in turn affect pressure and, ultimately, recovery.

1.2.2 Secondary Objective

To achieve a full analysis, the secondary objective of this research is to determine which reservoir "static" parameter (porosity or permeability) is most important when considering geomechanical effects. Three cases are analyzed (porosity considered alone, permeability considered alone, and porosity and permeability considered together as the coupling terms). It is expected that the most accurate results will be obtained when considering both parameters.

1.3 Methodology

To achieve these objectives, a "practical" external-two-way-coupled reservoir–geomechanical method is proposed using two commercial simulators. This is an attempt to capture the link between fluid flow and *in situ* effective stress. A complete description is presented in Chapter 3.

A comparison between streamline–only simulations and streamline–geomechanical simulations is done on elastic and isothermal synthetic cases. It is expected that changes in porosity and absolute permeability will be exhibited when the geomechanical behavior of the reservoir is taken into consideration.

The results will provide the basis for discussing the advantages and disadvantages of integrating geomechanics in streamline simulators.

1.4 Overview of Chapters

Chapter 1 gives a broad overview of the topic of this thesis and the objectives to be achieved, as well as a brief summary of the methodology used to accomplish those objectives.

Chapter 2 reviews some previous work relating to the incorporation of geomechanical parameters into reservoir simulation, highlighting findings relevant to this research. For a better understanding, this chapter also summarizes some of the theoretical aspects of streamline simulation and geomechanics.

Chapter 3 discusses in detail the steps followed in this study to link a reservoir streamline flow simulator with a geomechanical simulator. It also describes the cases to be studied and the applied simulators.

Chapter 4 details the model used to test the methodology developed in this research.

Chapter 5 provides the results obtained from the application of the external coupling, as well as an analysis and discussion of them.

Finally, Chapter 6 presents the conclusions and recommendations.

Appendices are included at the end, containing the programs used to link the simulators.

2
Literature Review

Interactions between rock deformation (stresses and displacements) and fluid flow in reservoirs have been studied by numerous researchers over the past decades. These researchers have recognized the importance of geomechanics in aspects such as borehole stability(de Sá and Soares 1997; Aadnov 1998; Bruno 2002; Ramos et al. 2002; Strenger-Proehl 2002), hydraulic fracturing (Advani et al. 1986; Berumen et al. 2000; Ji et al. 2007; Ammer et al. 2000; Chavez et al. 2004; Soliman et al. 2008), production-induced compaction and subsidence (Geertsma 1973; Hansen et al. 1995; Fredrich et al. 2000; Settari 2002), waterflooding (Heffer et al. 1994; Heffer et al. 1997; Rodrigues 2009), sand production, thermal fracturing, fault activation, and reservoir failure involving pore collapse (Dean et al. 2006).

Despite the complexity of the process, the subject of solving fluid flow equations together with geomechanical equations has been discussed in the literature and is still intensely researched (Stone et al. 2000; Settari 2002). The main objective of the coupling process is "to predict the evolution of stress-dependent parameters, such as porosity, rock pore compressibility, and permeability" (Settari and Walters 2001).

In such coupling approaches, there is not only the challenge of linking complex geomechanical processes, but also that of handling the field-scale models that are now commonplace. The iteratively coupled method, described below, seems to be the preferred method for field–scale problems (Samier et al. 2008; Pan et al. 2007).

The first sections of this chapter describe the basics of streamline simulation and geomechanics, both necessary concepts in reservoir-geomechanical simulations. Then, aspects of the coupled approach are described: its evolution and basic governing equations, as well as common coupling parameters.

2.1 Streamline Simulation

Since the theory of streamline simulation has been reported elsewhere (Batycky et al. 1997; Datta-Gupta 2000; Datta-Gupta and King 2007; Ingebrigtsen et al. 1999; Loromari et al. 2000; Schlumberger 2007), this section emphasizes only the points relevant to this research. The following discussion is based mainly on Datta-Gupta and King (2007), with more thorough discussion found in the referenced works.

2.1.1 General Description

Streamline simulation models convection–dominated flow in reservoirs based on the Implicit Pressure Explicit Saturation (IMPES) technique. Pressures are obtained as in any other conventional finite difference-based reservoir flow simulator. However, streamline simulation approximates 3D fluid flow calculations using the sum of 1D solutions along streamlines (Datta-Gupta 2000; Datta-Gupta and King 2007; Loromari et al. 2000).

Due to its versatility, streamline simulation has been used in a number of applications (Batycky et al. 1997; Datta-Gupta 2000; Datta-Gupta and King 2007), namely:

- The ranking of geostatistical models (equiprobable reservoir images)
- The rapid assessment of production strategies, such as infill drilling and gas injection
- Swept volume calculations
- The modeling of tracer flow and waterflooding
- Upgridding and upscaling
- Integration with production data for reservoir characterization
- Primary recovery and compressible flow
- Solvent flooding and compositional simulation

A streamline is represented by a set of points that intersects the grid cells (Schlumberger 2007). It is defined as “the curve that is locally tangential to the direction of the total interstitial velocity field” (Datta-Gupta and King 2007). This defi-

nition applies to compressible and incompressible fluids. It should also be noted that in streamlines the different phases or different components are not considered separately. **Fig. 2.1** shows the relationship between streamline and velocity in 2D. The components of velocity vector $\vec{v}$ are v_x and v_y; the local arc length $d\vec{r}$ has components dx and dy. **Fig. 2.2** shows the schematic transformation of velocity into streamlines.

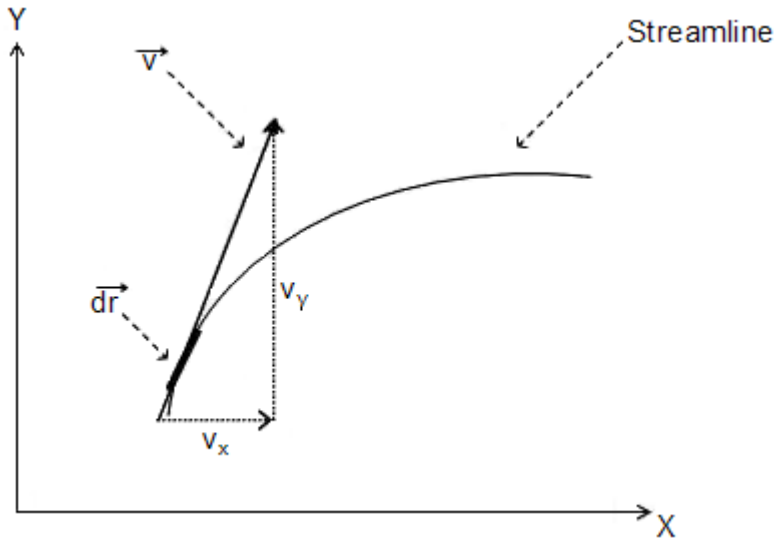

Fig. 2.1—Relationship between streamline and velocity in 2D (Datta-Gupta and King 2007).

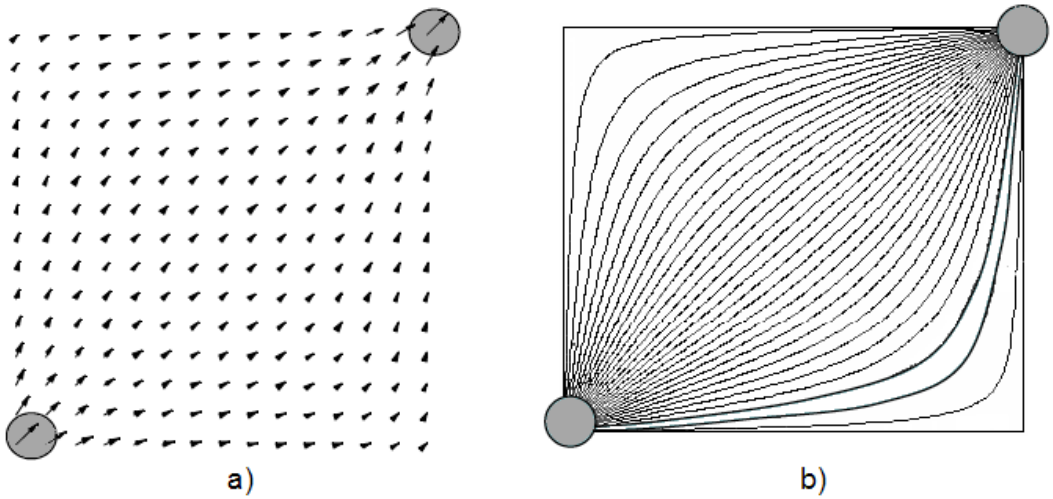

Fig. 2.2—Schematic transformation of velocity into streamlines. a) velocity field and b) streamlines(Datta-Gupta and King 2007).

Distance is replaced by the time of flight (TOF), where all streamlines are transformed into straight lines (Datta-Gupta 2000; Datta-Gupta and King 2007; Schlumberger 2007). This means that the 3D mass conservation equations are transformed into 1D equations, in terms of the time of flight, τ (Datta-Gupta and King 2007; Schlumberger 2007).

Put simply, TOF is defined as the time it takes for a particle to travel between two points on a streamline (Schlumberger 2007). **Fig. 2.3** shows schematically the relationship between streamlines and times of flight.

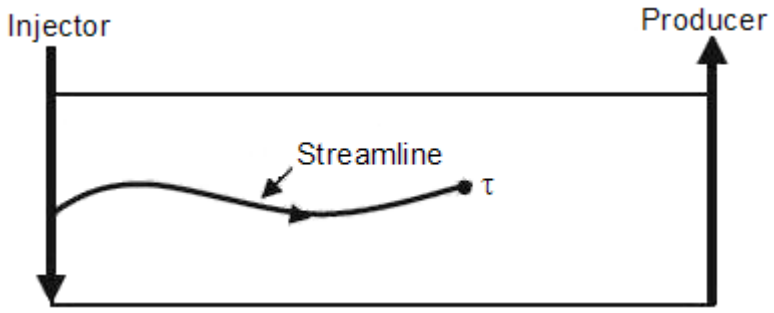

Fig. 2.3—Relationship between streamlines and time of flight (Datta-Gupta and King 2007).

Let ξ be the arc length, or distance traveled along a streamline from an injector to a given point (x,y,z), and let $\frac{\vec{v}}{\phi}$ be the interstitial velocity. Then, the TOF, τ, is defined as

$$\tau(x, y, x) = \int_{\xi} \frac{\phi}{|\vec{v}|} d\xi \quad \text{.....(2.1)}$$

Eq. 2.1 gives the time required to reach a point on the streamline based on velocity $\vec{v}$ along the streamline.

As a differential relationship, the TOF can be expressed as:

$$\vec{v} \cdot \nabla \tau = \phi \quad \text{.....(2.2)}$$

If a function F is defined along a streamline (Ingebrigtsen et al. 1999),

$$\vec{v}\cdot\nabla F=\vec{v}\cdot\left(\frac{\partial F}{\partial\tau}\frac{\partial\tau}{\partial x},\frac{\partial F}{\partial\tau}\frac{\partial\tau}{\partial y},\frac{\partial F}{\partial\tau}\frac{\partial\tau}{\partial z}\right)=\frac{\partial F}{\partial\tau}\vec{v}\cdot\nabla\tau=\phi\frac{\partial F}{\partial\tau} \quad \text{(2.3)}$$

then the transformation operator on streamlines can be expressed as:

$$\vec{v}\cdot\nabla=\phi\frac{\partial}{\partial\tau} \quad \text{(2.4)}$$

This equality is used to transform saturation equations from 3D to 1D along streamlines (Ingebrigtsen et al. 1999).

This form of discretization places a higher resolution in regions of faster flow, since streamlines tend to cluster in regions of high permeability (Datta-Gupta and King 2007). The permeability, porosity, and total mobility effects of the 3D domain are incorporated along a streamline by means of the τ coordinate (Ingebrigtsen et al. 1999).

Time of flight can be considered a measure of spatial distance along streamlines. Datta-Gupta and King (2007) suggest stating that the distance between two points 50 ft apart be described as the distance that can be covered in 1 hr while travelling at 50 ft/hr.

Fig. 2.4 presents three cases with different degrees of heterogeneity and the corresponding streamlines and times of flight. A 2D cross section is presented with an injector on the left and a producer on the right. Fig. 2.4a presents a homogeneous permeability field. The corresponding streamlines present a uniform geometry and as expected, the streamlines arrive at the same time, as observed with the TOF. Figs. 2.4b and 2.4c present heterogeneous cases, having an almost stratified pattern the last one. As a result, the streamlines concentrate in regions of high flow and different streamlines arrive at different times. The scales were increased for Figs. 2.4b and 2.4c.

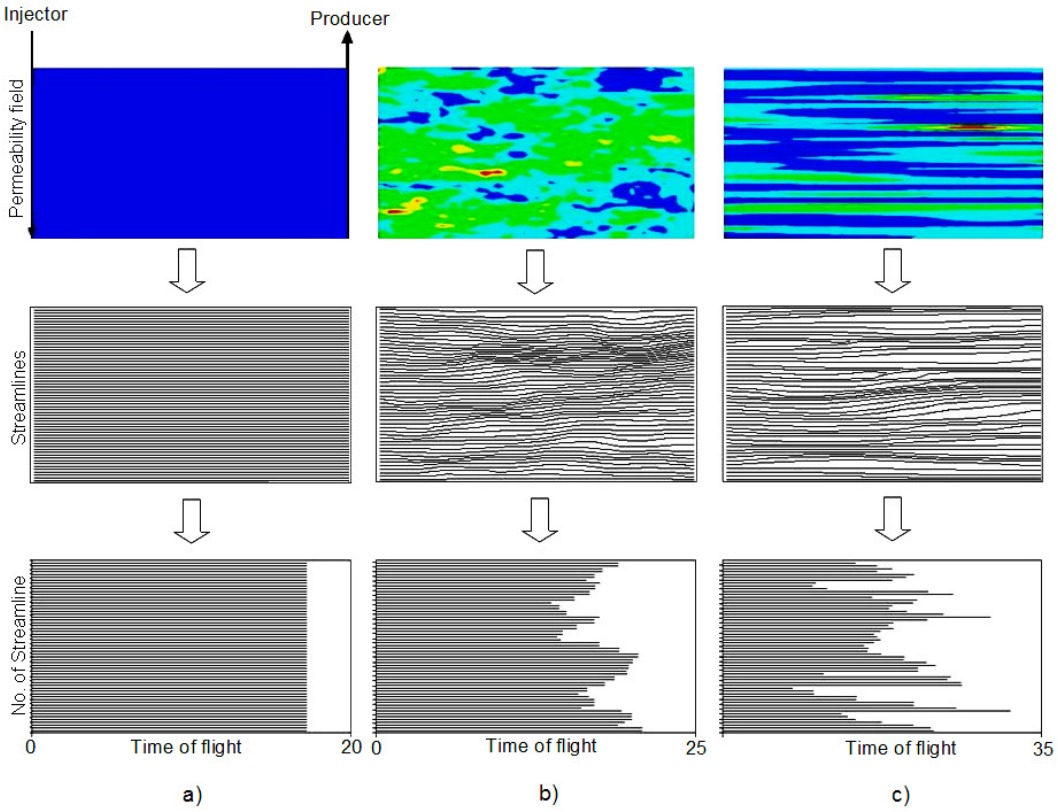

Fig. 2.4—Permeability, streamline geometry and time of flight. a) homogeneous permeability field, b) heterogeneous permeability field, c) heterogeneous field, almost stratified (Datta-Gupta and King 2007).

Streamline technique comprise two major steps: generating streamlines and solving the 1D fluid transport equations along those streamlines (Ingebrigtsen et al. 1999).

Gravity effects, capillarity, and changing well rates, all considered transverse mechanisms, are accounted for in a separate step using operator splitting techniques. Saturation solutions are split in two steps: fluxes along streamlines and fluxes across streamlines. Because of this, the global timestep may be divided into many local steps as required while solving for saturation. (Datta-Gupta 2000; Datta-Gupta and King 2007; Ingebrigtsen et al. 1999; Koutsabeloulis and Hope 1996)

The basic steps, visualized in **Fig. 2.5**, for streamline simulation are (Batycky et al. 1997; Datta-Gupta 2000; Datta-Gupta and King 2007; Ingebrigtsen et al. 1999; Loromari et al. 2000; Schlumberger 2007):

1. Once the grid has been populated and the initial and boundary conditions defined, the pressure solution is found for a global timestep. The pressure field is generated using a finite-difference or a finite-element method that yields a system of equations solved with a multigrid method. (Batycky et al. 1997; Datta-Gupta 2000; Datta-Gupta and King 2007; Ingebrigtsen et al. 1999)
2. The velocity is computed at gridblock faces.
3. The streamlines are generated (Batycky et al. 1997; Ingebrigtsen et al. 1999; Schlumberger 2007); streamlines usually start from injectors and are traced forward. They tend to cluster in high–permeability regions (Batycky et al. 1997; Datta-Gupta 2000).
4. The TOF is computed along the streamlines.
5. The saturations are mapped onto streamlines.
6. The saturation equation is solved for each streamline, using a 1D numerical technique.
7. The gravity segregation is solved, iterating as necessary.
8. Saturations are mapped back to the grid.
9. The pressure solution is found for the next timestep.
10. Return to Step 2.

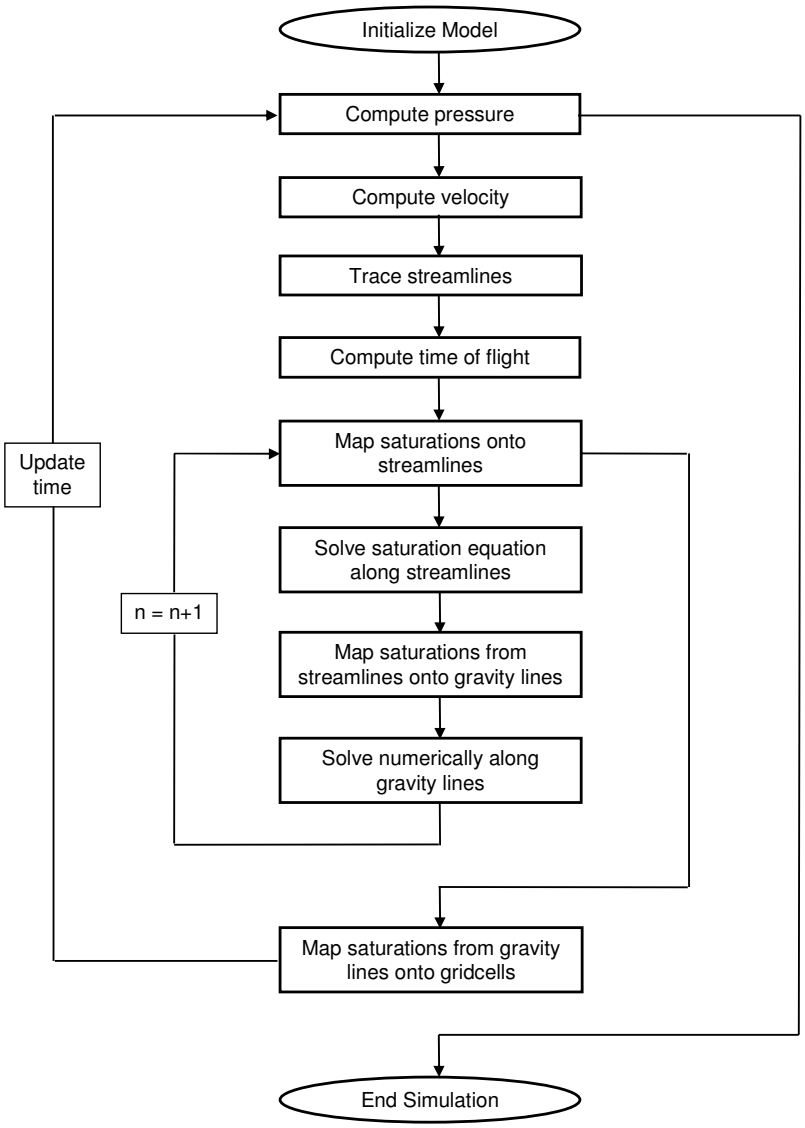

Fig. 2.5—Streamline simulation flowchart (Loromari et al. 2000)

There are some relevant aspects about streamline simulation that should be mentioned:

1) the fastest front can be moved at more than one gridblock per global timestep because fluid transport is decoupled from the grid; therefore there is the opportunity of using larger timesteps in the simulations (Batycky et al. 1997);

2) streamlines do not need to be updated frequently because they tend to stay constant, leading to faster computation (Datta-Gupta and King 2007);

3) streamlines should be updated whenever a new pressure solution is calculated (Schlumberger 2007);

4) for unsteady-state simulations, the streamlines vary with time, creating the need to map saturations from the old set of streamlines to the new one (Datta-Gupta 2000; Datta-Gupta and King 2007);

5) while gravity and compressibility are already included in commercial software, capillarity is still under research (Datta-Gupta and King 2007);

6) the modeling of fluid flow and transport in naturally fractured reservoirs and compositional streamline simulation are still considered advanced functions for streamline simulators (Datta-Gupta and King 2007).

Finally, as Datta-Gupta and King (2007) note, streamline simulation is still a "young" technique compared to conventional simulations (e.g. finite-difference or finite-element techniques). As such, there are still many issues to be worked out. In fact, their book is the first to provide a compilation of the subject.

These authors also state that streamline simulation is by no means a substitute for conventional techniques. Instead, it should be seen as a complementary tool when taking decisions, since streamline-based simulators can easily model highly detailed problems (although not complex physics).

2.1.2 Streamline-Based Simulations in Coupled Approach

Streamline-based simulations in coupling situations are intended to obtain accurate and efficient solutions for field–scale problems. Streamline-based techniques are fast and stable, even for large timesteps, and numerical dispersion is insignificant. (Koutsabeloulis and Hope 1996).

The motivation for this research comes from the fact that only a few authors had used streamline simulation in coupled approaches (Heffer et al. 1994; Koutsabeloulis and Hope 1996; Jha and Juanes 2006) and even fewer had used it for field–scale problems.

Heffer et al. (1994) used a tracking method for saturation and temperature fronts, using velocity vectors calculated at the fronts from the previous timestep. They demonstrated that the preferred directionality during waterflood operations is "stress–related and progressive with time".

Koutsabeloulis and Hope (1996) compared a partially coupled scheme using a finite element stress analysis simulator with a streamline fluid flow simulator. They were interested in studying rock deformation and changes in "reservoir effective stress state during HP/HT and/or waterflooding operations".

Jha and Juanes (2006) used streamlines to calculate the velocity fields for their cases (with and without gravity). They focused on developing a computational model using a finite-element method for the mechanical problem and a mixed finite-element method for the flow problem.

2.2 Basics of Geomechanics

The following overview is based on Fjaer et al. (2008).

2.2.1 Elasticity

This concept is the foundation of rock mechanics and is defined as the "ability to resist and recover from deformations produced by forces".

Linear elasticity—in which Young's modulus and Poisson's ratio play a fundamental role—denotes situations in which the relationships between stresses and resulting strains are linear.

2.2.1.1 Young's Modulus and Poisson's Ratio

According to Hooke's law (**Eq. 2.5**), given a stress, the strain response will depend on the proportionality constant of the material, known as Young's modulus, E (Rodrigues et al. 2007)

$$\sigma = E\varepsilon \quad (2.5)$$

where σ is the stress, E is Young's modulus, and ε is the elastic strain, defined as, **Eq. 2.6**:

$$\varepsilon = \frac{\Delta L}{L} \quad (2.6)$$

where L is the length of the sample.

Poisson's ratio, **Eq. 2.7**, is defined as the ratio of the transversal to the longitudinal strains (Rodrigues et al. 2007),

$$\upsilon = -\frac{\varepsilon_{trans}}{\varepsilon_{long}} \quad (2.7)$$

where ν is Poisson's ratio, ε_{trans} is the transversal strain, and ε_{long} is the longitudinal strain.

2.2.2 Stress, σ

Simply put, stress is the force applied to a unit area, and can be classified as normal or shear stress. The former occurs when force is perpendicular to the section where the force is applied, whereas the latter occurs when force is parallel to the section.

2.2.2.1 Effective Stress, σ'

Effective stress describes the relative contribution of total stress, σ, and pore pressure, p, to the deformation of rock. This means that fluid supports some portion of the applied load, while sediment particles sustain the remaining load. **Eq. 2.8** de-

scribes the relationship between them (Rodrigues et al. 2007; Rodrigues 2009; Tran et al. 2005a).

$$\sigma' = \sigma - \alpha p \quad (2.8)$$

where σ' is effective stress, σ is total stress, p is pore pressure, and α is the Biot coefficient, which is related to the grain compressibility of the porous material (being equal to one for incompressible grains) (Itasca 2006).

2.2.3 Volumetric strain, ε_v

Volumetric strain is defined as the relative volume change, **Eq. 2.9**,

$$\varepsilon_v = \varepsilon_x + \varepsilon_y + \varepsilon_z \quad (2.9)$$

where ε_v is volumetric strain, ε_x is strain in the x-direction, ε_y is strain in the y-direction, and ε_z is strain in the z-direction.

2.3 Coupled Geomechanics-Reservoir Flow Simulation

Although it is true that reservoir simulation has a long history and has been used to model a wide variety of reservoir problems, conventional simulators still cannot reproduce some phenomena that occur during production, such as subsidence, compaction, casing damage, wellbore stability, and sand production. It is required to have both an understanding of the porous flow of reservoir fluids and an understanding of reservoir stresses and displacements to explain these phenomena. (Dean et al. 2006; Tran et al. 2004)

Most conventional reservoir simulators do not incorporate stress changes and rock deformations with changes in pressure and temperature during production (Tran et al. 2004). Moreover, they assume that a porous medium does not deform—the bulk volume of each grid cell remaining constant—and considers rock compressibility, c_r, the only mechanical parameter in the model. However, this scalar quantity cannot represent the behavior of rocks by itself. Even for linearly elastic and iso-

tropic materials, different compressibility values are obtained depending on the loading path. (Gutierrez et al. 2001; Tran et al. 2005a)

In some problems, the geomechanical response has a great impact in the performance of the reservoir. For example, as a reservoir is depleted, the weight of the overburden is increasingly supported by the solid rock matrix. This can lead to pore reduction or collapse (in response to the increased stress). This can translate into compaction of the reservoir, which in turn causes subsidence of the surface and damage to well casings, which in turn causes significant production loss. There are several field examples of this behavior: Ekofisk and Valhall fields (North Sea); Belridge Diatomite and Wilmington fields (California); Goose Creek (Texas); and oil reservoirs bordering Lake Maracaibo (Venezuela) (Fredrich et al. 2000; Geertsma 1973; Tran et al. 2004)

Conventional reservoir simulators also exclude the surrounding formation (burden), although it is well known that it interacts with the reservoir. Burden deformation is dependent on the pore pressure distribution in the reservoir, which in turn is controlled by the deformation of the surrounding formation (Gutierrez et al. 2001). Therefore, it should be considered in any study, even when its pressure does not change (Rodrigues 2009). The surrounding formation comprise: the overburden (rock and soil lying between the seabed or surface and the reservoir); the sideburden (rock layer adjacent to the reservoir); and the underburden (rock lying below the reservoir) (Samier et al. 2006).

Additionally, there are some cases where the pore pressure can increase above the initial reservoir pressure during depletion. One of such cases can occur with reservoirs contained within a stiff non pay region. Dean et al. (2006) showed that for this kind of problems, geomechanical effects can cause the fluid pressures to increase at the boundary of the reservoir during the initial stages of depletion. They explained that the reservoir pressure can increase as the reservoir is depleted because some of the vertical load that was supported at the center of the reservoir is transferred to the edges of the reservoir. This means that the amount of pressure increase at the edge of the reservoir is a strong function of the contrast in elastic

moduli between the reservoir and nonpay regions. However, this pressure increase cannot be observed if geomechanical calculations are not included.

Fredrich et al. (2000) presented a good example of why geomechanical simulation should be used as a reservoir management tool. They could identify better operating policies to mitigate casing damage, and incorporate the effect of well failure in economic analyses to determine different infilling and development options.

Fluid flow and geomechanics form a set of domains that cannot be analyzed separately. Thus, it becomes essential to perform coupled reservoir-geomechanical simulations. Computational advances are making these feasible, even on a field-scale.

2.3.1 Background and Historical Review

Terzaghi (1925), Biot (1941), and Geertsma (1957) are recognized as the pioneers in the study of the solid–fluid deformations and their interactions to describe deformation and flow in porous, elastic materials (Yale 2002).

In 1925, Terzaghi was the first person to analyze the coupled deformation and fluid-flow problem with his 1D consolidation theory. He established the fundamentals of geomechanics by defining the concept of effective stress. Since then, Terzaghi's 1D work has been applied widely, such as in settlement problems in saturated soils. (Gutierrez et al. 2001)

Based on Terzaghi's work, Biot (1941) investigated the effect of solid and fluid deformations on single-phase flow and pressure in porous media, extending the theory of consolation into a more general 3D case.

In 1957, Geertsma (1957) attempted to link geomechanics with flow simulation by defining pore compressibility (Gutierrez et al. 2001; Yale 2002), giving a better insight into the relationship between pressure, stress, and volume (Tran et al. 2004).

Since then, there have been many reports of geomechanical modeling. It has been used as a tool to evaluate alternative development plans. For example, in the

Belridge field, California, stresses were predicted to develop strategies to minimize additional subsidence and fissuring, as well as to reduce axial compressive type casing damage (Hansen et al. 1995).

Another example is the case presented by Berumen et al. (2000). They developed a geomodel of the Wilcox sands in the Arcabuz-Culebra field in the Burgos Basin, northern Mexico. This model, combined with fracture and reservoir engineering, was used to improve fracture treatment designs and improve the planning of well location and spacing.

Several authors have also presented different formulations for coupling geomechanics and reservoir flow simulations. These will be discussed in the next subsections.

2.3.2 Governing Equations

For completeness, the main equations used by each type of simulator are presented.

2.3.2.1 Basic Flow Equations

Since the case presented in this study is a black-oil model, black-oil equations are the only type of equations presented in this section.

Three-phase flow equations are obtained based on mass conservation and Darcy's law (Cunha, 2006; Ertekin et al., 2001; Rodrigues 2009), **Eqs. 2.10-2.12**:

$$\text{Oil: } \nabla\left[\lambda_o\left(\nabla p_o - \gamma_o \nabla z\right) + r_s \lambda_g \left(\nabla p_g - \gamma_g \nabla z\right)\right] = \frac{\partial}{\partial t}\left(\frac{\phi S_o}{B_o} + \frac{r_s S_g}{B_g}\right) + q_w + q_g r_s \quad \text{.....(2.10)}$$

$$\text{Gas: } \nabla\left[\lambda_g\left(\nabla p_g - \gamma_g \nabla z\right) + R_s \lambda_o \left(\nabla p_o - \gamma_o \nabla z\right)\right] = \frac{\partial}{\partial t}\left(\frac{\phi S_g}{B_g} + \frac{R_s S_o}{B_o}\right) + q_g + q_o R_s \quad \text{...(2.11)}$$

$$\text{Water: } \nabla\left[\lambda_w\left(\nabla p_w - \gamma_w \nabla z\right)\right] = \frac{\partial}{\partial t}\left(\frac{\phi S_w}{B_w}\right) + q_w \quad \text{.....(2.12)}$$

where λ is the phase mobility; γ is the fluid specific weight; ϕ is porosity; S is the saturation; q is the rate; r_s is the solution gas/oil ratio into gas phase; R_s is the solution gas/oil ratio into oil phase; p is the pressure; B is the formation volume factor; t is time; z is the depth from a reference pressure datum; and o, g, and w are subscripts for oil, gas, and water, respectively.

Additional equations, **Eqs. 2.13-2.15**, include the sum of saturations and capillary functions (Peaceman 1977).

$$S_o + S_g + S_w = 1 \quad (2.13)$$

$$p_{cwo} = f(S_w) \quad (2.14)$$

$$p_{cgo} = f(S_g) \quad (2.15)$$

where p_c is capillary pressure.

2.3.2.2 Basic Equations for a Deformable Porous Medium

Besides the forces acting on the surface of a body, there are forces acting on every point of the body itself. These 'body forces', f (e.g. gravity), "give rise to stress gradients", that is, total stress increases with depth. For a stressed body to be in equilibrium, all forces acting on the body must cancel out. The following equations apply, **Eqs. 2.16**, **2.17**, and **2.18** (Fjaer et al. 2008):

$$\frac{\partial \sigma_x}{\partial x} + \frac{\partial \tau_{yx}}{\partial y} + \frac{\partial \tau_{zx}}{\partial z} + \rho f_x = 0 \quad (2.16)$$

$$\frac{\partial \tau_{xy}}{\partial x} + \frac{\partial \sigma_y}{\partial y} + \frac{\partial \tau_{zy}}{\partial z} + \rho f_y = 0 \quad (2.17)$$

$$\frac{\partial \tau_{xz}}{\partial x} + \frac{\partial \tau_{yz}}{\partial y} + \frac{\partial \sigma_z}{\partial z} + \rho f_z = 0 \quad (2.18)$$

where f is the body force per unit mass, σ is the stress, and ρ is the density of the medium.

A constitutive equation for the solid porous media is also required. For an elastic medium, **Eq. 2.19** is used:

$$\sigma = E\varepsilon \quad (2.19)$$

where ε is the strain.

2.3.2.3 Coupled Equations

In conventional reservoir simulators, rock compressibility is the only parameter used to "account for" rock deformation, and it is assumed that the bulk volume of each gridblock remains constant at the initial value, V_b^o. Thus, the gridblock pore volume is expressed as **Eq. 2.20** (Dean et al. 2006):

$$V_p = V_p^o\left[1 + c_r\left(p - p_0\right)\right] \quad (2.20)$$

where V_p^o represents the initial pore volume; p, the fluid pressure; and c_r, the rock compressibility, which is entered by the user as part of the input data.

When a flow simulator is coupled with a geomechanical program, porosity changes caused by geomechanics must be considered. Thus, in order to model a deformable porous medium using a flow simulator that assumes constant porosity, "reservoir" and "true" porosities must be defined, **Eqs. 2.21** and **2.22** (Tran et al. 2004; Tran et al. 2005a).

$$\phi^* = \frac{V_p}{V_b^o} \quad (2.21)$$

and

$$\phi = \frac{V_p}{V_b} \quad (2.22)$$

where ϕ^* is the reservoir porosity; ϕ, the true porosity; V_p, the current pore volume; V_b, the current bulk volume; and V_b^o, the initial bulk volume.

These two porosities can be related using **Eq. 2.23** (Tran et al. 2005a):

$$\phi^* = \left(1 - \varepsilon_v\right)\phi \quad (2.23)$$

2.3.3 Solutions for the Coupled Approach

Numerous authors have presented different methods for modeling geomechanical behavior with multiphase flow. These methods can be classified in three major categories:

- Full coupling (wherein flow and deformation equations are solved simultaneously);
- Partial coupling (wherein equations for fluid flow as well as for the geomechanical response are solved separately, i.e., separate models); and
- Pseudo-coupling (wherein a conventional reservoir simulator itself computes some geomechanical responses, or wherein a geomechanical simulator itself computes simple fluid flow responses).

Dean et al. (2006) compared some of the different approaches. They could not determine which technique worked best since the problems analyzed yielded outcomes of varying accuracy and efficiency. Thus, they concluded that technique selection will depend on "ease of implementation, program availability, numerical stability, and computational efficiency".

2.3.3.1 Fully Coupled Solution

Considered the most rigorous approach, in this kind of solution, flow and geomechanical variables (pressure, temperature, saturations, compositions, displacements, stresses and strains) are calculated simultaneously through a system of equations, usually using finite element techniques. This method is sometimes called "implicit coupling" because of the simultaneous solution of the variables (Tran et al. 2004). It is the most stable approach and preserves second–order convergence, giving "good solutions" which can be used as benchmark for other coupling approaches (Tran et. al 2005a; Tran et. al 2005b; Dean et al. 2006). However, not all researchers agree. Regarding complex and large scale reservoirs, Samier et al. (2006, 2008) stated that "the feasibility and accuracy of such simulators… have yet to be proved".

The method's main advantage is that it can work with anisotropic and non–linear models, and with cases where the rock is weak and porosity changes are large, such as in compaction and subsidence problems (Samier et al. 2006; Stone et al. 2003; Tran et al. 2005b). However, a major drawback is the high CPU requirement compared to that of other coupled approaches—that is, it is slower as it solves more variables (Stone et al. 2003; Dean et al. 2006).

Another disadvantage of the fully coupled approach is that it requires explicit knowledge of the simulation model equations used to describe the dynamic system. This requires access to the internal code of the simulator, something that is not possible for commercial simulators (unless you are one of the programmers of the simulator).

2.3.3.2 Partially Coupled Solution

In this approach, also known as "external" or "modular", the stress and fluid flow equations are solved separately using geomechanical and reservoir simulators, respectively. This is done through an interface code (hence the name of external coupling) developed to allow communication between the simulators. In other words, the coupling of the components is obtained by passing data between the simulators, and, if necessary, iterating on a timestep basis (Settari and Mourits 1998; Settari and Walters 2001).

The changes in pressure and/or temperature that occur in the reservoir simulator are passed to the geomechanical simulator to calculate strains and stresses. Then, the updated strains and stresses are used to compute porosity and permeability, which in turn are passed back to the reservoir simulator. An iterative method is recommended to obtain convergence (Settari and Walters 2001).

The main advantage of the approach is the possibility and ease of using existing geomechanical simulators in combination with standard reservoir simulators and their full capabilities without changing the code (Dean et al. 2006; Samier et al. 2006; Settari and Mourits 1998; Tran et al. 2004). However, this can become a dis-

advantage, as the user is constrained by software limitations. Hence, coupling existing simulators may require more code development (Dean et al. 2006).

This method can be subdivided into two large categories: explicit coupling and iterative coupling.

Explicit Coupling (or Loose Coupled Approach)

Simulators perform calculations for fluid flow at each timestep, whereas the geomechanical calculations for the displacements are done during selected timestep. Importantly, this means the two are performed on different time scales. The frequency of geomechanical updates depends on changes in pore volume during timesteps; if pore volumes change slowly, then few geomechanical updates are required (Dean et al. 2006). This coupling subtype is sometimes considered an "iterative" scheme with only one iteration (Stone et al. 2000). A weakness of this approach is the possibility of timestep restrictions due to stability and accuracy (Dean et al. 2006).

This approach can be subdivided into two categories:

- Two–Way Coupling: At user–defined steps or even at each timestep, the pressure and/or temperature calculated by the reservoir simulator are sent to the geomechanical code, which updates the stresses and strains and either "returns" the porosity and permeability changes to the reservoir simulator, or passes these updates directly to the reservoir for calculation. Doing this at each timestep is only recommended when there is "significant compaction" or when there is a reduction in permeability over the stress ranges (Stone et al. 2003; Samier et al. 2006; Tran et al. 2004).

- One–Way Coupling: Modifications are not sent back to the reservoir simulator, hence the name "one-way". The information is passed only from the reservoir simulator to the geomechanics simulator. Hence, changes in reservoir flow variables affect the geomechanics variables, but reservoir flow is not affected by geomechanical responses. This is considered the weakest link between reservoir

flow and geomechanics. (Samier et al. 2006; Tran et al. 2004; Tran et al. 2005b) Some authors also refer to this method as "explicit" coupling (Tran et al. 2004; Tran et al. 2005a).

Iterative Coupling

The two simulators solve flow and displacement variables in a separate and sequential manner. To guarantee convergence, iterations are performed within each stress step before continuing to the next stress step (Dean et al. 2006; Samier et al. 2006; Tran et al. 2004). The exchange of information is normally done through a driver or interface, which also checks for convergence (Tran et al. 2004).

When properly suited, results can be similar to those obtained with the fully coupled approach. This is usually accomplished with a "sufficiently tight" convergence tolerance, which is normally based on pressure or stress changes between the last two iterates of the solution (Settari and Mourits 1998; Dean et al. 2006; Tran et al. 2004; Tran et al. 2005b).

Since it may display a first–order convergence rate, one of the main disadvantages of this method is that it may require a large number of iterations for "difficult problems", where, for example, changes in pressure are significantly large and/or the material is non-linear (Dean et al. 2006; Tran et al. 2005b).

Another disadvantage of this "classical" iterative scheme, as defined by Samier et al. (2008), is that at each stress step, the reservoir simulation must be restarted from the previous converged step. This restart-based scheme can be difficult to implement in practice if the user is not able to modify the internal codes of the simulators. Therefore, a novel iterative scheme was proposed wherein the information is passed (that is, pressure/stress iterations are performed) after a complete run of the reservoir simulation. Porosity and permeability modifications are calculated at various times, and the complete reservoir simulation is repeated. Iterations continue until convergence is achieved.

Some authors, like Tran et al. (2005a), call this "two–way coupling", since calculated information is exchanged between the reservoir and geomechanical simulators.

Because of the complexity and large computing requirements of the coupled models, iterative coupling appears to be the most "popular" method for field–scale simulation (Settari 2002; Tran et al. 2005a).

2.3.3.3 Pseudo-Coupling

Standalone commercial simulators can compute simplified coupled approaches. Some conventional reservoir simulators can calculate some geomechanics responses such as compaction and horizontal stress changes through simple relations between porosity and vertical displacement, porosity and stress, or permeability and stress. Besides the constant porosity option available in all reservoir simulators (wherein pore volumes are only functions of pore pressure), options can be used which multiply porosity and permeability versus pore pressure. Porosity and absolute permeability are updated through empirical models, which are entered as tables of porosity and permeability versus pressure and, sometimes, water saturation. That is, they are functions of pressure and water (Samier et al. 2006; Tran et al. 2004).

On the other hand, some geomechanical codes can simulate the process for single phase fluid flow (Stone 2000). CPU time is normally small, providing a means to make rough estimates and, to an extent, to reproduce field observations without rigorous geomechanics calculations (Tran et al. 2005b).

2.3.4 Parameters of Coupling

There are two main parameters that can be used to perform the coupling between stress and flow: pore volume and/or flow properties (Gutierrez and Lewis 1996; Settari and Mourits 1998). Depending on the reservoir and the desired information, volume coupling or stress–dependent permeability coupling is selected.

Some authors use volume coupling, some use coupling through flow properties, and still others state that the two can be included in the same step.

2.3.4.1 Volume Coupling

In volume coupling, also called "pore compressibility" or "deformation–fluid pressure" coupling, rock deformation affects fluid pressure and vice versa (Gutierrez and Lewis 1996). Porosity is a function of the reservoir's pressure and temperature variations—obtained from the reservoir model—and of the variables calculated from the geomechanics model (stress and strains) (Samier et al. 2006; Settari and Mourits 1998). Volume coupling is important in problems with large changes in porosity, as in unconsolidated heavy oils and oil sands, and soft compacting reservoirs (Settari and Mourits 1998).

Several formulations for volume coupling can be found in the literature. Tran et al. (2004) present a highly-recommended summary of the evolution of the porosity formulation. However, as mentioned by Rodrigues (2009), these are useful only with access to the simulators' internal codes.

This research is inspired by Rodrigues' (2009) work, which uses Tortike and Farouq Ali's (1993) equations "because of their robustness, simplicity, and similarity to modern approaches ". The equations are presented in the next chapter.

2.3.4.2 Coupling Through Flow Properties (or Stress-Permeability Coupling)

In this type of coupling, changes in permeability and relative permeabilities are the result of stress changes (Gutierrez et al. 2001; Settari and Mourits 1998). Most reservoir-flow simulators assume a fixed absolute permeability, as well as a fixed porosity. Others include permeability or transmissibility modifiers as a function of pore pressure; however, the true reservoir behavior is not captured (Heffer et al. 1994; Stone et al. 2000). Absolute permeability may change due to changes in stress during production. Davies and Davies (1999) indicated that the rate of permeability declines when stress is highly variable.

Permeability is dependent not only on pore pressures, but also on mean stress, shear stress and strain, and loading conditions (known as stress path in geomechanics) to which the rock is subjected (Gutierrez et al. 2001). For large-scale reservoir problems with a high degree of heterogeneity, variations in permeability can be very large (Wan et al. 2003), which in turn can cause changes in the directionality of fluid flow (Gutierrez et al. 2001; Settari and Mourits 1998). By using an explicit coupling simulation model, Gu and Chalaturnyk (2005) concluded that permeability, cleat spacing and *in situ* stresses are the main parameters most sensitive and influenced during coal-bed methane production. Thus, it is necessary to understand and model dynamic permeability changes.

There are different ways to model the relationships between stress and permeability, including the classic permeability–porosity model, the modeling of mean effective stress versus permeability, and that of permeability versus $\sigma_1 - \sigma_3$, (the difference between the maximum and minimum principal stresses) (Stone et al. 2000; Tran et al. 2005a). However, there is no simple linear method to account for the effects of stress on permeability (Samier et al. 2006).

Changes in permeability under various conditions of effective stress and strain can also be measured in the laboratory (Davies and Davies 1999; Tran et al. 2005a). One example of this has used triaxial loading (Rodrigues 2009).

Function of Porosity.

When permeability is expressed as a function of porosity, the former is considered an indirect function of geomechanical response. From Tran et al. (2005a), **Eqs. 2.24** and **2.25**:

$$\phi^* = \phi^*\left(\phi, \varepsilon_V\right) \quad \text{.....(2.24)}$$

and

$$k = k\left(\phi^*\right) \quad \text{.....(2.25)}$$

where ϕ^* represents reservoir porosity; ϕ, true porosity ; and k, permeability.

Function of Volumetric Strain or Mean Effective Stress

This type of function is necessary when permeability cannot be accurately predicted only by considering it a function of porosity, such as in diagenetically altered reservoirs (Davies and Davies 1999). Absolute permeability is expressed as a direct function of volumetric strain or mean effective stress. Different authors have recognized the possibility of multiple relationships between permeability and stress (Davies and Davies 1999). Thus, several equations are suggested in the literature.

2.3.5 Upscaling

When geomechanical and reservoir grids are independent, geomechanical simulation is usually performed on coarser grids because of the large size of the geomechanical domain, which is composed of the reservoir and its surroundings. Thus, upscaling and downscaling techniques are used to transfer information between the two models. This research does not address this particular issue because it implies different approaches, as explained in the next sections.

2.3.6 Other Challenges for Reservoir-Geomechanics Coupling

The degree of coupling is not the only issue to be addressed. Others include "the degree of non–linearity (elastic versus plastic), the treatment of multiphase flow coupled to geomechanical response, fracture flow". Each of these is currently under intense research. (Settari and Walters 2001; Yale 2002)

Overall, the interaction between reservoir fluid flow and solid deformation still poses many problems for researchers such as accuracy, convergence, and computing efficiency (Tran et al. 2004). The aim is to ensure that coupled codes have the same capabilities as existing commercial simulators (Settari and Walters 2001).

3
Methodology

Instead of developing a fully coupled simulator, which is extremely time-consuming, this research links two separate existing commercial simulators through a common interface. These have been "optimized for specific classes of applications" (Minkoff et al. 1999).

The two-way coupling approach has been adapted to perform reservoir–geomechanical modeling so as to provide a preliminary understanding of the effects of geomechanical parameters on permeability and porosity. Permeability and porosity, in turn, affect the pore pressure profile, and ultimately, the final recovery factor.

The methodology is based on the work of Minkoff et al. (1999), Rodrigues (2009), and Samier et al. (2008). Despite focusing on different aspects and using different methodologies, the works of these authors share three main attractive characteristics: 1) the codes of the commercial simulators need no modification; 2) any two commercial simulators can be used, depending on the objectives and requirements of the research, allowing exploitation of their special features; and 3) they have the potential to obtain fully coupled solutions.

3.1 Proposed Two-Way Coupling Approach

Dean et al. (2006) could not describe better the essence of the two-way coupling approach: "displacements enter the fluid flow equations through the calculation of reservoir pore volume; and fluid pressures enter the displacement calculations through the stress/strain constitutive equations".

The method presented in this thesis consists of running the model in the streamline simulator for the full time interval with fixed porosity and absolute permeability. Pore pressures are recorded at every timestep for each gridblock.

Then, the interface code reads and organizes these data according to the geomechanical simulator's input requirements. The simulation of the geomechanical deformation covers the same total time interval, using the pore pressures as external loads, to determine displacements and stress updates for each timestep.

The resulting volumetric strains are converted to porosity and permeability (used as the coupling terms) updates for the different timesteps; these updates are transformed into porosity and permeability multipliers.

Due to simulator limitations, only an average of these values is calculated for each gridblock in the interface module, which are fed back (the average multipliers) to the streamline simulator for the next complete run to calculate the pressure in every gridblock.

This means that another set of fixed values for porosity and absolute permeability are used throughout the second run, but these values now consider an average of the changes in stresses and strains. No temperature variation is considered in this research.

Fig. 3.1 presents the conceptual workflow for this algorithm, including the programs used in this research. FLAC^{3D} (Itasca Consulting Group, Minneapolis, 2006), a finite-difference geomechanical simulator, is coupled to FrontSim™ (Schlumberger Geoquest, Paris 2007), a streamline-based fluid flow simulator. A MATLAB (MathWorks, Inc. 2007) code is used as the common interface.

Fig 3.1 also shows the equations used to calculate the updates for porosity and permeability. These equations are explained in detailed in the next subsections.

Finally, Fig 3.1 indicates that before the coupling, the geomodel should be run for equilibrium, using exclusively the geomechanical simulator. This step is further explained in the next subsections as well.

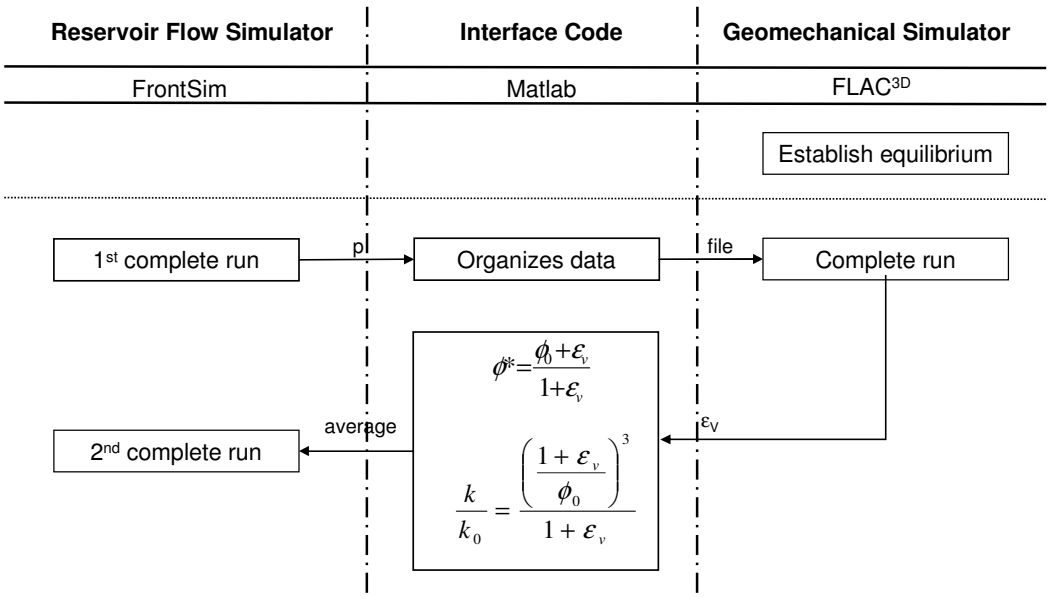

Fig 3.1—Proposed two-way coupling workflow.

The computer used for this study is a Dell Precision Workstation 690, Quad Core Intel Xeon Processor E5345 2.33 GHz, 4 GB RAM, 667 MHz, nVidia Quadro running the Windows XP-32 operating system.

3.1.1 Porosity Equation

An equation similar to Eq. 2.14 may be used to calculate the "corrected" pore volumes for each timestep. Based on Rodrigues' (2009) discussion, a simplified version of Tortike and Farouq Ali's (1993) equation, **Eq. 3.1**, is used because it addresses the problem of true porosity and reservoir porosity. Temperature effects are not considered. This equation assumes that porosity varies linearly with volumetric strain, ε_v, and that solid grains are incompressible.

$$\phi^* = \frac{\phi_0 + \varepsilon_v}{1+\varepsilon_v} \quad \text{.....(3.1)}$$

where ϕ_0 is the initial porosity and ε_v is the volumetric strain.

3.1.2 Permeability Equation

When a flow simulator is coupled to a geomechanical program, it is also important to establish a relationship, either experimentally or theoretically, between permeability and stress to account for the stress dependence of the permeability (Gutierrez et al. 2001).

In the experimental approach, correlations are obtained through triaxial tests which measure the response of permeability to stress (Rodrigues 2009). Most of the equations in the theoretical approach are developed from the concepts of porosity (Eq. 2.13), pore compressibility (**Eq. 3.2**) and an assumed relationship between permeability and porosity (Rodrigues 2009).

$$c_p = -\frac{1}{V_p}\frac{dV_p}{dp} \quad \text{.....(3.2)}$$

where c_p is the pore compressibility, V_p is the pore volume, and dV_p/dp is the gradient of pore volume.

Following Rodrigues' (2009) work, **Eq. 3.3** (Tortike and Farouq Ali 1993) is used to calculate the permeability updates for each gridblock, since this permeability ratio represents the effect that porosity and volumetric strains have on fluid flow.

$$\frac{k}{k_0} = \frac{\left(\frac{1+\varepsilon_V}{\phi_0}\right)^3}{1+\varepsilon_V} \quad \text{.....(3.3)}$$

where k_0 is the initial permeability and k is the current reservoir permeability.

3.1.3 Motivation and Justification

It is acknowledged that this approach is simplistic and insufficient to capture the true geomechanical responses within a reservoir. However, this research is considered as a starting point in the investigation of incorporating geomechanics in streamline simulations. According to Williams et al. (2004), investigations should start with the "simplest possible model and simulator appropriate to the business

decision", in order to start exploring the advantages and disadvantages of using these two types of simulators.

The advantage of this methodology is that it does not require explicit knowledge of the simulator flow equations, thereby making computations less tedious.

3.2 General Cases

As this method is intended to be general and applicable to any kind of problem, this section only provides an overview of the analyzed cases for each study case presented in this thesis; details of the study cases are given in the next chapter.

It should be emphasized that all cases are run in prediction mode (i.e., no history match is done), and consider elastic isothermal deformations.

3.2.1 Uncoupled Case (Base Case)

The base case, which comprises only the reservoir, does not consider geomechanics. It is used as a reference against which to compare results obtained from cases that do consider geomechanical behavior. Pore pressures obtained from the base case at each timestep become the external loads for cases that consider geomechanical parameters. This case is referred to as Uncoupled Case.

3.2.2 Coupled Cases

The next step is to explore the relative influences of geomechanical processes on reservoir behaviour, namely if the average porosity and/or permeability—obtained after running the geomechanical model—affect the reservoir pressure profile. Three cases are chosen to provide a complete analysis of which "static" parameter is most important in this respect:

1) Using permeability as the only coupling term (utilizing Eq. 3.5 to convert volumetric strains into permeability changes), leaving porosity constant. This case is referred to as Permeability Case.

2) Using porosity as the only coupling term (utilizing Eq. 3.3 to convert volumetric strains into porosity changes), leaving permeability constant. This case is referred to as Porosity Case.

3) Using both permeability and porosity as the coupling terms (using both Eqs. 3.3 and 3.5). This case is referred to as Poro&Perm Case.

The most accurate results are expected when considering both parameters.

3.3 Description of Simulators

3.3.1 FrontSim

FrontSim is Schlumberger's 3D, three-phase, compressible black-oil streamline simulator. It includes gravity effects, compressibility, temperature tracking and the capability to simulate changes in well conditions (Koutsabeloulis and Hope 1996).

3.3.1.1 Limitations

Initially, only streamline simulators with an incorporated geomechanical package were considered for use (i.e., using a pseudo-coupling approach). After some research, it was found out that commercial streamline simulators with such capabilities do not exist. This means that FrontSim, by itself, is not prepared to solve geomechanical problems, as opposed to Eclipse 100 (Schlumberger's black-oil simulator), or STARS (CMG's compositional simulator).

The next logical step was to consider a geomechanical simulator coupled with FrontSim and to try to develop a methodology similar to that of Samier et al. (2008). This methodology used an external iterative coupled approach with complete runs, modifying the pore volumes in the "Schedule" section of the flow simulator input file. However, this could not be done either, as only Eclipse 100, the simulator used by Samier et al. (2008), can modify pore volumes after the run has begun, i.e., after declaring the initial static variables (Schlumberger 2007).

Despite this difficulty, the iterative approach was still considered, as was the restart option, which allows the user to "restart" the run from a given report time of a previous run. As in other commercial conventional (finite-difference based) reservoir simulators, it is not possible to change the static properties in streamline simulators once they are established at the beginning of a process. Consequently, it is not possible to iterate internally at each timestep without changing the internal code (as in the "classic" iterative approach described in Section 2, which is implemented within research codes). Therefore, the idea was to use the restart files at each timestep, changing the porosity and/or permeability before each run in order to account for volumetric changes. In other words, a "new model" would be created at each timestep using the restart option, allowing changes in the static properties, and iteration. However, this could not be done because FrontSim can only run these restart files as long as the grid and geometry properties remain unaltered (Schlumberger 2007).

Next, Rodrigues' (2009) method was considered an alternative, as it also uses explicit iterative coupling. That research uses IMEX, CMG's black-oil simulator, as the flow simulator. It uses lookup tables of compressibility, where porosity and permeability multipliers are entered, varying with pressure, to account for volumetric strain changes. However, once again, this could not be done because FrontSim does not allow the input of porosity and permeability or their multipliers as functions of pressure.

Despite these limitations, the simulator was deemed appropriate as it is much faster to adapt to its shortcomings than to develop a new code with the necessary characteristics to run reservoir-geomechanical simulations.

3.3.2 FLAC3D

FLAC3D is Itasca's 3D finite-difference geomechanical simulator capable of solving different constitutive equations (e.g. elastic-plastic, creep, elastoviscoplastic, etc). The convention adopted by this simulator is to consider compressive stress and compressive strain as negative (Itasca 2006).

FLAC3D reads pore pressures from the nodes of the gridblocks (up to eight), and not from the center, like FrontSim does. To solve this "compatibility problem", so that FLAC3D could be able to "load" the fluid pressures, a subroutine was written in MATLAB, using tri-linear interpolation to convert one value (block-centered pressure) into eight (node-pressures). This method was formulated and validated by Rodrigues (2009).

It should be noted that the description of the input file of FLAC3D has a different structure and requires "three fundamental components" in order to run: a) a finite-difference grid; b) a constitutive model and material properties, and c) boundary and initial conditions (Itasca 2006).

3.3.2.1 Constitutive models

FLAC3D can model elastic and plastic materials. This research focuses exclusively on elastic problems.

Young's modulus (E) and Poisson's ratio (υ) are the parameters that describe the elasticity condition. In FLAC3D, these are entered indirectly, as the user has to use **Eqs. 3.6** and **3.7** to convert them into bulk modulus (K) and shear modulus (G), and enter them into the input file instead (Itasca 2006).

$$K = \frac{E}{3(1-2\upsilon)} \quad \text{.....(3.6)}$$

$$G = \frac{E}{2(1+\upsilon)} \quad \text{.....(3.7)}$$

where E is Young's modulus, υ is Poisson's ratio, K is the bulk modulus, and G is the shear modulus.

3.3.2.2 Boundary conditions

It is common to have either stress or displacement boundary conditions. Usually the bottom of the grid has a zero displacement condition while the sides and top have specified stresses (Stone et al. 2000).

3.3.2.3 Equilibrium

Prior to the streamline-geomechanical run, it is mandatory to establish equilibrium conditions in the geomodel. This can be accomplished either by timestepping the simulation to equilibrium (i.e., stepping forward after the declaration of the variables) to allow gravitational stresses to develop within the model, or by directly establishing it in the input file (i.e., without stepping), using specific keywords (*ini* and *apply*) with their corresponding values (Itasca 2006).

It is advised to monitor the maximum unbalanced force (the resultant force at each gridpoint) and z-displacements to determine if the model has reached equilibrium; the unbalanced force should approach a small value and the displacement histories should become constant (Itasca 2006).

3.3.2.4 Limitations

Since the main purpose of this research is to test the features of a streamline simulator considering geomechanical behaviour, the intent was to work with a detailed field-scale model (more than a million gridblocks for the reservoir alone, not including the non-pay region). However, the Windows XP Professional 32-bit computer used could not support the creation of this model in FLAC^{3D}. At least 64 bits is required to handle such large models.

The creation of an equivalent geomodel was considered, using upgridding and pseudo-upscaling (when transferring the pore pressures to the geomodel) and downscaling (when transferring the strains to the flow simulator). However, this was abandoned because researchers do not agree regarding on which methods are best suited for different kinds of problems. Moreover, results would be harder to interpret and analyze; if errors were present, it would be difficult to determine if they were caused by the method itself or because of an error in choosing the upscaling and/or downscaling techniques. To avoid issues of scaling up and scaling down, this approach handles the same grid cell structure in both simulators, i.e., the same number of cells.

As a final comment, FLAC^{3D} cannot be considered a user-friendly program, at least when compared to commercial reservoir flow simulators. The user is required to perform many calculations before entering data into the input file. For example, data should be introduced in consistent units, while in flow simulators, data entered in different units are converted internally. Another example is that the user is really encouraged to "initialize internal stresses such that they satisfy equilibrium and gravitational gradient", i.e., they should match. Finally, even when there is a user interface, the user should create files from scratch. There are no "builders" that allow the user simply to enter the values and let the program compile the input file, which is very common in most commercial flow simulators.

The above points mean that users should be particularly familiar with the program, something which can take months, according to some experts. Even those well trained in the program must exercise a great deal of care when using it to avoid inaccurate results.

4
Study Cases: Description

This research validates the two-way coupling approach described in the previous chapter by running two study cases: Study Case 1 and Study Case 2. The former is a single-phase fluid (water) model with one producer at the center of the reservoir. The latter handles a two-phase fluid (oil and water) model, with one injector and one producer, located diagonally across the reservoir.

It should be mentioned that although these two study cases are fairly straightforward, and that pressure histories have the potential to be reproduced by typical reservoir simulators with the proper choice of compressibilities (Dean et al. 2006), they were chosen because geomechanical responses still can be observed.

In other words, although no strong geomechanical effects might be observed, they were chosen for the sake of simplicity. Coupling these two areas is a complex task, and handling complex models will just make analyses more difficult.

Despite the simplicity of the models, it was intended to work with models that could prove the validity of this approach. The study cases are elastic with no lateral or bottom movement, and do not consider the surrounding formation.

This research should be considered as a first step toward a more complex coupling. There are many study cases (Minkoff et al. 1999) that handle simple algorithms, and still are able to obtain good results for analysis. Such a case is Dean's et al. (2006) work.

4.1 Study Case 1: Single-Phase

The problem number 1 that was presented by Dean et al. (2006) in SPE paper 79709, was chosen as the first study case. It was chosen because the authors pro-

vided detailed descriptions (fluid-flow and geomechanical parameters) and results of the simulations. This facilitates the possibility to compare the performance of this two-way coupling approach, since its results can be compared with tested cases.

Dean et al. (2006) compare three different coupling techniques: explicitly coupled, iteratively coupled, and fully coupled, providing all the data they used as well as their results to be used for comparison with other geomechanical-fluid flow simulators.

This SPE paper presents four different models, but Problem 1 was particularly addressed because it is the simplest to build, especially in the geomechanical code, where equilibrium should be established prior to the coupling simulation.

It does not include a non-pay region, making it possible to focus on the reservoir at this initial stage. Since the model is detailed in Dean et al. (2006), the following subsections only present a summary of it.

It should be indicated that their Problem 3 was the first model to be considered, as it includes the surrounding formations (a more realistic geomechanical problem). It also has the particularity that it captures an increment in pressure at the border of the reservoir (a behaviour that cannot be reproduced by any only-reservoir-flow simulation). However, precisely because this method is conceptually simple, this feature would have never been seen. It was deemed inappropriate to try to compare the results obtained in the SPE paper with those obtained using this methodology because it was known in advance that the results would never resemble those of Dean et al. (2006).

Some general comments are necessary before the raw data of this problem is presented. Dean et al. (2006) focused exclusively on porosity changes, leaving the absolute permeabilities constant. By including the permeability changes, this research is meant to go one step further.

For this particular problem, Dean et al. (2006) present the average pressure and subsidence with one single line for the three techniques, in their Figs. 2 and 3, re-

spectively, meaning that the same results were obtained using all of the coupling approaches they compared.

Two models were created, one for the streamline simulator and other for the geomechanical simulator. Both models have 1210 cells, all of which are active; 11 cells in the x-direction, 11 in the y-direction, and 10 layers in the z-direction. Each cell is 200 x 200 x 20 ft. The top surface of the reservoir is located at a depth of 6,000 ft.

The MATLAB code, FrontSim and FLAC^{3D} input files for this study case can be found in **Appendices A-C**, respectively.

4.1.1 FrontSim™

Table 4.1 presents a summary of the reservoir model properties. **Fig. 4.1** illustrates the model generated in FrontSim. It is a single-phase (water) depletion example with one producer located at the center of the model, completed throughout the 10 layers of the reservoir, with a wellbore radius of 0.25 ft. The well produces at a rate of 15 000 B/D for 500 days, with a timestep size of 10 days.

Table 4.1—Summary of reservoir parameters, Study Case 1.

Porosity, ϕ	0.20
Horizontal permeability, k_x and k_y (md)	50.0
Vertical permeability, k_z (md)	5.0
Formation volume factor @ 14.7 psi, B_w	1.0
Viscosity, μ_w (cp)	1.0
Density @ 14.7 psi, ρ_w (lbm/ft^3)	62.4
Fluid compressibility, c_f (psi^{-1})	$3x10^{-6}$
Initial fluid pressure @ 6000 ft, p_i (psi)	3000
Hydrostatic gradient, (psi/ft)	0.433
Rock compressibility, c_r (psi^{-1})	$3.71x10^{-4}$

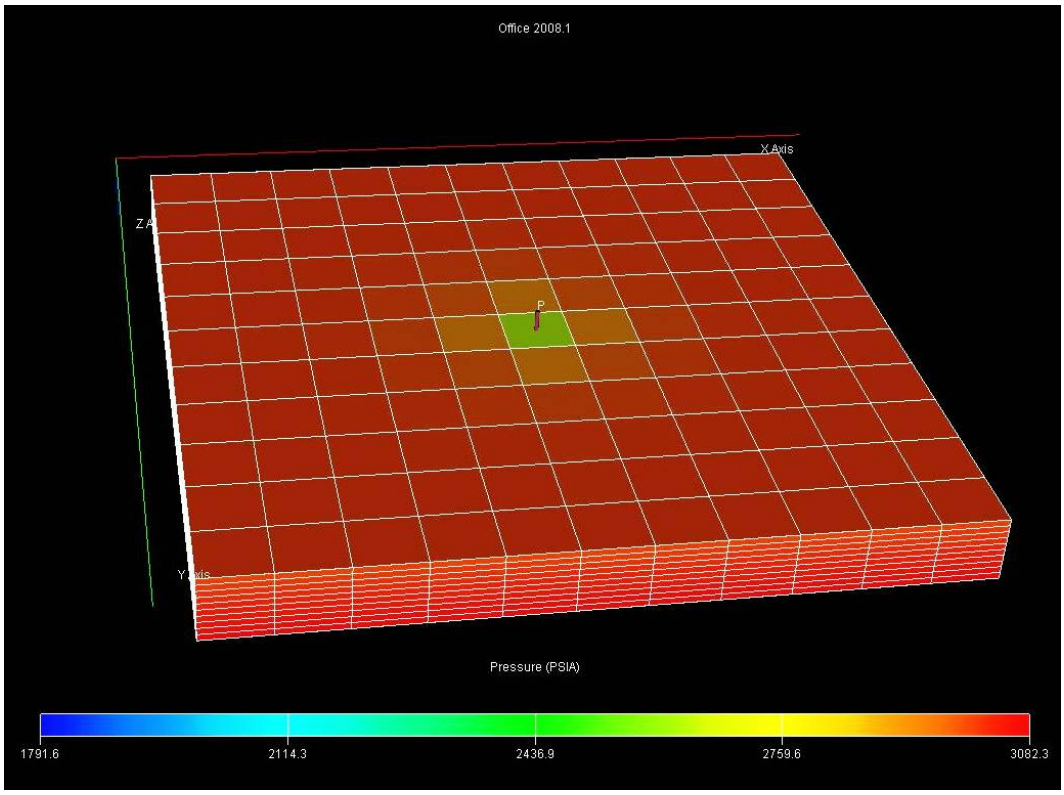

Fig 4.1—FrontSim grid showing the well location, Study Case 1.

The results obtained from this FrontSim model is the Uncoupled Case. For the coupled cases, the porosity and/or permeability maps were modified accordingly (i.e. the rest of the parameters remained the same).

For the results, which will be presented in the next chapter, four observation points were chosen to monitor the changes in pressure, porosity, permeability and volumetric strains. Considering Fig. 4.1 as the reference, the points are located at the

- Top. This cell is at the center of the reservoir, where the well is located. The ID for this cell, in the FLAC^{3D} model is Cell 1150.

- Bottom. Also located at the center of the reservoir, where the well is located. The ID for this cell, in the FLAC^{3D} model is Cell 61.

- Left Bound. This cell is at the center, in the vertical direction. The ID for this cell, in the FLAC^{3D} model is Cell 661.

- Right Bound. This cell is at the center, in the vertical direction. The ID for this cell, in the FLAC^{3D} model is Cell 671.

4.1.2 FLAC^{3D}

The flow-model and the geomodel have the same number of grids (same size and orientation). This allowed the "direct" transfer of data [pore pressures (after transforming the block-centered pressure into eight node-pressures) and volumetric strains] between the models.

Table 4.2 presents a summary of the geomodel properties, and **Fig. 4.2** shows the geomodel grid generated in FLAC^{3D}.

Table 4.2—Summary of geomodel characteristics, Study Case 1.

Young's modulus, E (psi)	1x10^4
Poisson's ratio, υ	0.3
Initial vertical stress @ 6000 ft, σ_{zi} (psi)	6000.0
Vertical stress gradient, (psi/ft)	1.0231
Initial horizontal stresses, σ_{xi} and σ_{yi} (psi)	4000.0
Bottom and sides normal displacements of grid	0.0
Tangential stresses (all faces)	0.0
Biot's coefficient, α	1.0

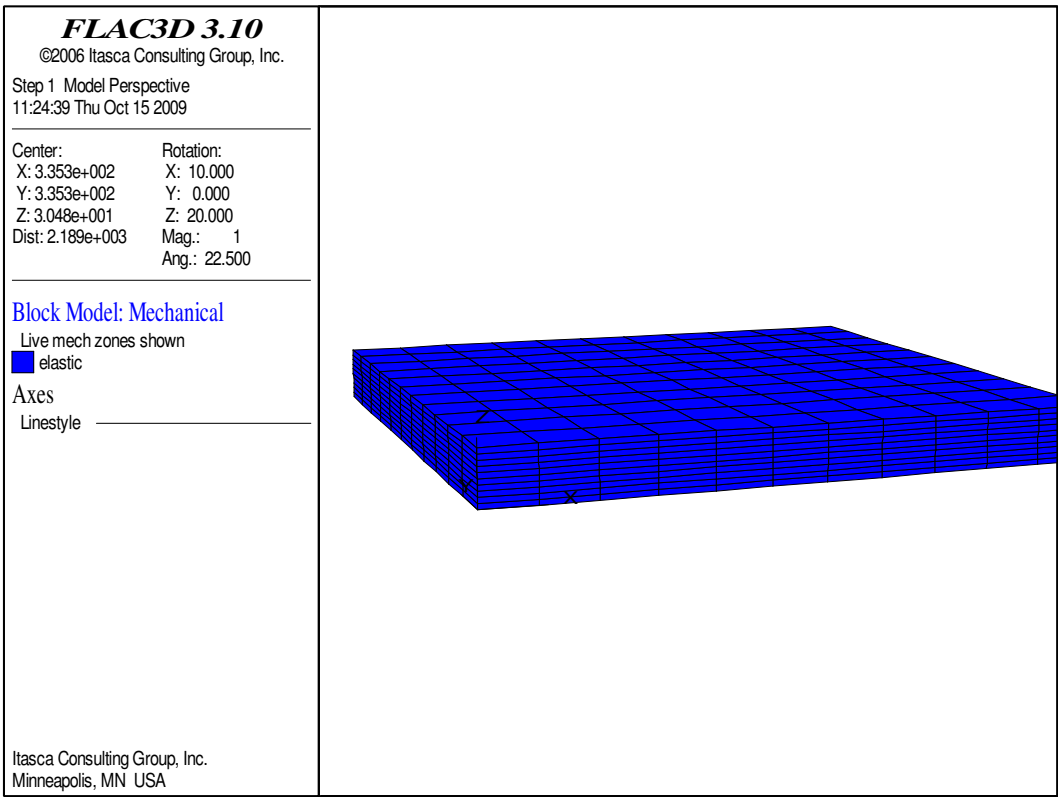

Fig. 4.2—Geomodel for Study Case 1, built in FLAC3D.

A sketch of the model is portrayed in **Fig. 4.3**, showing that the bottom and lateral boundaries are fixed, and the top surface of the model is free to move in z-direction. Although not realistic (it has been seen that reservoir boundaries, including bottom, displace), this model was chosen because of easiness to establish equilibrium in the geomechanical run.

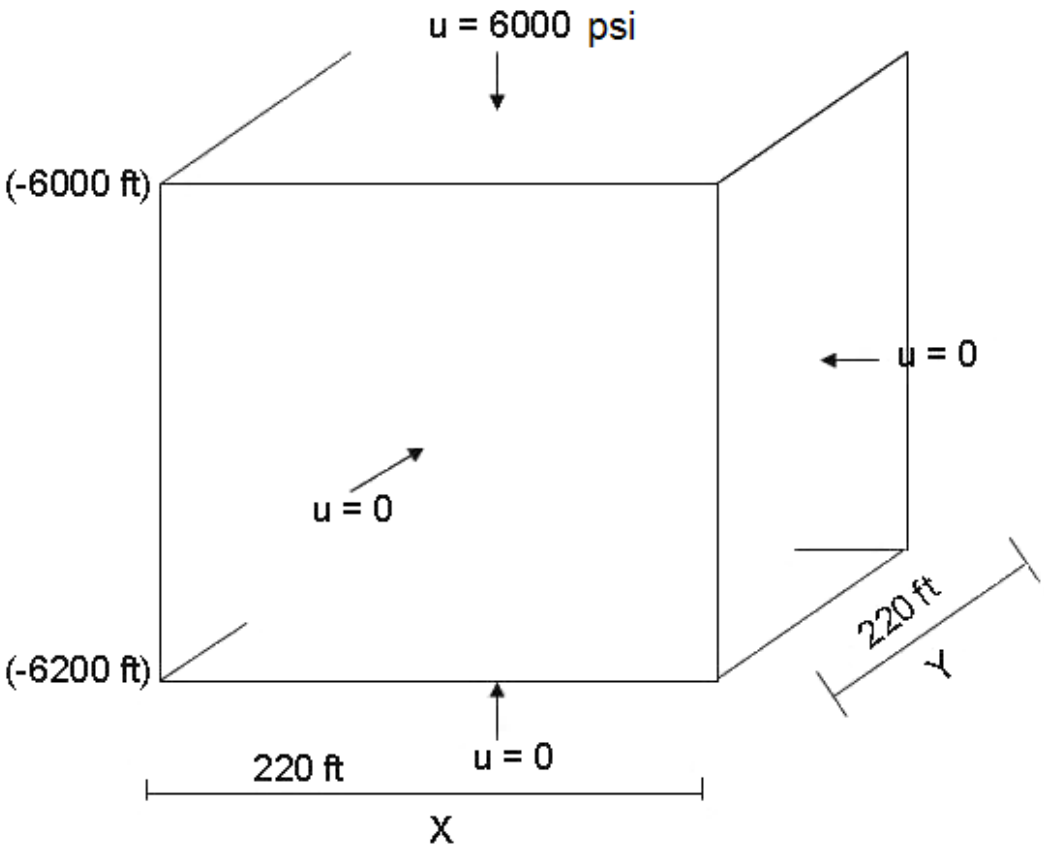

Fig. 4.3—Boundary conditions of the FLAC^{3D} model. Values in parentheses represent the depth. The single values represent the total distance. *u* stands for displacement (modified from Dean et al. 2006 and Rodrigues 2009).

4.2 Study Case 2: Two-Phase Flow

It was considered to have at least two study cases to have more tools for the analyses of results. This problem aims to deal with a "more" complex case: more fluids, more cells, as well as being run for a longer period of time.

It was also deemed appropriate to test an injection case since streamline simulators are well suited for this kind of problems. In other words, depletion cases were recently incorporated to capabilities of the simulators. Although they have been tested to work (either in depletion or injection cases), it is still convenient to work with problems that are well established for this kind of simulators.

This is also a synthetic, elastic, thermal case, adapted from the one of the tutorials of FrontSim (ECL_SAMPLE3D.DATA). One of the interesting features of this model is that permeability is heterogeneous.

As with Study Case 1, two models were created; one for the streamline simulator and another for the geomechanical simulator. Both models have 62 500 cells; 50 cells in the x-direction, 50 in the y-direction, and 25 layers in the z-direction. Each cell is 65.62 x 65.62 x 13.12 ft. The top surface of the reservoir is located at a depth of 6561.68 ft.

FrontSim and FLAC^{3D} input files for this study can be found in **Appendices D-E**, respectively.

4.2.1 FrontSim™

Table 4.3 presents a summary of the reservoir model properties. It is a two-phase (oil and water) model with one producer and one injector, located diagonally at the corners of the reservoir. Both wells are completed throughout the 25 layers of the reservoir, with a wellbore radius of 0.25 ft. The well produces at a liquid rate of 34 465 B/D for 10 years, with a timestep size of 730 days.

Table 4.3—Summary of reservoir parameters, Study Case 2.

Porosity, ϕ	0.20
Average horizontal permeability, k_x and k_y (md)	504.05
Vertical permeability, k_z (md)	0.1*k_x
Oil formation volume factor @ 4409.15 psi, B_o	1.0
Oil viscosity, μ_o (cp)	1.0
Oil density @ 14.7 psi, ρ_o (lbm/ft^3)	48.69
Water formation volume factor @ 4409.15 psi, B_w	1.0
Water viscosity, μ_w (cp)	1.0
Water density @ 14.7 psi, ρ_w (lbm/ft^3)	63.30
Water compressibility, c_w (psi^{-1})	3x10^{-6}
Initial pressure @ 6,561.68 ft, p_i (psi)	4409.15
Rock compressibility, c_r (psi^{-1})	3.71x10^{-4}

Table 4.4 presents a summary of the descriptive statistics for the horizontal permeability. **Fig. 4.4** presents the histogram of the data. It is seen that the frequency has a uniform distribution.

Table 4.4—Summary of descriptive statistics for horizontal permeability, Study Case 2.

Mean	504.05
Standard Deviation	285.54
Range	989.96
Minimum	10.03
Maximum	999.98

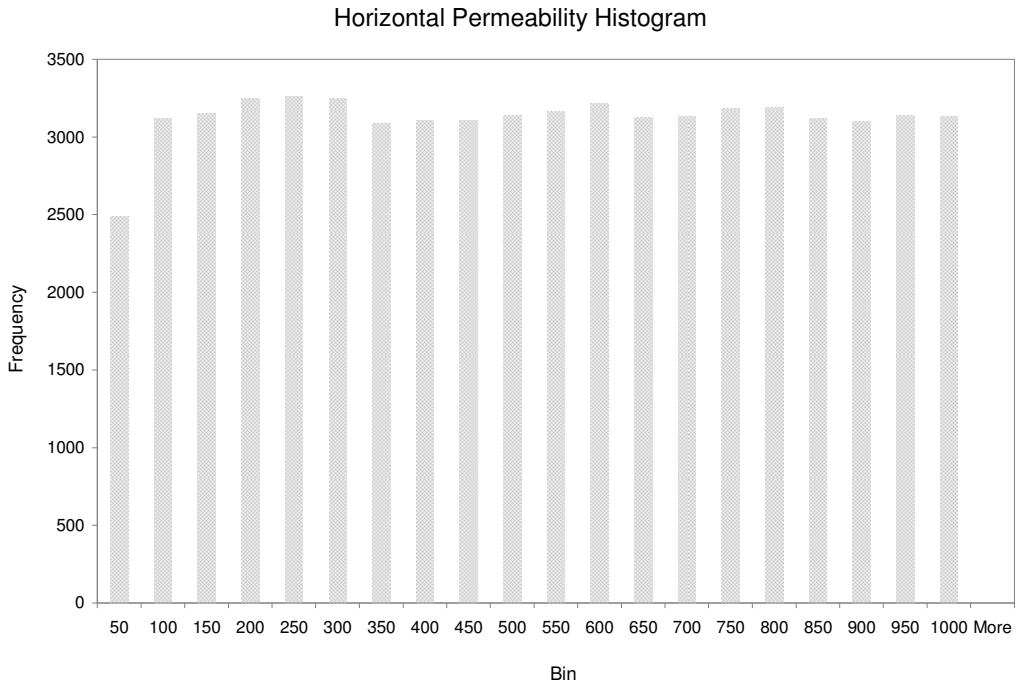

Fig. 4.4—Histogram for horizontal permeability, Study Case 2.

As with Study Case 1, the results obtained from this FrontSim model are referred as Uncoupled Case. For the coupled cases, the porosity and/or permeability maps were modified accordingly (i.e. the rest of the parameters remained the same).

4.2.2 FLAC3D

The flow-model and the geomodel have the same number of grids (same size and orientation), to allow the "direct" transfer of data between the models.

The geomodel was built using the same data as in Study Case 1 (Table 4.2). **Fig. 4.5** presents the model generated by FLAC3D.

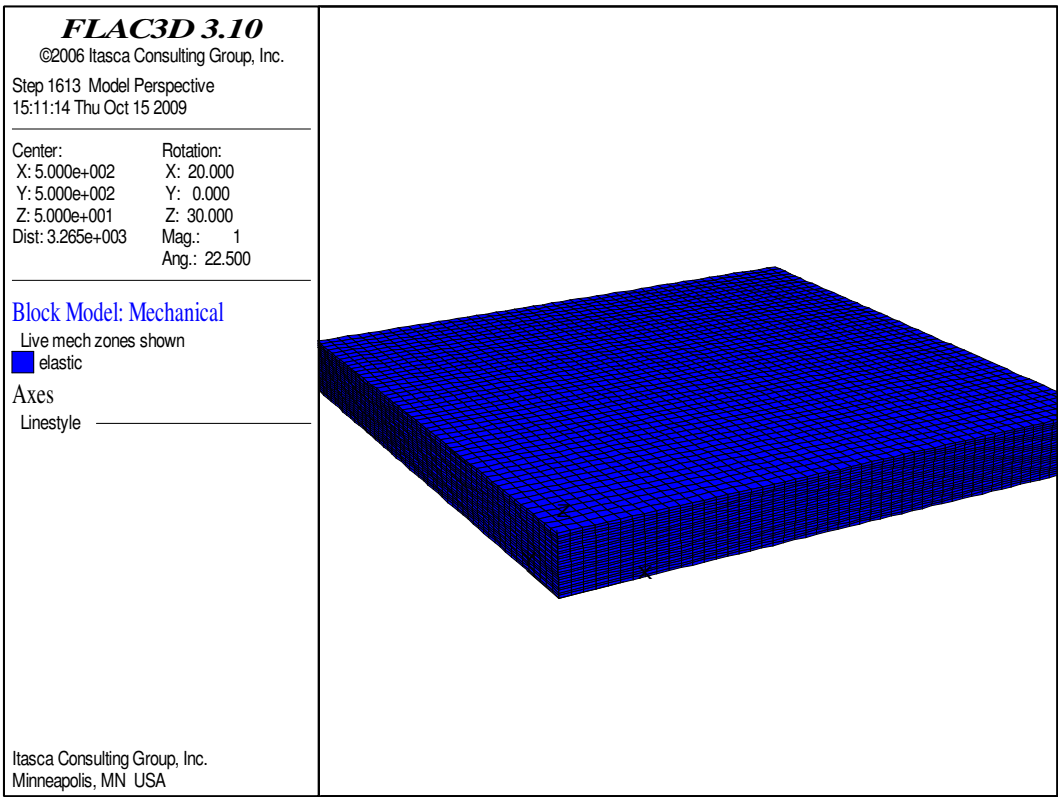

Fig. 4.5—Geomodel for Study Case 2.

For the results, which will be presented in the next chapter, six observation points were chosen to observe the changes in pressure, porosity, permeability and volumetric strains. Considering Fig. 4.5 as the reference, the points are located at the

- Top Left. This cell is at the left "upper" corner of the reservoir, where the injector is located. The ID for this cell, in the FLAC3D model is Cell 62 451. The

ID of one of the gridpoints surrounding this is cell is 67 596 (top right corner of the cell that is not on the boundary).

- Top Right. This cell is at the right "lower" corner of the reservoir, where the producer is located. The ID for this cell, in the FLAC^{3D} model is Cell 60 050. The ID of one of the gridpoints surrounding this is cell is 65 125 (top left corner of the cell that is not on the boundary).

- Bottom Left. This cell is at the left "upper" corner of the reservoir, where the injector is located. The ID for this cell, in the FLAC^{3D} model is Cell 2451. The ID of one of the gridpoints surrounding this is cell is 5 000 (bottom right corner of the cell that is not on the boundary).

- Bottom Right. This cell is at the right "lower" corner of the reservoir, where the producer is located. The ID for this cell, in the FLAC^{3D} model is Cell 50. The ID of one of the gridpoints surrounding this is cell is 198 (bottom left corner of the cell that is not on the boundary).

- Left Boundary. This cell is at the center, in the vertical direction. The ID for this cell, in the FLAC^{3D} model is Cell 33 751. The ID of one of the gridpoints surrounding this is cell is 32 488 (bottom left corner of the cell).

- Right Boundary. This cell is at the center, in the vertical direction. The ID for this cell, in the FLAC^{3D} model is Cell 33 800. The ID of one of the gridpoints surrounding this is cell is 32 538 (bottom right corner of the cell).

5
Results, Discussion, and Analysis

This chapter presents the results of two synthetic isothermal elastic cases, which were used to test the two-way coupling approach [using porosity (Porosity Case), permeability (Permeability Case), and permeability and porosity (Poro&Perm Case) multipliers as the coupling factors). The performance of this approach is mainly evaluated by comparing these results with those obtained from the streamline-only simulation (referred as the Uncoupled Case).

One reason for using multipliers, and not the actual maps, of porosity and permeability as the coupling parameters is that they are easier to implement in the code. But in fact, there are no differences in the results when using one or the other.

Another advantage of using them is that it is easier to appreciate the magnitude of the changes in the values (e.g. instead of using a value of 0.205, it uses 1.025, given that 0.2 is the original porosity).

5.1 Study Case 1

As indicated in Section 4.1.1 (see for more details), four points were chosen to monitor the progress of the process. These points are referred as Top [the top-center cell (ID 1150)], Bottom [bottom-center (ID 61)], Left Bound (ID 661), Right Bound (ID 671).

The different steps of the two-way approach are illustrated by presenting the different results (volumetric strains, porosity and permeability multipliers, and pore pressures) obtained for these four cells.

The average reservoir pore pressure profiles obtained from the Uncoupled and Coupled Cases are also presented, and compared with the profile obtained by Dean

et al. (2006) as well for completeness. GetData Graph Digitizer™ was used to re-produce Dean et al.'s (2006) graph.

5.1.1 Geomechanical Equilibrium (Preliminary Phase)

Prior to the pore pressure loading, it is necessary to establish the equilibrium state in the geomodel. For Study Case 1, which has simple geometry, boundary and initial conditions, it was established in the input file. This means that values were written in such a way that the equilibrium was already established even without running it. However, just to corroborate it, the model was run.

The histories of the maximum unbalanced force and z-displacements, and shear stresses were assessed, for the four chosen cells, to check for the initial equilibrium state. The first two plots are not shown since all of them are blank, i.e. the values are zero, corroborating that equilibrium was established in the input file.

Fig. 5.1 shows the shear stresses for these cells; they have a value of zero (another indicator of equilibrium), since the grid orientation coincides with the principal axes. The minus signs for the normal stresses indicate compression.

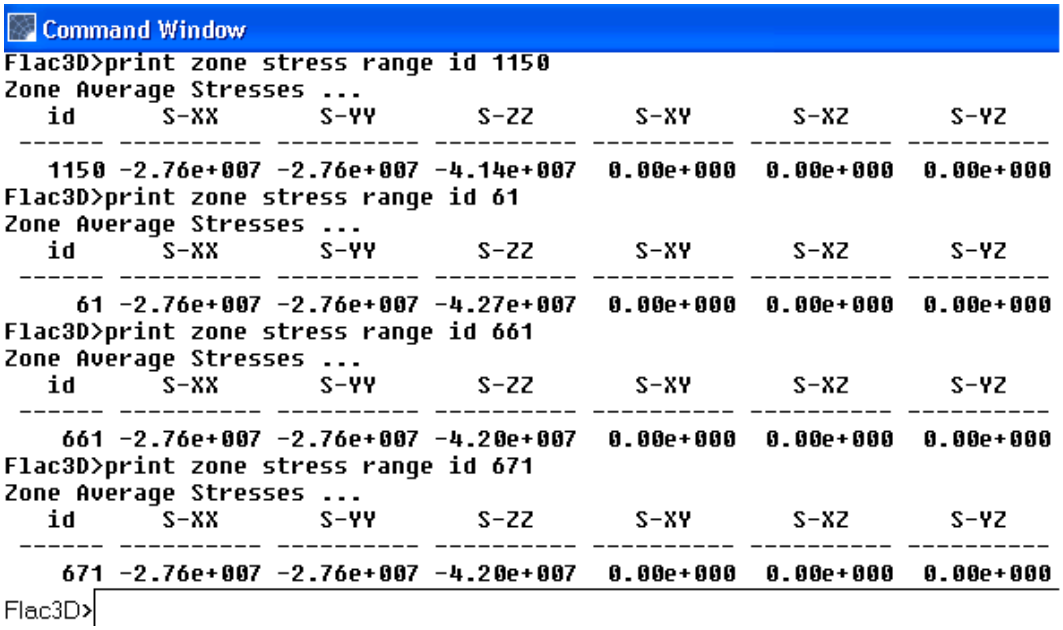

Fig 5.1—FLAC3D results showing no shear stresses, S-XY, S-XZ, S-YZ, at the top (ID 1150), bottom (ID 61), and boundaries (ID 661 and 671) of geomodel, Study Case 1.

Finally, initial vertical stresses were also checked for equilibrium for the whole geomodel, **Fig. 5.2**. Each layer has a different constant value, having the largest value at the bottom, denoting equilibrium as well.

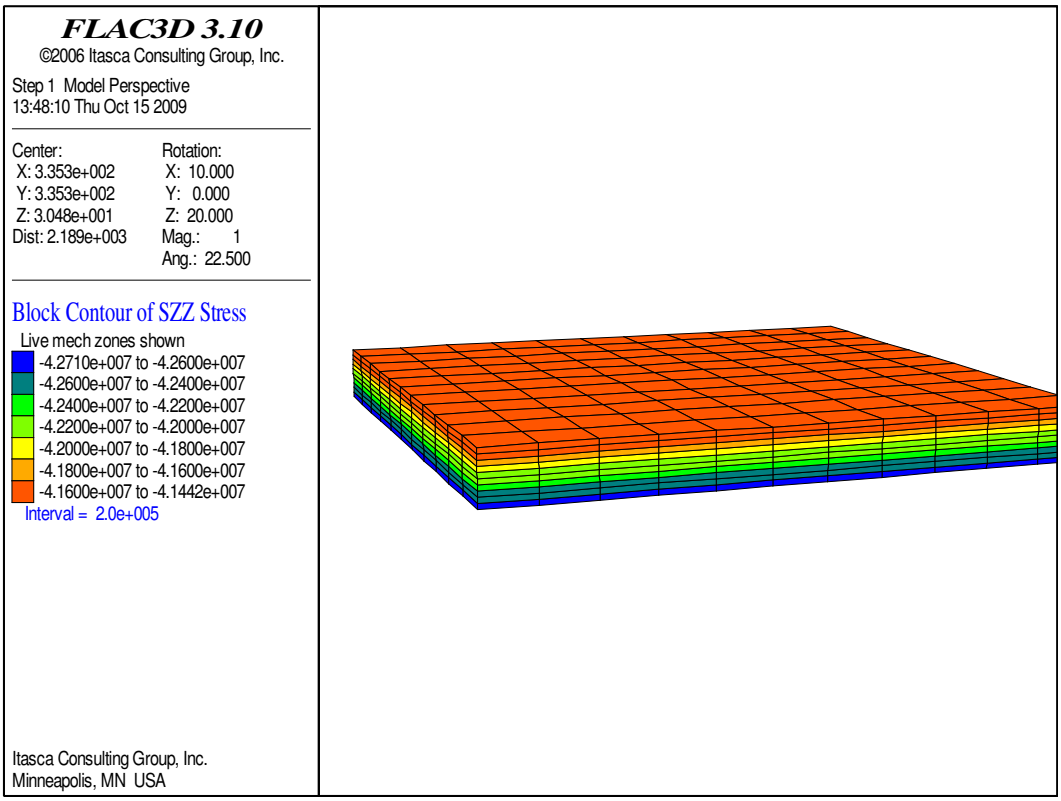

Fig. 5.2—Initial vertical stresses after equilibrium run, Study Case 1.

5.1.2 Volumetric Strains

After the complete run of the Uncoupled Case, the pore pressures were passed to FLAC3D (as external loads), for it to calculate the volumetric strains for each gridblock at each timestep. **Fig. 5.3** shows the volumetric strains profile of the Top, Bottom, Left Bound, and Right Bound Cells.

Independently of the simplicity of the two-way approach, it can be seen that the external loads do not have a significant impact on the geomodel response. Looking at the scale of the graph, the changes are quite small, and usually, at least in practice, would be neglected. However, despite this fact, some comments are in order.

To facilitate the analysis of the results, the four cells (points of observation) can be divided into two groups, according to the displayed behaviour (shape) in the graph: Vertical (Top and Bottom Cells) and Horizontal (Left Bound and Right Bound Cells).

At the beginning of the run (the first 40 days), both groups exhibit a disturbance (although opposite behavior), which is probably due to the disequilibrium that is created when the reservoir starts producing. After this period, the graph "stabilizes".

The Vertical Group shows a decrement at the beginning of the simulation, and then and increment, reaching its peak at 40 days. After this period, it enters into a dynamic equilibrium, decreasing at an almost constant rate for the rest of the simulation, which is in agreement for a depletion case. The changes in volumetric strains are more pronounced for the Top Cell (the slope is steeper). This is most likely due to the boundary conditions; the top of the reservoir is free to move, while the bottom is fixed. At the bottom, even though it is fixed, it still has to support the weight of the layers above.

On the other hand, the Horizontal Group shows an increment at the beginning of the run; then it decreases, reaching its lowest value at 40 days. After this period, it starts increasing again until it reaches the original value (zero volumetric strains) at 300 days, remaining the same for the rest of the simulation. Although these changes were observed, it is fair to say that they are minimal. Moreover, in practice, they can be considered as zero, especially if it is taken into account that only 500 days were simulated. This behaviour was expected due to the boundary conditions imposed; there is no lateral movement. If other behavior was observed, it would have indicated an error in the input file(s).

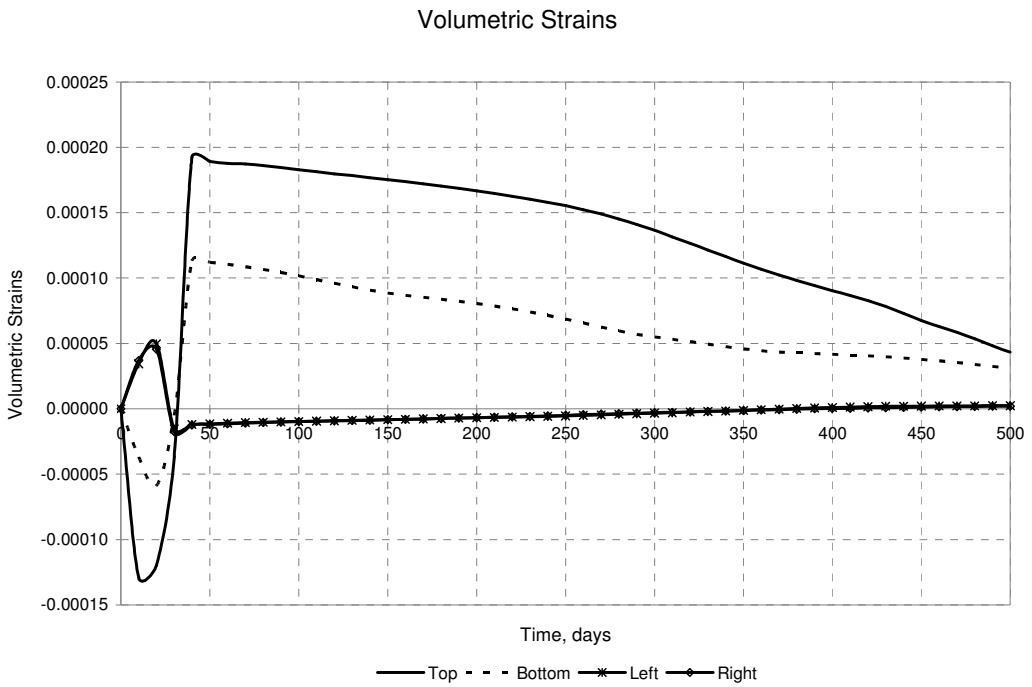

Fig. 5.3—Volumetric strain profile for cell at the top-center cell (ID 1150), bottom-center (ID 61), left boundary (ID 661), and right boundary (ID 671).

Considering the characteristics of this study case (elastic, homogeneous, one-phase, depletion, and one well), the outcome is, at some point, even expected. However, it should be mentioned that a larger change was anticipated.

If a more complex model was considered, e.g. considering plasticity, it was more likely to get a significant response. However, as indicated in Section 3.3.2.4, FLAC^{3D} is not user friendly, quite the contrary. The user must have some level of expertise to manipulate it. It should be borne in mind that this is just a starting point in investigating the possibility of coupling geomechanics and streamline simulators. Most of the times, when starting a research of this nature, elastic models are used. Once it is proved that they work, more complex models are built.

Another option for registering larger changes in the geomechanical response, could had been by considering each change, not after a complete run of the reservoir simulator, but after each timestep. However, due to streamline simulator's limitations, this was hard to implement.

For all these reasons (and also because of time constraints), it was decided to continue with the testing of the approach using this study case.

Since this geomechanical response is passed on throughout the coupling simulation, as will be seen in the next subsections, the results should be carefully handled. The analysis should be done qualitatively more than quantitatively. With these small values of volumetric strains, it can be expected that the changes in average reservoir pressure will not be significant for the coupled cases.

5.1.3 Average Porosity and Permeability Multipliers

Figs. 5.4 and **5.5** illustrate the calculated porosity and permeability multipliers, respectively, for each timestep for the four cells (top, bottom, and boundaries).

As anticipated, the graphs present the same behavior as that of the volumetric strains (they were calculated using them).

Although porosity and permeability multipliers present the same behavior, the scales are different; being one order of magnitude larger for permeability. This can lead us to think that permeability is somewhat more sensitive to changes in geomechanical parameters than porosity.

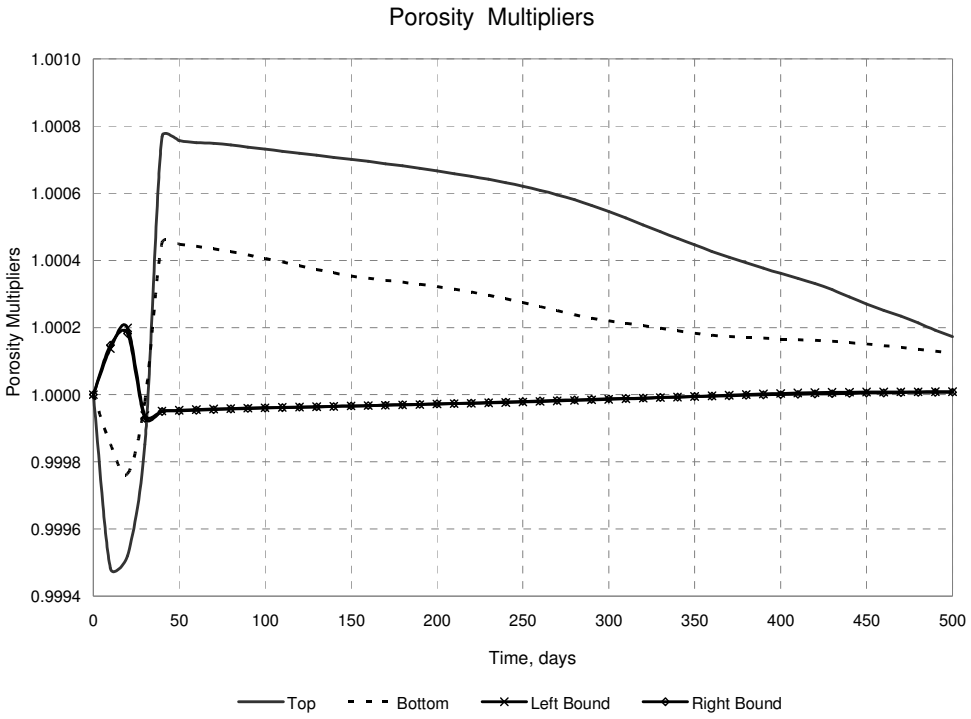

Fig. 5.4—Porosity multipliers profile for cell at the top-center cell (ID 1150), bottom-center (ID 61), left boundary (ID 661), and right boundary (ID 671).

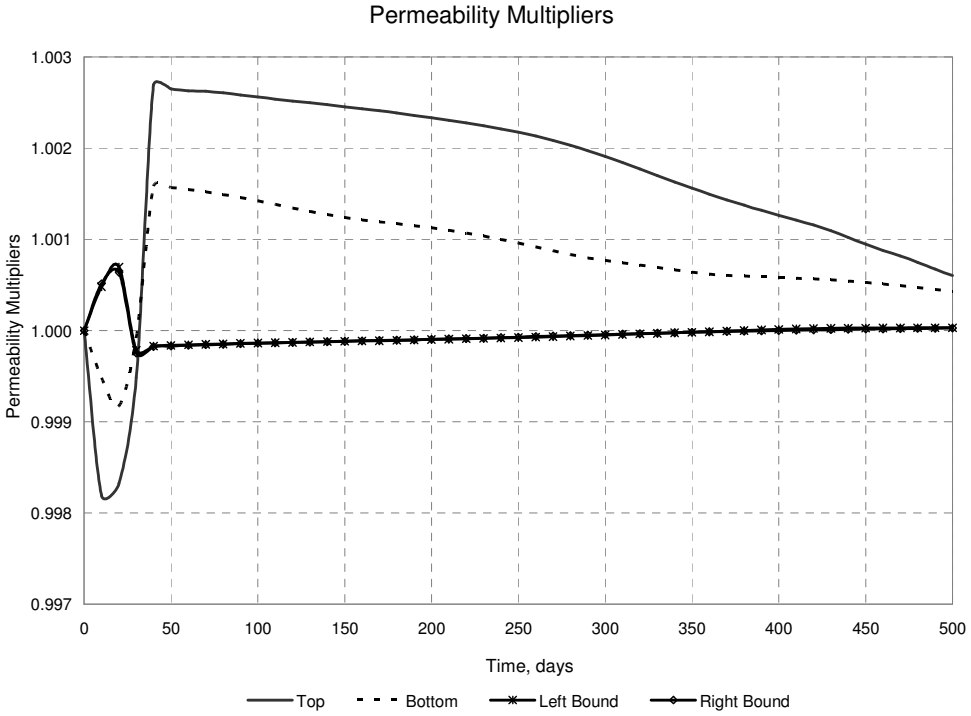

Fig. 5.5—Permeability multipliers profile for cell at the top-center (ID 1150), bottom-center (ID 61), left boundary (ID 661), and right boundary (ID 671).

To facilitate comprehension of the magnitude of the changes, **Figs. 5.6** and **5.7** show the relative difference, in percentage, of porosity and permeability, respectively, compared to the original values. Changes are not even bigger than 0.08% and 0.3% for porosity and permeability, respectively.

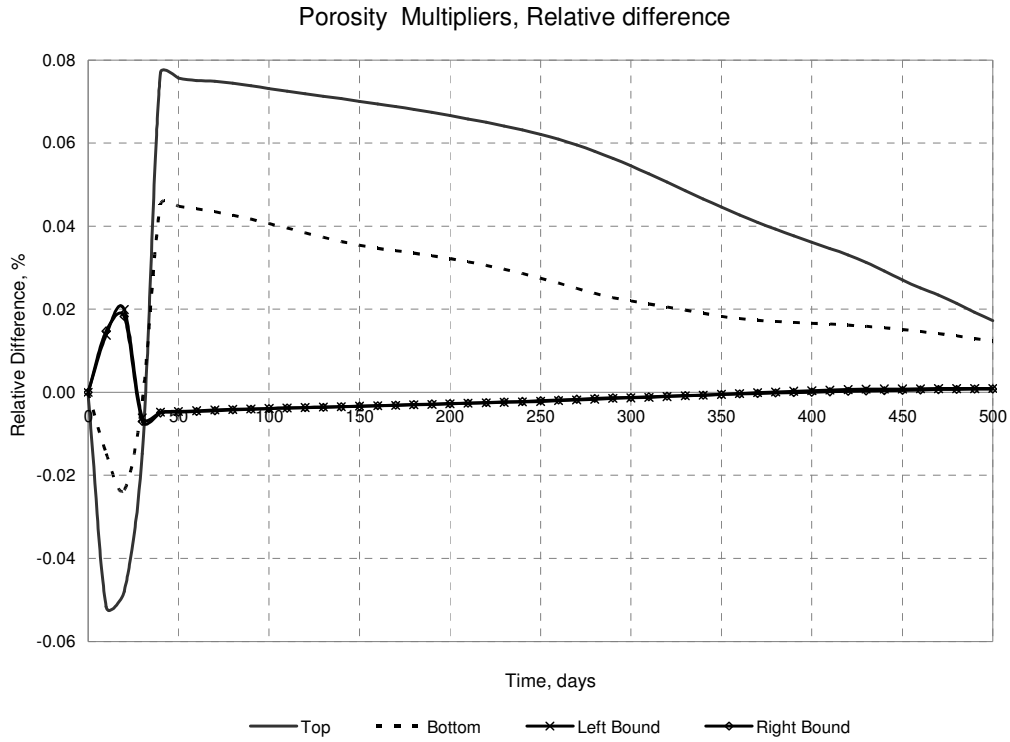

Fig. 5.6—Relative difference of porosity, in percentage, for cell at the top-center cell (ID 1150), bottom-center (ID 61), left boundary (ID 661), and right boundary (ID 671).

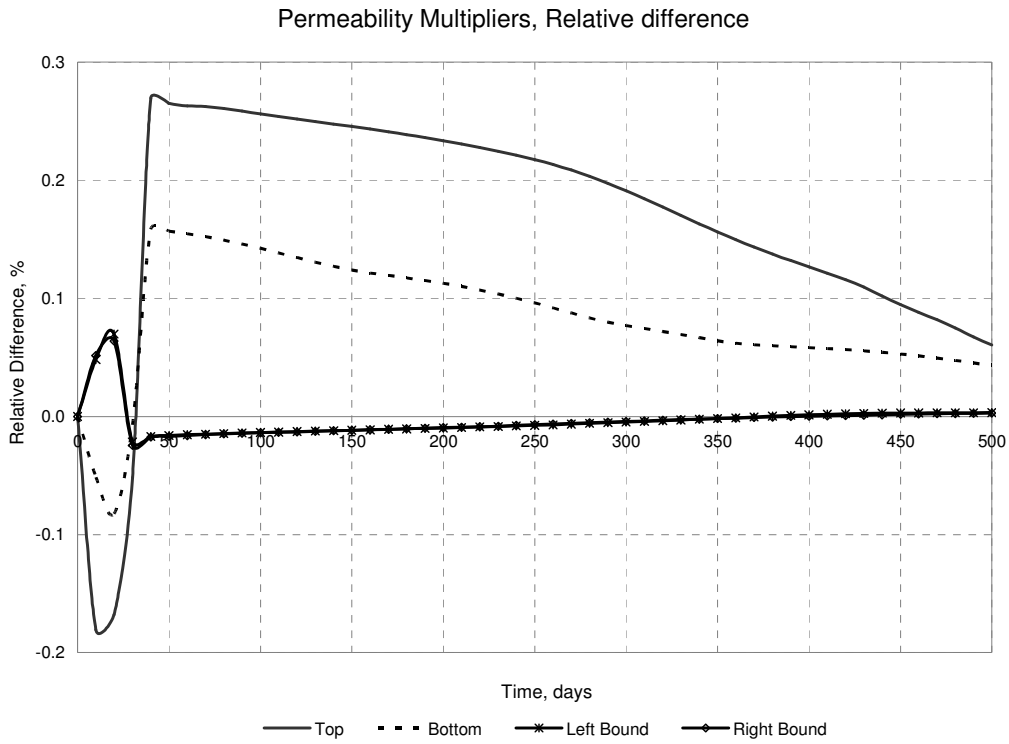

Fig. 5.7—Relative difference of permeability for cell at the top-center (ID 1150), bottom-center (ID 61), left boundary (ID 661), and right boundary (ID 671).

Table 5.1 provides the average porosity and permeability multipliers—computed for these four gridcells—that were used in the coupled cases. The average values are in agreement with what was previously stated (the permeability shows a "larger" difference). These final values are quite small, and usually, at least in practice, would be neglected. But once again, this is a simple algorithm which only takes into account an average value of the changes in porosity and permeability.

Table 5.1—Average porosity and permeability multipliers used for the four observation cells.

	Top Cell	Bottom Cell	Left Cell	Right Cell
Average porosity multiplier	1.00047	1.00024	0.99999	0.99999
Average permeability multiplier	1.00166	1.00083	0.99996	0.99996

5.1.4 Pore Pressure Profiles

5.1.4.1 Pore Pressure Profiles at Monitored Cells

The next step in the process is to obtain the pore pressures for each cell considering the new values of porosity and permeability. **Fig. 5.8** shows the pressures for the four cells used to monitor the performance for the uncoupled and coupled cases.

It can only be observed one line per figure despite that there are four cases (uncoupled and coupled cases). Since the values of the multipliers are so small, no visible difference can be observed.

Nonetheless, qualitatively analyzing the figures, two types of behavior can be observed: the ones in the vertical direction (Top and Bottom Cells), and the ones in the horizontal direction (Left Bound and Right Bound). For the former, the reservoir is in unsteady state for the first 100 days, and then it enters into pseudo-state. For the latter, the pressure drop is small during the first days. Then also enters a pseudo-steady state. This is also in agreement with the boundary conditions.

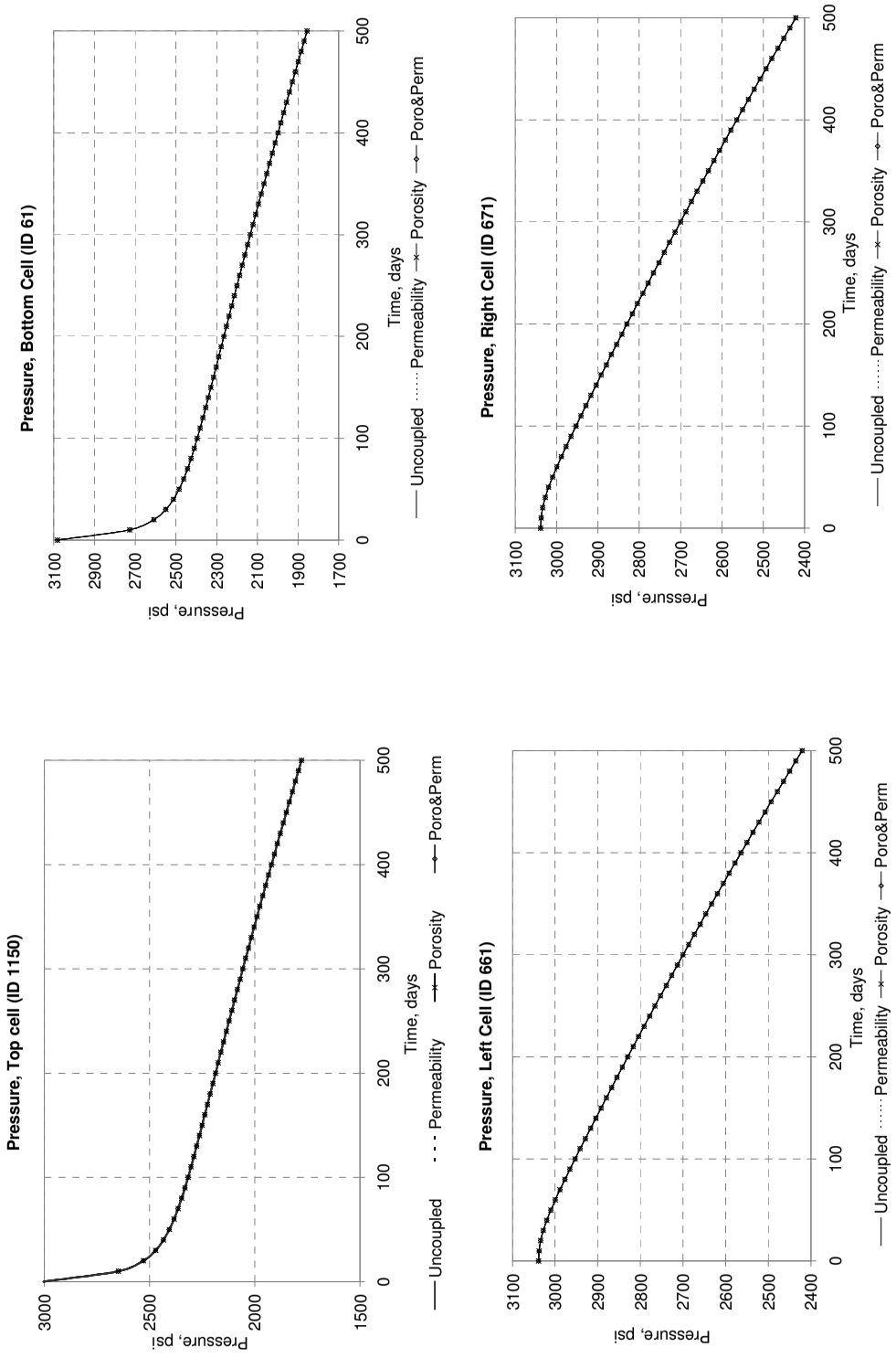

Fig. 5.8—Pore pressure profile for cells at the bottom-center (upper left), right boundary (upper right), top-center (lower left), and left boundary (lower right).

5.1.4.2 Average Reservoir Pressure Profiles

Fig. 5.9 displays the average reservoir pressure for the uncoupled and coupled cases. Additionally, the results obtained by Dean et al. (2006), referred as SPE79709, are also included to be used as benchmark.

Although the figure show a standard depletion response (i.e., the pressure is decreasing), no change is observed between the uncoupled and coupled cases. Except for the SPE79709 case, the rest of the lines overlap each other (i.e., only one line is recognized). This means that the changes in the average pressures between the uncoupled case and the coupled cases are not significant. This result was expected, considering the fact that the changes in porosity and permeability were minimal.

Dean et al. (2006) did not present the values for the case when geomechanics is ignored (i.e., the Uncoupled Case). Therefore, this is an opportunity to understand how significant the differences in the responses are when geomechanics are considered in the process.

For instance, the pressure profile matches the results of Dean et al.'s (2006) at the beginning of the run, implicating that the geomechanical effects are not immediately felt (at least not at an early stage of the run). This can allow the usage of only reservoir flow simulators, which is faster and more economically to implement, during the early stages for certain problems.

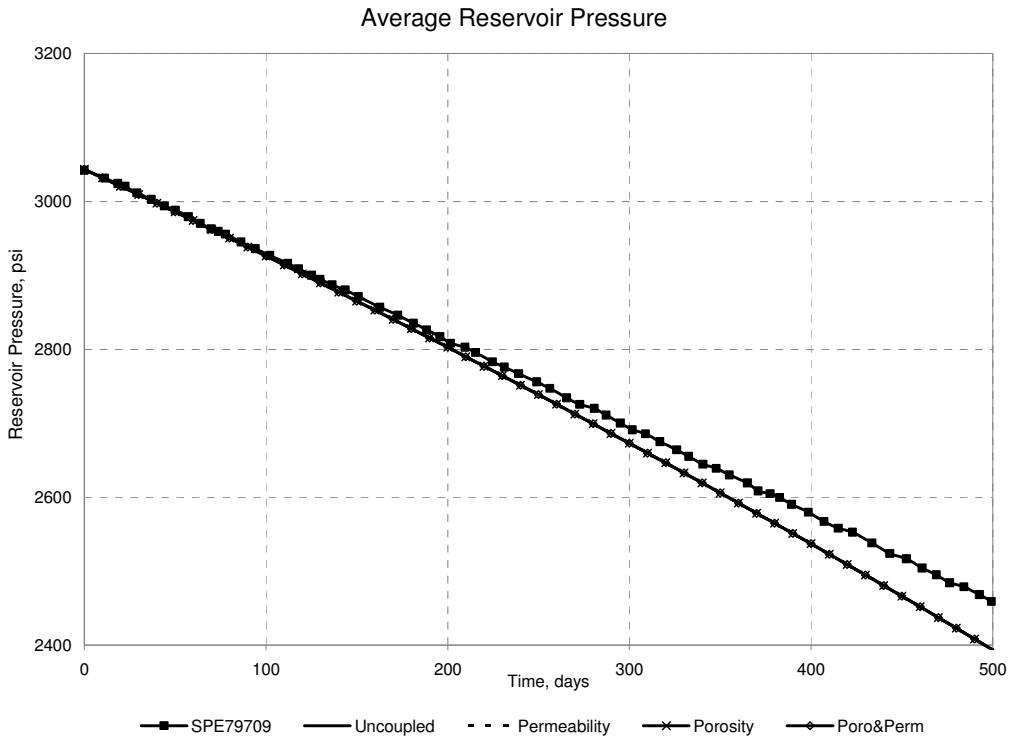

Fig. 5.9—Average reservoir pressure profile for all cases, Study Case 1.

When applying one of Dean et al.'s (2006) coupling approaches, it is clearly noted that the pressure is higher than that of the Uncoupled Case, having approximately a 2.68% difference at the end of the run. Although this quantity might look relatively small, it should be borne in mind that this problem represents a short period of time, which is rarely the case in real problems. Usually, the life of a reservoir extends for several years during the depletion phase. If secondary and/or tertiary recoveries are also considered, not only the life of the reservoir is extended but also more geomechanical factors enter to play.

Resuming the discussion about the differences between the coupled cases, although no differences can be appreciated to the naked eye, in fact, they exist. In practice, these differences are neglected. However, since the purpose of this research is to start exploring the possible impact that geomechanics may have on reservoir-flow parameters, these differences are discussed further and analyzed.

In order to appreciate the magnitude of the changes obtained from the coupled cases, the relative differences (in percentage) in relation to the Uncoupled Case are calculated and illustrated in **Fig. 5.10**.

There is a clear deviation in the Porosity Case (considering porosity as the coupling term) and Poro&Perm Case (considering porosity and permeability as the coupling terms) from the Uncoupled Case, following both of them the same trend—presenting some fluctuations that repeat in periods. These cases indicate that there is some increment in the pressure values when considering the geomechanical response, just like showed by Dean et al. (2006). Moreover, the Porosity Case presents a "larger" relative difference.

On the other hand, the Permeability Case (considering only permeability) has the closest results to the Uncoupled Case (the line runs parallel to the Uncoupled Case), having even lower values. This is an unexpected result since it was observed that permeability was the parameter with the "largest" changes when considering the volumetric strains. It would have been interesting if Dean et al. (2006) also included the changes in permeability.

Although these differences were noticed, no concrete conclusion can be drawn regarding the determination of the most influential coupling parameter. In practice, these changes are neglected and considered to be, basically, the same result, i.e. no changes.

Nevertheless, it can be stated that some deviations in the pressure profile were perceived, giving enough reasons to keep investigating the inclusion of geomechanics in streamline simulation.

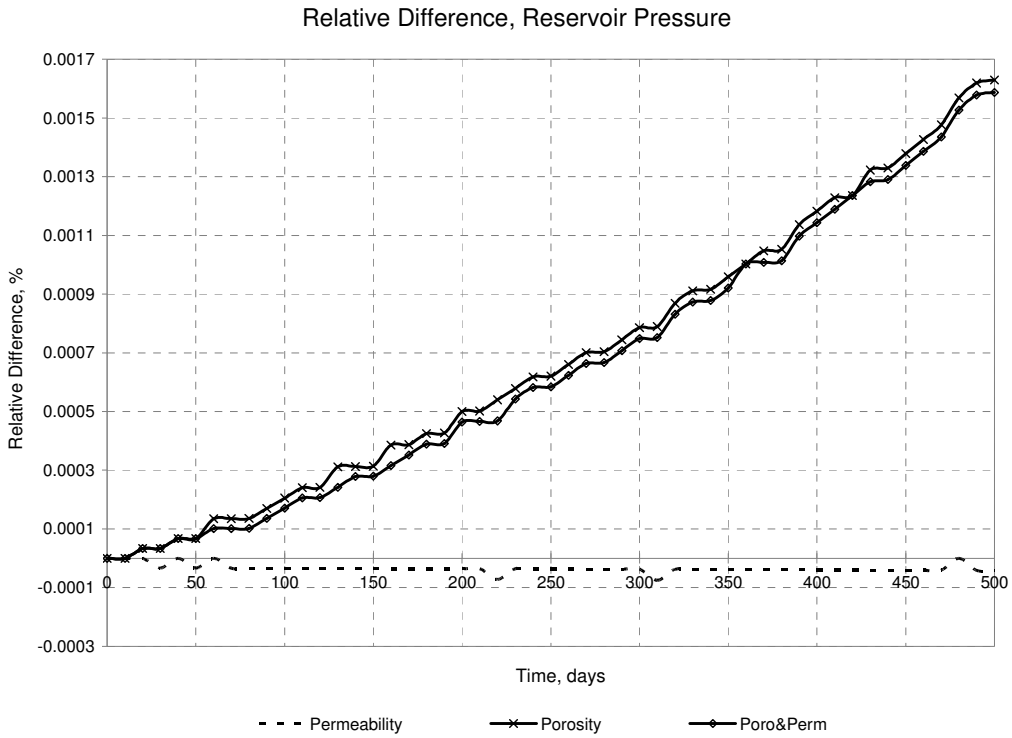

Fig. 5.10—Relative difference in reservoir pressure when compared against the Uncoupled Case, Study Case 1.

Finally, since this problem has a fixed production, there is no need to plot it (the production is the same for all the cases, uncoupled and coupled).

5.1.5 Geomechanical Parameters

Dean et al. (2006) also presented the subsidence at the top of the reservoir where the well is located. This figure is not presented here since basically there was no subsidence using the two-way approach. They calculate a subsidence of 12.2 ft after 500 days, while this approach of $5x10^{-4}$ ft.

The map of vertical stresses for the whole model is not included either because no difference is observed from the equilibrium state presented in Fig. 5.2.

5.1.6 Smaller Timesteps

Dean et al. (2006), in one of their problems (No. 3), suggest using smaller timesteps for the explicitly coupled approach in order to improve the accuracy of results. This idea was tested for this study case, using one-day timesteps.

Fig. 5.11 illustrates the average reservoir pressure profile for the uncoupled and coupled cases; no improvements are observed. It is just a reproduction of Fig. 5.9, with the only difference that this one has more points. The rest of the data obtained in the process are not presented since they are also just a reproduction of the previous figures.

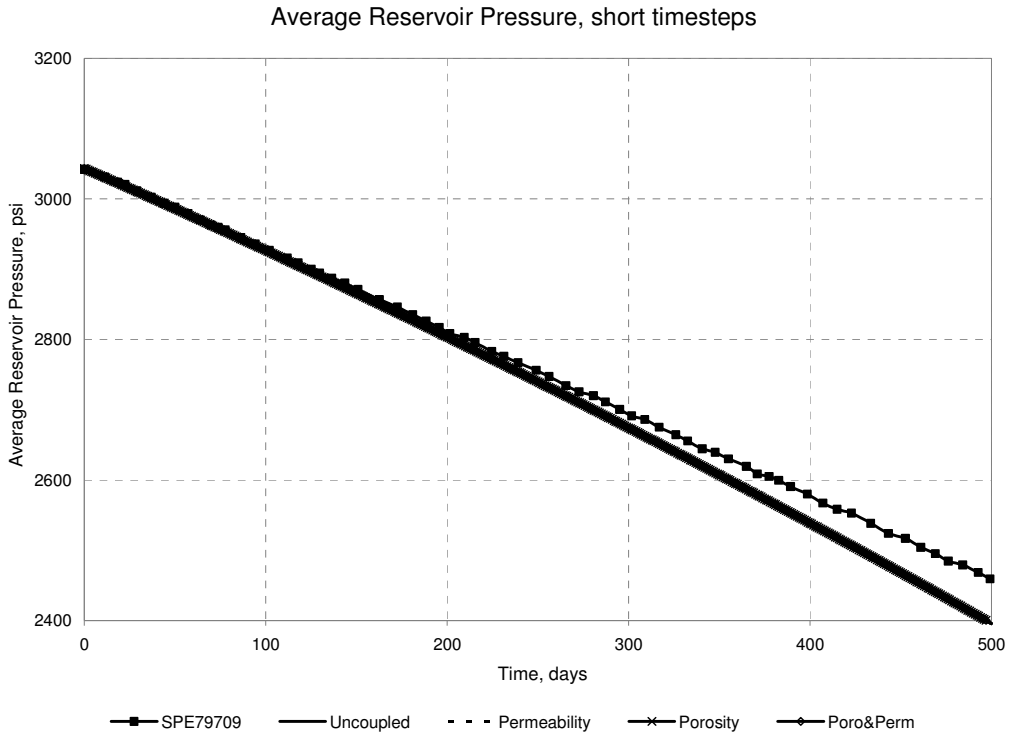

Fig. 5.11—Reservoir pressure profile for all cases, using one-day timesteps, Study Case 1.

5.1.7 Increment in Number of Gridblocks

Despite the fact that the results were somewhat expected, still another idea was tested to see if there could be an improvement: adding more gridblocks. This

was done with the purpose of testing all possibilities before drawing any final conclusions.

None of the parameters were changed in any of the models (reservoir and geomechanical), except for the number of cells: 50x50x10 (25 000 cells) with 44x44x20 ft. **Fig. 5.12** shows the model built in FLAC3D.

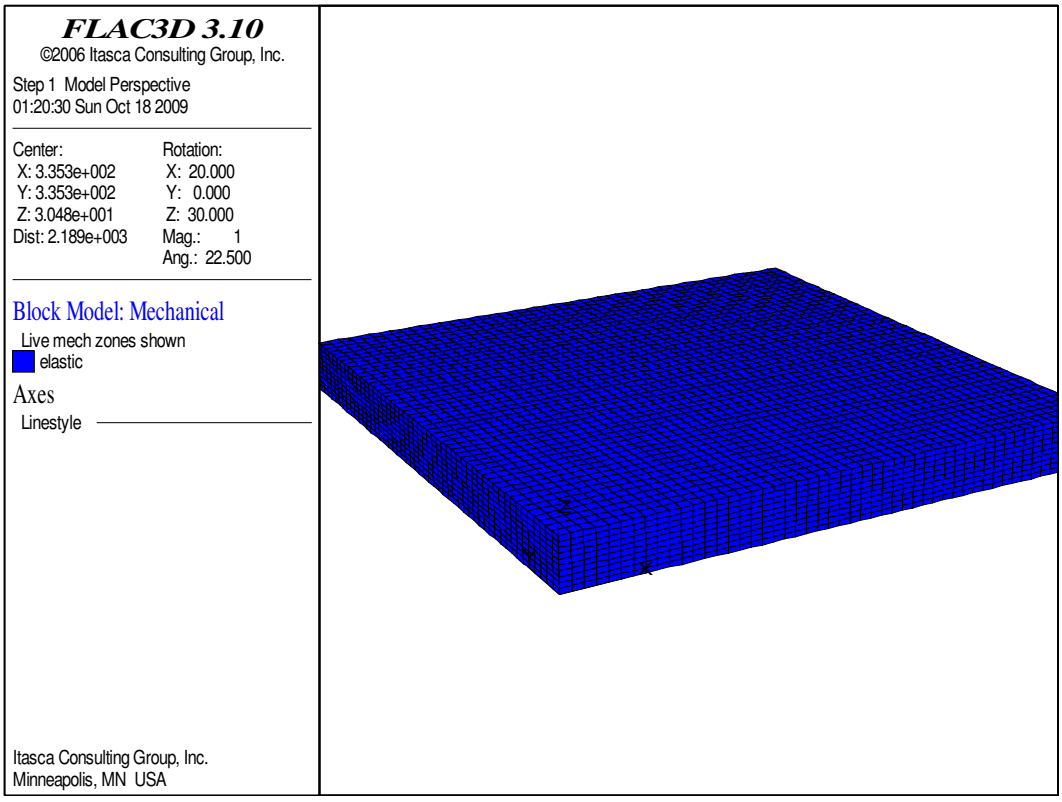

Fig. 5.12—Study Case 1, with more gridblocks.

Fig. 5.13 illustrates the average reservoir pressure; no improvement is observed. Moreover, the simulation time increased considerably, because of the increment in gridblocks [a large portion of the computational time can be spent in geomechanical calculations (Dean et al. (2006)].

Adding more cells not always justifies the consumption of computational resources, as demonstrated in this study case.

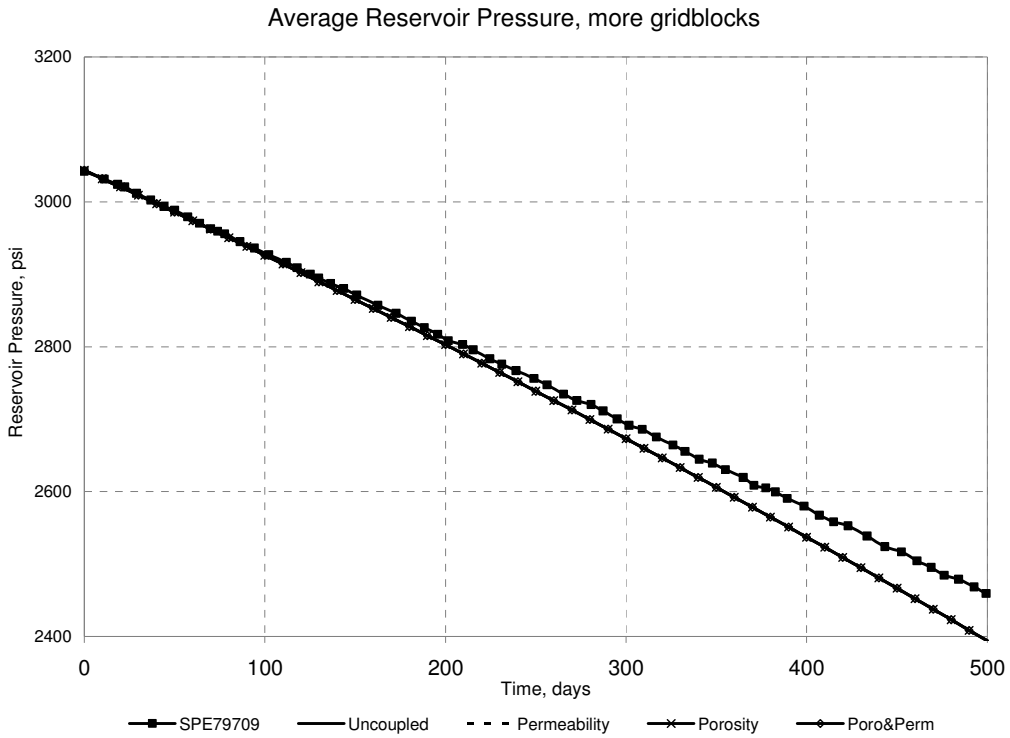

Fig. 5.13—Reservoir pressure profile for all cases, using more gridblocks, Study Case 1.

5.1.8 Simulation Time

This subsection presents, **Table 5.2**, the simulation elapsed time run for the Uncoupled Case; the coupled cases using 10-day timestep; the coupled cases using 1-day timestep; and the coupled cases using more gridblocks.

The 10-day coupled simulation is one order of magnitude faster than the 1-day coupling simulation, and two orders of magnitude "slower" than the uncoupled simulation. On the other hand, the coupling simulation using more gridblocks is two orders of magnitude larger than the 10-day coupled simulation, making it clear that geomechanical calculations consume most of the computational resources in a coupled approach.

It can also be seen that the relationship in computational time is not linear. The time simulation increases much more when incrementing the number of cells in the model than when incrementing the number of timesteps.

Consequently, prior to conducting a study it should be determined if the coupling approach will represent a significant advantage, since time will be sacrificed. However, it is rare to be able to determine this *a priori*.

Table 5.2—Comparison of total elapsed time runs among different simulations, in seconds.

FrontSim (s)	FrontSim-FLAC^{3D} (s) 10-day timestep	FrontSim-FLAC^{3D} (s) 1-day timestep	FrontSim-FLAC^{3D} (s) More gridblocks
5.3984	3.0242e2	4.1108e3	5.8478e5

5.2 Study Case 2

The whole process is illustrated once again (volumetric strains, permeability and porosity multipliers, and pore pressures), but this time to compare if the performance of the two-way approach is the same as with Case Study 1.

Six cells are monitored: two at the top, where the wells are [Top Inj (ID 62 451) and Top Prod (ID 60 050)]; two at the bottom, where the wells are [Bottom Inj (ID 2451) and Bottom Prod (ID 50)]; and two at the boundaries [Left Bound (ID 33 751) and Right Bound (ID 33 800)] of the model.

Since this model has no benchmark (it was not based on a previous study), the comparison is basically made between the uncoupled and coupled cases. But as was learned from Study Case 1, results are carefully handled, and not considered to be 100% accurate. They are just considered to be a possible guide of what the real results might look like.

Pore pressure, and oil and water production rates are used as parameters of comparison between the Uncoupled and coupled cases (Permeability Case, Porosity Case, and Poro&Perm Case).

Subsidence is not analyzed since there is no way to compare it with another similar problem and verify if the results are accurate or not, or at least if they follow the trend. This study case does not tackle

In view of the fact that no improvement was gained when increasing the number of timesteps, nor the number of gridblocks, this study case does not deal with these issues, especially because it already has a large number of cells, and the wells do not change conditions. One of the advantages of using streamline simulation is that it can take longer timesteps, reducing the simulation time, especially when fluids are incompressible, and wells do not change conditions, which is the case. In fact, the original data set just had one timestep of 10 years.

5.2.1 Geomechanical Equilibrium (Preliminary Phase)

As the input data was a little bit more complicated than that of Study Case 1, equilibrium could not be established right from the beginning, i.e. directly in the file. The geomodel was run for equilibrium; to verify it, the histories of the maximum unbalanced force and z-displacements of the selected cells were plotted, **Figs. 5.14** and **5.15**.

In Fig. 5.15, the boundary cells (Left Bound and Right Bound) are not included because the graphs are blank, indicating that they were in equilibrium right from the beginning.

It is observed that the maximum unbalanced force approaches to a small value, and the displacements histories become constant (at the end of the run), indicating that an equilibrium state has been reached after the run.

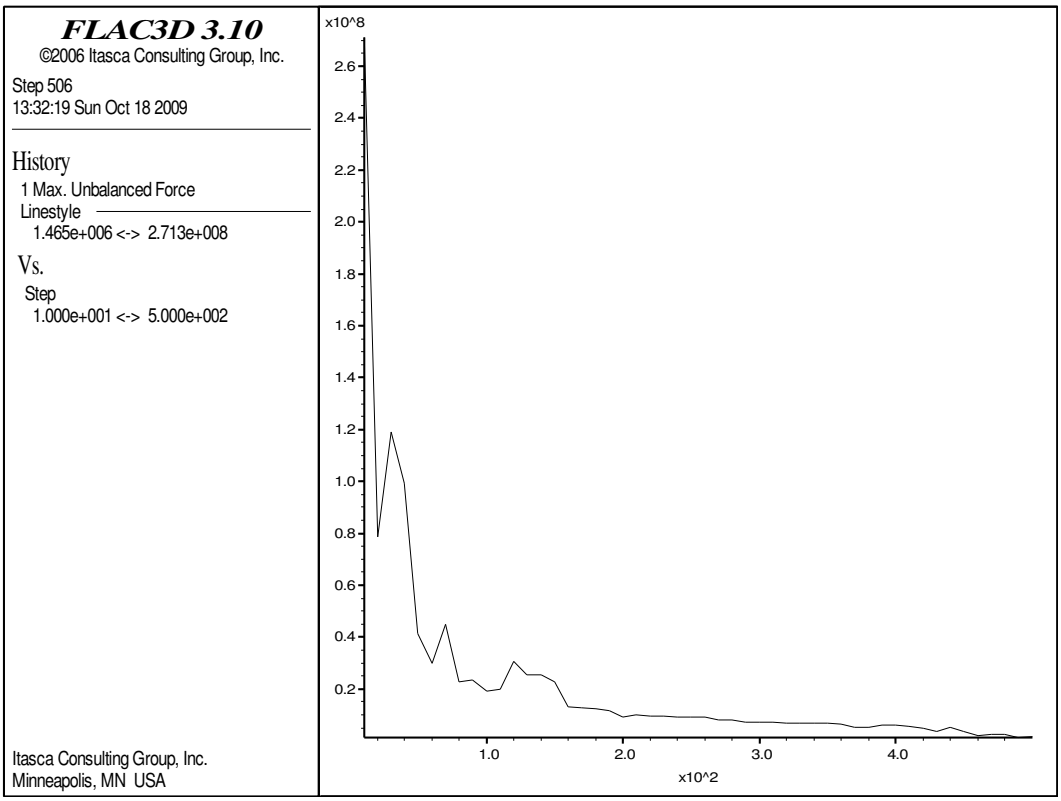

Fig 5.14—Maximum unbalanced force, Study Case 2.

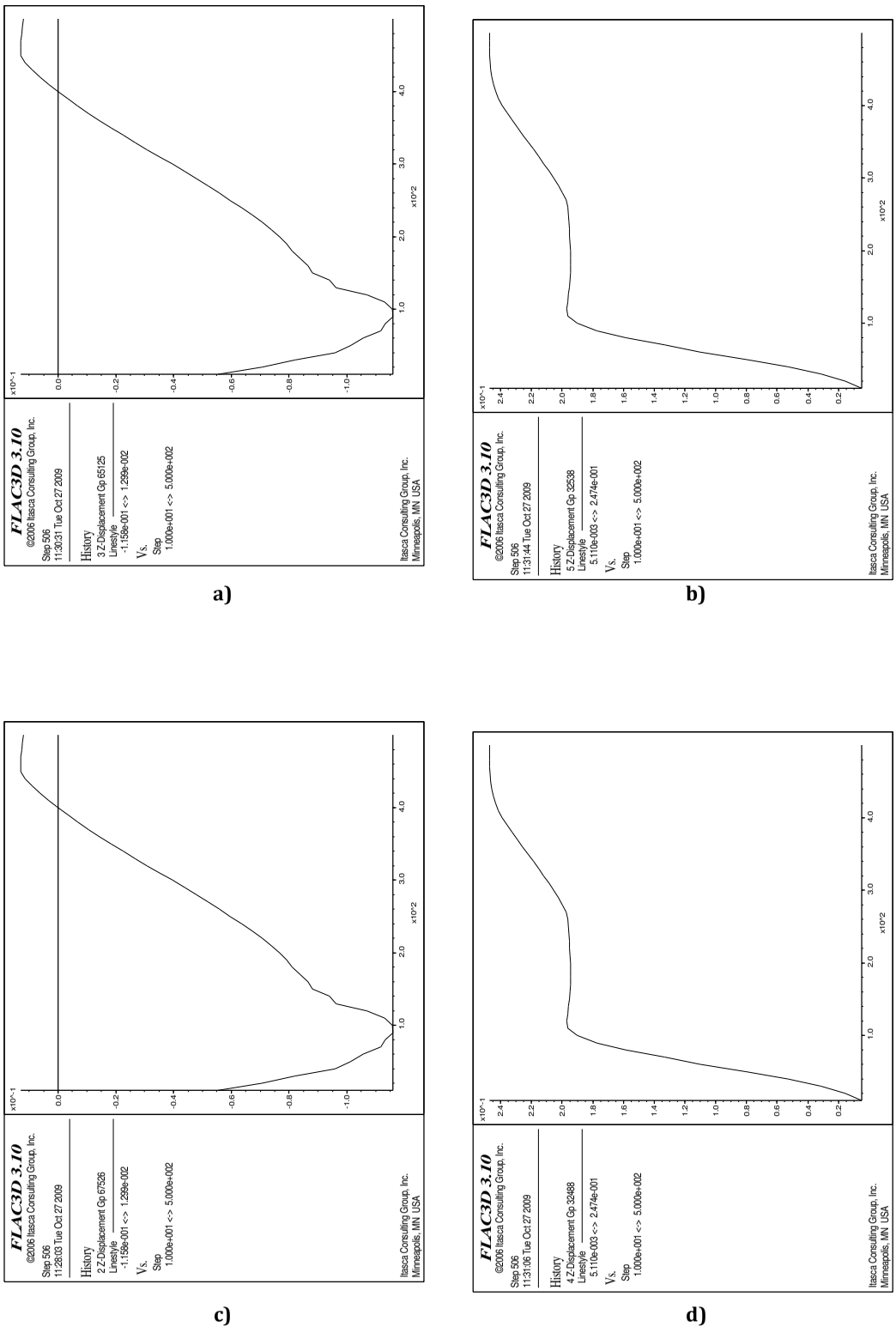

Fig 5.15—Z-displacements after equilibrium run, evaluated at gridpoints a) 65 125, surrounding Cell 60 050; b) 198, surrounding Cell 50; c) 67 526, surrounding Cell 62 451; and d) 5000, surrounding Cell 2451.

Fig. 5.16 displays the shear strains for the six cells. Although the same geomechanical parameters were used as in Study Case 1, it can be observed that they have non-zero values (another indicator that is a more elaborated problem). If the values of the shear stresses are 1% of the normal stresses, it is considered to be in equilibrium. The minus signs for the normal stresses indicate compression.

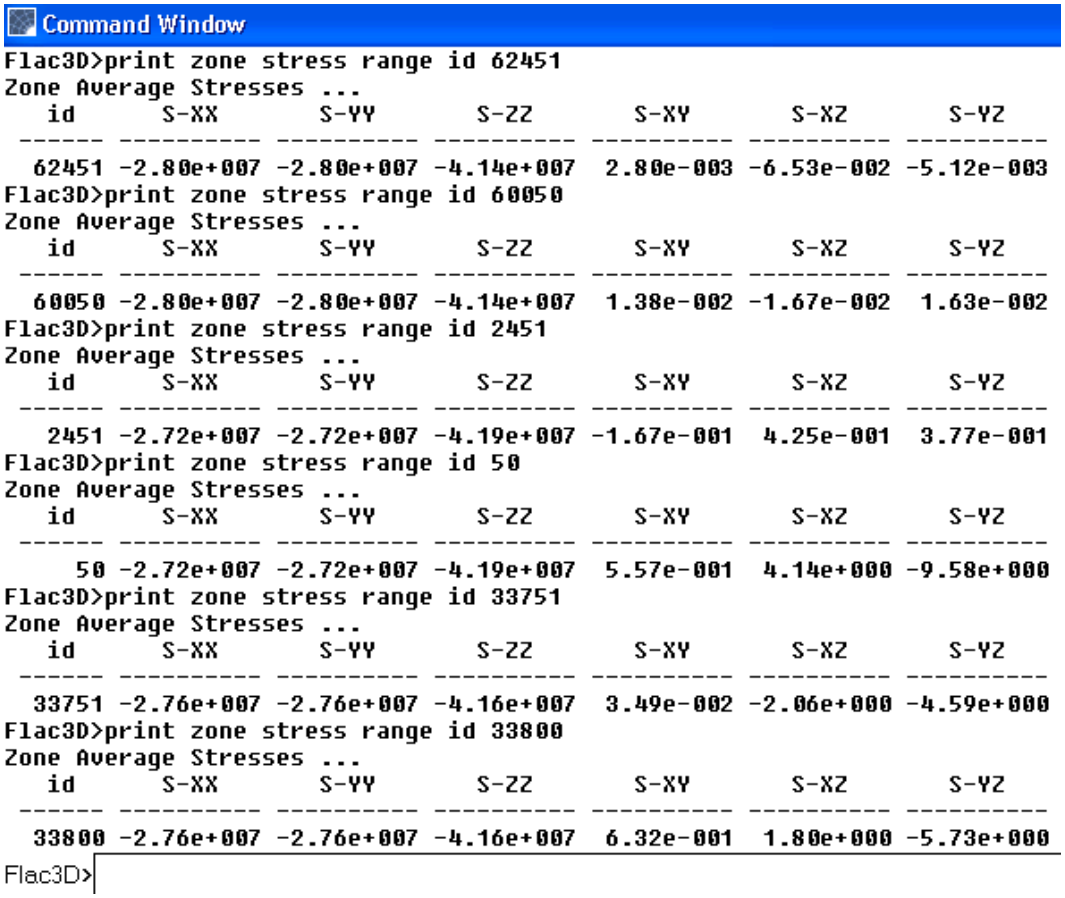

Fig 5.16—FLAC^{3D} results showing no shear stresses, S-XY, S-XZ, S-YZ, at the top (IDs 62 451 and 60 050), bottom (IDs 2451 and 50), and boundaries (IDs 33 751 and 33 800) of the geomodel, Study Case 2.

Finally, the initial vertical effective stresses were also plotted, **Fig. 5.17**, to check the equilibrium state. Due to the number of cells, the resolution got affected, but it can still be appreciated each layer has a different constant value, having the largest value at the bottom, indicating equilibrium.

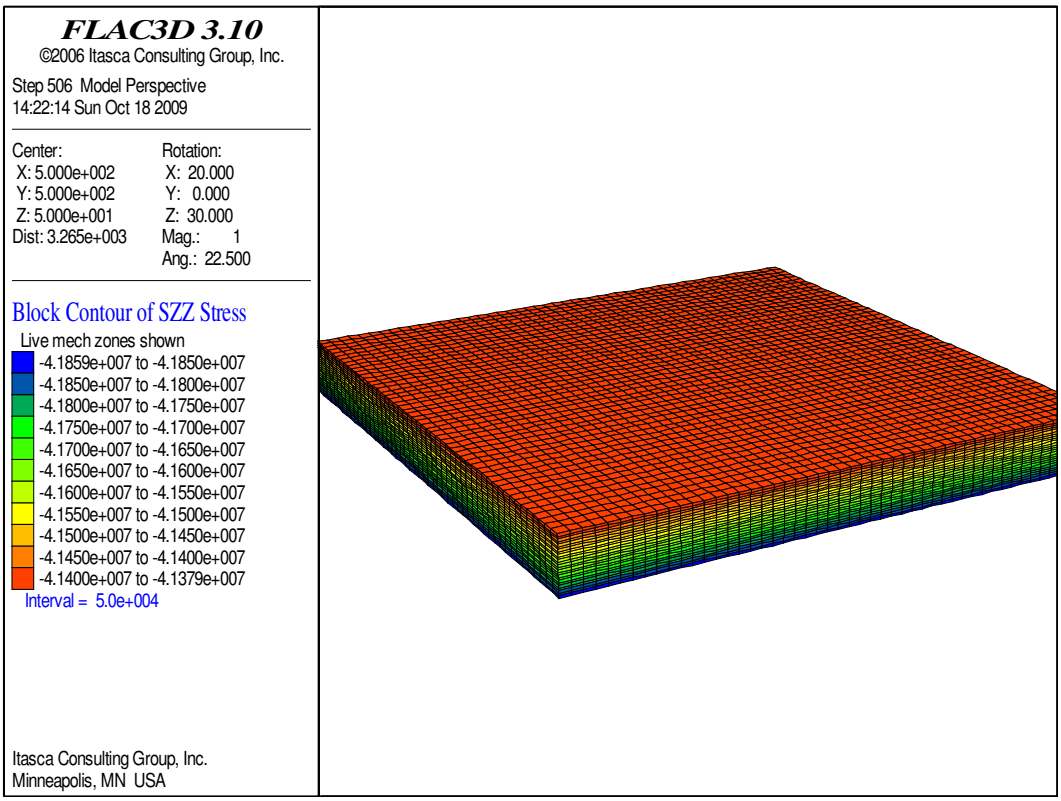

Fig. 5.17—Initial vertical stress in after equilibrium run, Study Case 2.

5.2.2 Volumetric Strains

After the complete run of the Uncoupled Case, the volumetric strains were calculated by FLAC3D after considering the pore pressures as external loads for each timestep. **Fig. 5.18** shows the volumetric strains for the six cells.

Again, the six cells can be divided into three groups according to the behavior they display: Top (Top Inj and Top Prod), Bottom (Bottom Inj and Bottom Prod), and Boundary (Left and Right Bound).

Except for the boundaries, which are almost constant and equal to zero, the behavior displayed by the cell is completely different from the one observed for Study Case 1; it is a "mirror" figure. The Top group decreases at a constant rate up until 500 days; then, there is a small bump, and then it has a constant value of -0.009 until the end of the simulation. On the other hand, the Bottom group has the opposite be-

havior; it increases at a constant rate up until 500 days; then, there is a small bump, and then it has a constant value of 0.009 until the end of the simulation.

This means that the Top group decreases its relative volume, while the Bottom group increases its relative volume.

It is also important to indicate that the scales of the graphs of the two study cases (for this parameter) are different by two orders of magnitude, revealing that more mechanisms enter into play when considering injection.

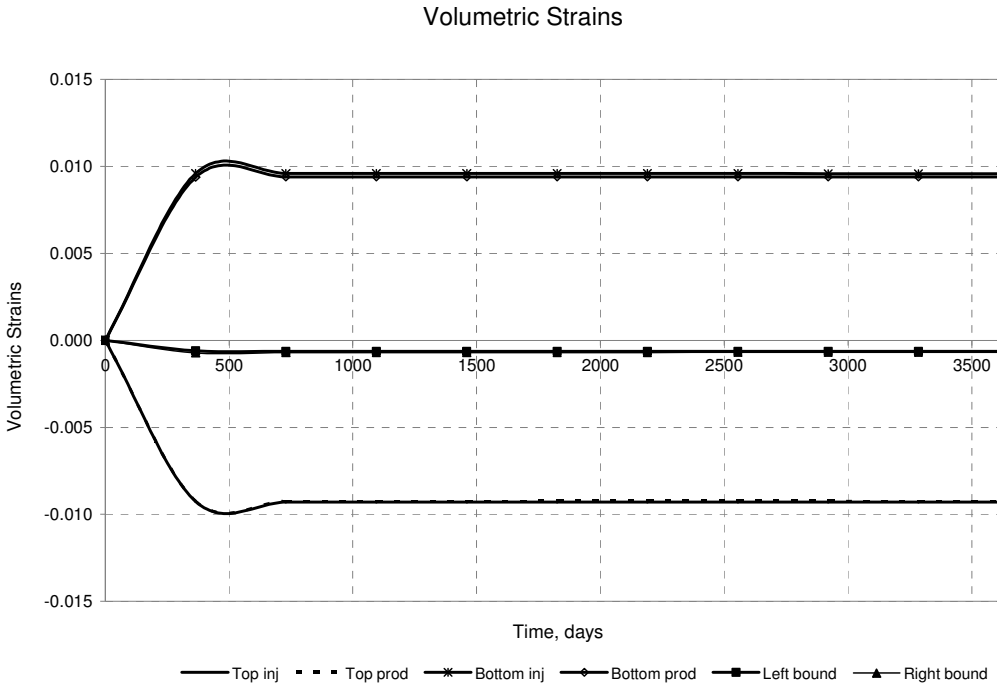

Fig. 5.18—Volumetric strain profile for cell at the top corner cell where injector is (ID 62 451); top corner where producer is (ID 60 050); bottom corner cell where injector is (ID 2451); bottom corner where producer is (ID 50); left boundary (ID 33 751), and right boundary (ID 33 800).

5.2.3 Porosity and Permeability Multipliers

Figs. 5.19 and **5.20** present the calculated porosity and permeability multipliers, respectively, for each timestep for the six cells. As expected, the graphs present the same behavior as that of the volumetric strains.

The scale of the graphs is also larger than that of Study Case 1, suggesting that the magnitude of the changes is problem-dependent.

Because of the formulas that were used, the variation in permeability is greater than the variation in porosity.

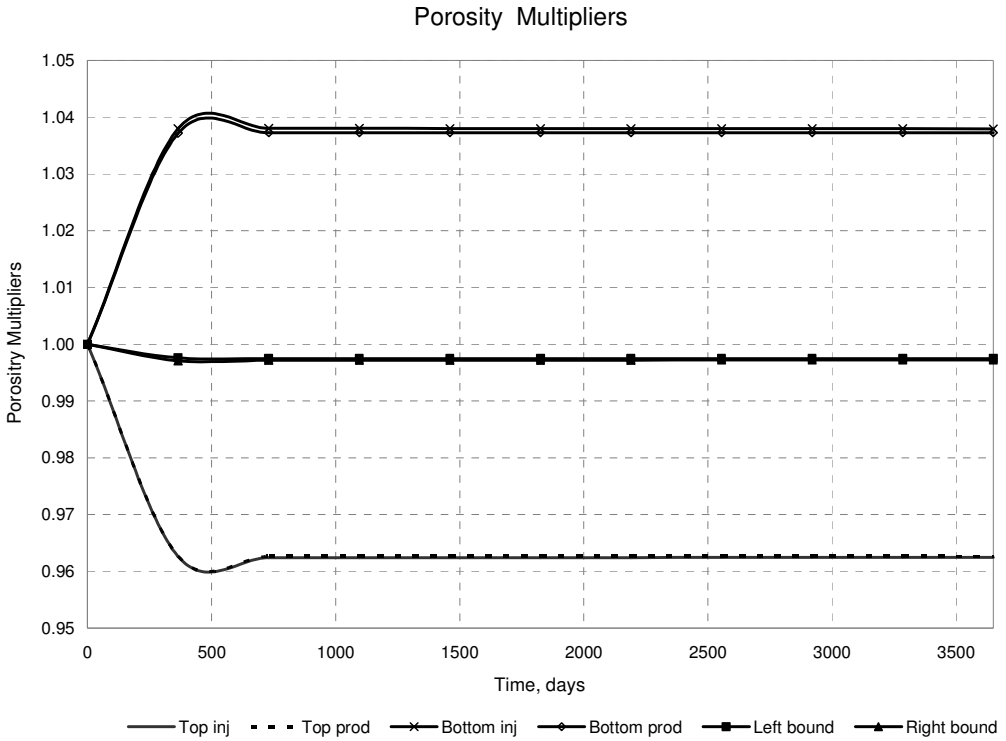

Fig. 5.19—Porosity multipliers profile for cell at the top corner cell where injector is (ID 62 451); top corner where producer is (ID 60 050); bottom corner cell where injector is (ID 2451); bottom corner where producer is (ID 50); left boundary (ID 33 751), and right boundary (ID 33 800).

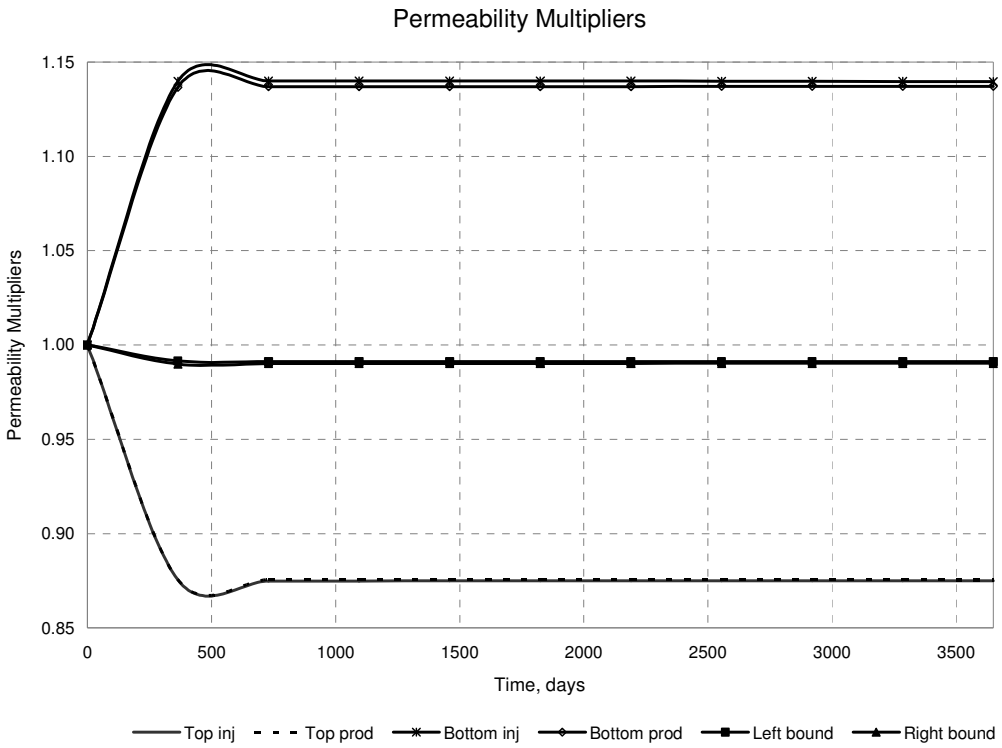

Fig. 5.20—Permeability multipliers profile for cell at the top corner cell where injector is (ID 62 451); top corner where producer is (ID 60 050); bottom corner cell where injector is (ID 2451); bottom corner where producer is (ID 50); left boundary (ID 33 751), and right boundary (ID 33 800).

Table 5.3 provides the average porosity and permeability multipliers—computed for these six gridcells—that were used in the coupled cases. The average values are in agreement with what was previously stated (the permeability shows a "larger" difference). These final values are definitely larger than those of Study Case 1; it should be expected to see some changes in pore pressure (as it will be seen in the next subsections).

Table 5.3—Average porosity and permeability multipliers used for the six observation cells, Study Case 2.

	Top Inj	Top Prod	Bottom Inj	Bottom Prod	Left Bound	Right Bound
Average porosity multiplier	0.96587	0.96603	1.03454	1.03386	0.99772	0.99745
Average permeability multiplier	0.88640	0.88692	1.12718	1.12457	0.99203	0.99109

5.2.4 Pore Pressure Profiles

5.2.4.1 Pore Pressure Profiles at Monitored Cells

Although the changes in porosity and permeability multipliers are larger than in the previous study case, still just one line can be distinguished for the different subcases (uncoupled and coupled). They are presented in **Appendix F**.

5.2.4.2 Average Reservoir Pressure Profiles

Fig. 5.21 displays the average reservoir pressure profile for the coupled and uncoupled cases.

Although the monitored cells did not reveal any change throughout the simulation for the coupled and uncoupled cases, the average reservoir pressure reveals a deviation from the Uncoupled Case. The difference is not too big, but still can be appreciated to the naked eye. As suspected, these changes were perceived only after longer time was simulated.

For most of the period simulated, the four subcases (Permeability, Porosity and Poro&Perm) present the same behavior. However, approximately at 2190 days, the four cases deviate from each other, having the Porosity Case the greatest value of pore pressure at the end of the run, whereas the Permeability Case has the lowest value. It should also be mentioned that the Permeability and Poro&Perm cases have lower values than the Uncoupled Case.

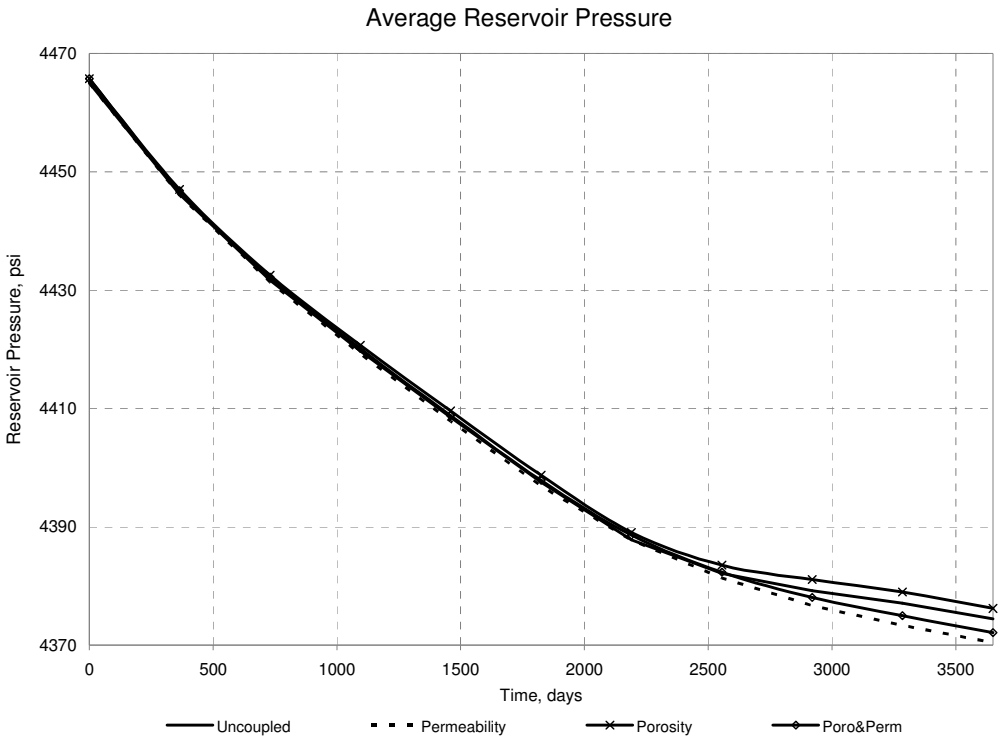

Fig. 5.21—Average reservoir pressure profile for all cases, Study Case 2.

In order to appreciate the magnitude of the changes obtained from the coupled cases, the relative differences (in percentage) in relation to the Uncoupled Case are calculated and illustrated in **Fig. 5.22**. Although the changes do not surpass the 0.11%, there is still a deviation from the Uncoupled Case.

The behavior the graphs present is certainly strange. Although different for each case, up until 1825 days, the three coupled cases present a stable behavior. After this period, they enter a “transition” period (from 1825 to 2555 days), and finally exhibit another stable behavior almost until the end of the run simulation. This demonstrates once again that the geomechanical response is case dependant.

This "strange” behavior can be better explained when production is analyzed (next subsection).

As previously stated, the Porosity Case calculates a higher pore pressure than the Uncoupled Case for the entire simulation run, where as the Permeability Case

calculates a lower pore pressure; the Poro&Perm Case registers values between these two. Following this line of reasoning, this behavior is similar to the one presented by Study Case 1. Nevertheless, this time the Poro&Perm Case presents a similar behavior to that of the Permeability Case, instead of the Porosity Case, as was seen in Study Case 1.

Considering these two study cases, it seems that the Poro&Perm Case reproduces the behavior of one of the other two coupled cases (Porosity or Permeability), depending on which one has the strongest influence. Study Case 1 was homogeneous (Poro&Perm "ran" parallel to the Porosity Case), whereas Study Case 2 is heterogeneous (Poro&Perm "ran" parallel to the Permeability Case).

It also seems that the Poro&Perm Case registers values that are between the results obtained by the other two coupled cases, as if porosity and permeability have counter effects. However, it would be too bold to affirm that this applies to all cases. More study cases need to be analyzed.

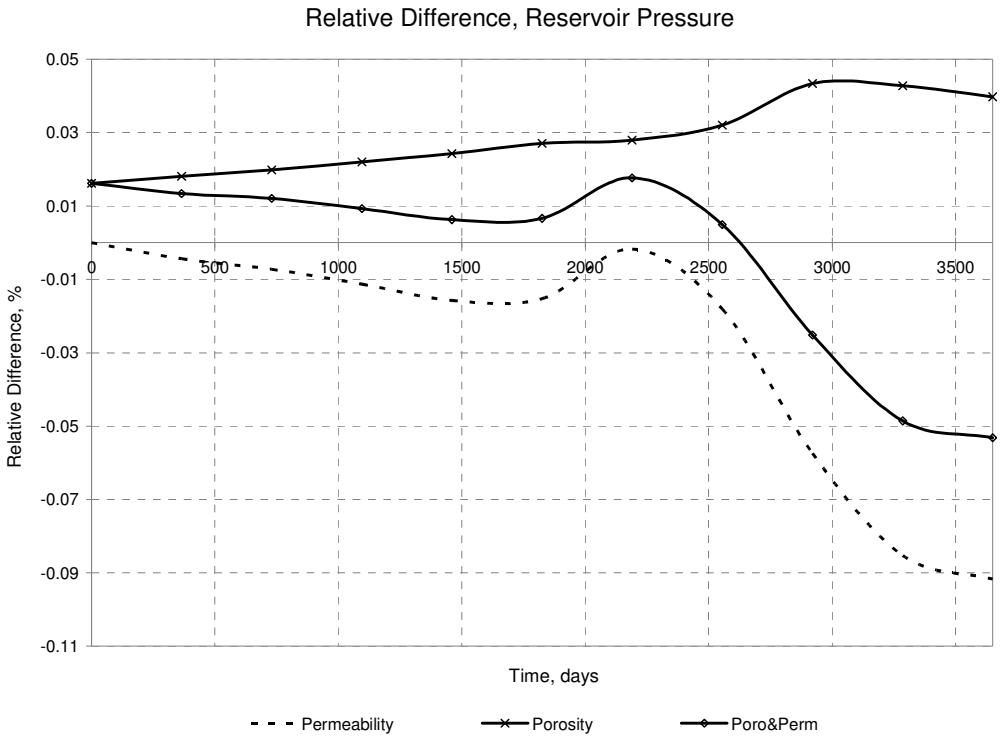

Fig. 5.22—Relative difference in reservoir pressure when compared against the Uncoupled Case, Study Case 2.

5.2.5 Production Data

5.2.5.1 Oil Production

Fig. 5.23 illustrates the field oil production rate (which is the same as the well oil production rate since there is only one producer), and cumulative oil production. For both graphs, it can be indentified only one line (although there are four cases presented) up until approximately 1825 days.

After this period, production rate starts declining, and the three coupled cases (for both graphs) deviate from the Uncoupled Case, following different "paths", at least until the 3285th day.

When analyzing oil cumulative production, the changes are not that noticeable for this period.

Although Study Case 2 is also a simple problem, larger changes can be appreciated when compared with Study Case 1. This is most likely due to the fact that more mechanisms enter to play (injection and production of another fluid).

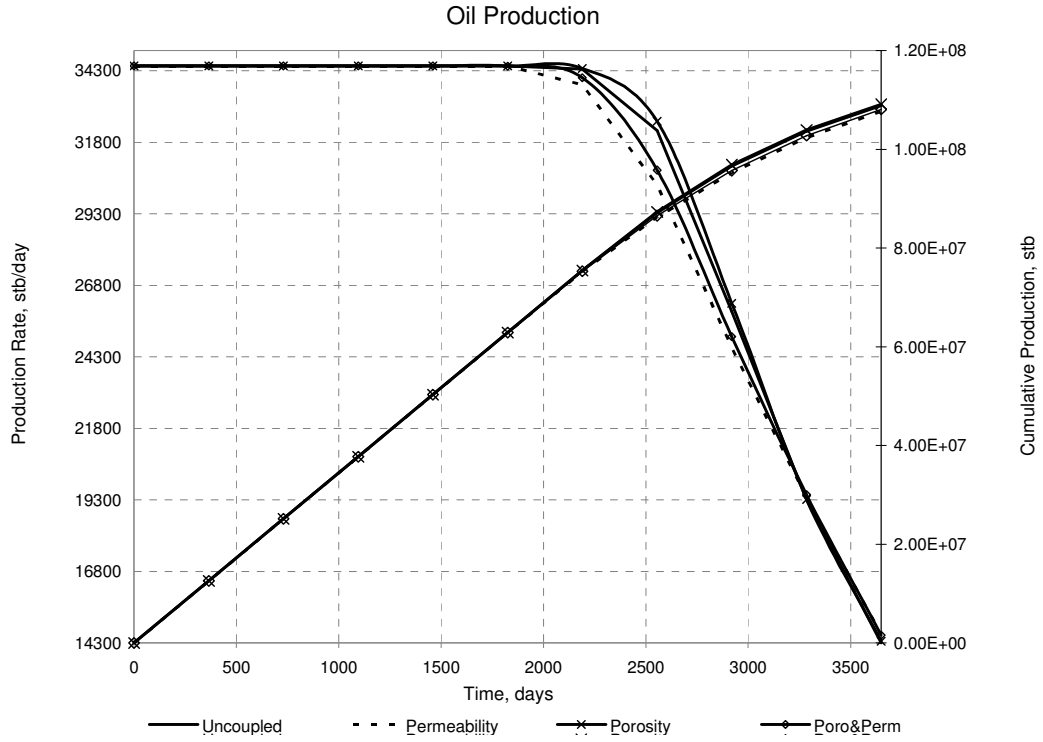

Fig. 5.23—Field oil production rate and cumulative oil production, Study Case 2.

The percentage relative difference between the Uncoupled and Coupled cases is also presented for oil production rate and cumulative oil production, **Fig. 2.24** and **2.25**, respectively, in order to perceive the magnitude of the changes.

It is clearly seen that the four cases produce the same amount of oil and at the same rate until 1825 days. Then the transition period is observed for both graphs, where the Permeability and Poro&Perm Cases register a lower production and a lower rate than that of the Uncoupled Case.

It is also noticed that after the transition period, oil production rate for the Permeability and Poro&Perm cases is larger than that of the Porosity Case, meaning that Permeability Case do not always underperform.

As for the cumulative oil production, it can be seen that Permeability and Poro&Perm cases start having a smaller differences from the Uncoupled Case after the transition period. The Porosity Case, although it decreases after the transition period, it still predicts a larger production from that of the Uncoupled Case.

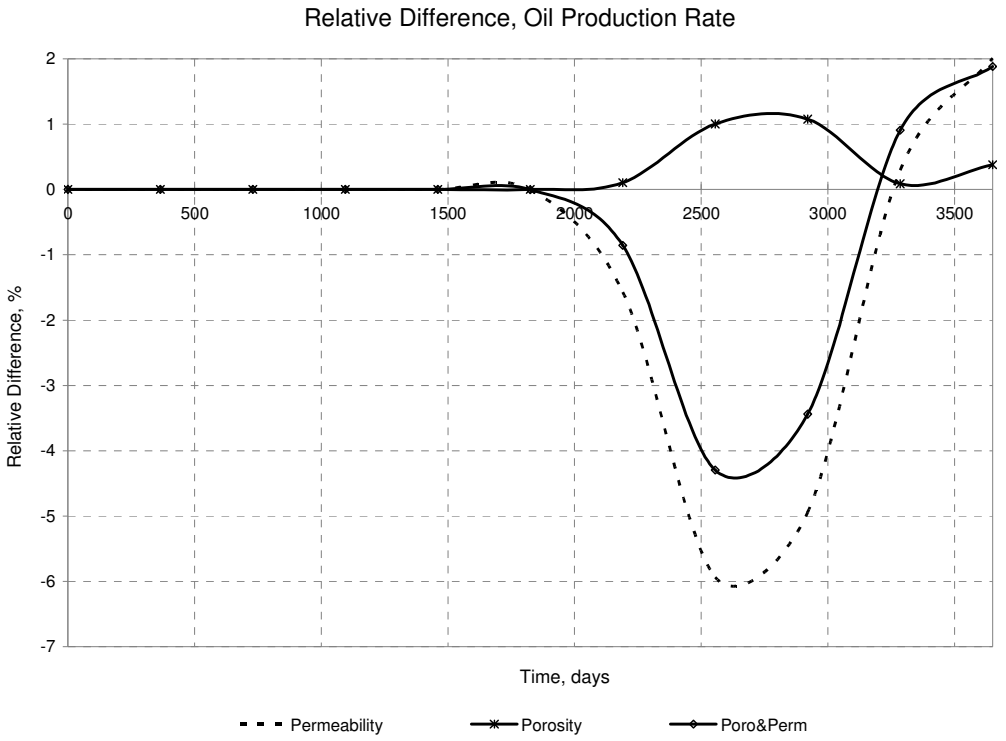

Fig. 5.24—Relative difference in oil production rate when compared against the Uncoupled Case, Study Case 2.

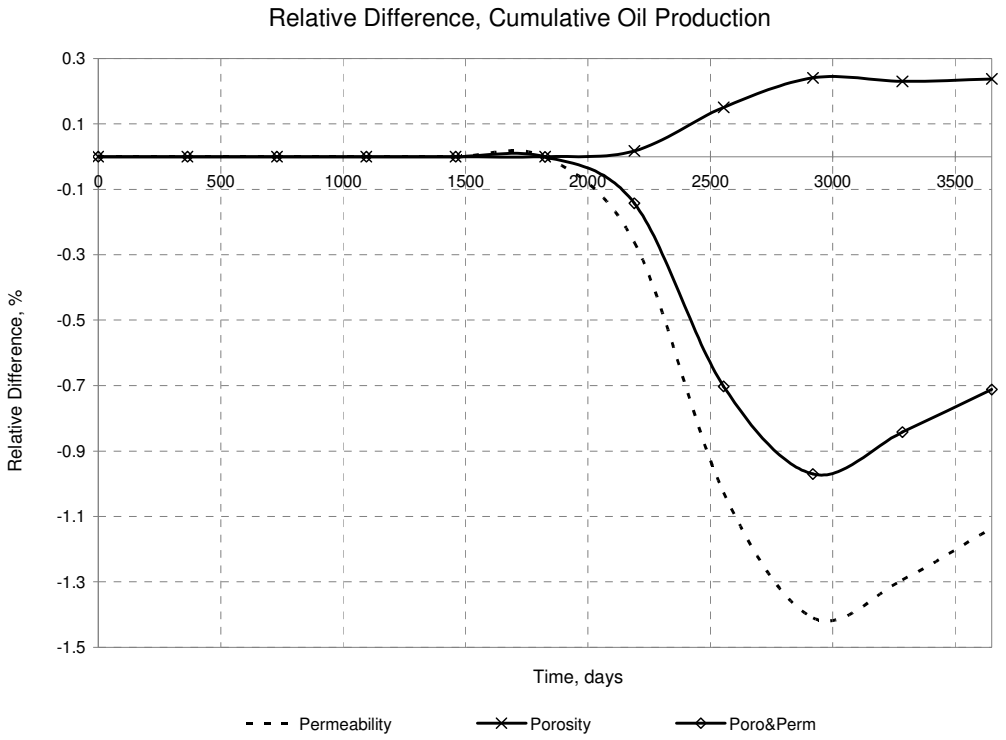

Fig. 5.25—Relative difference in cumulative oil production when compared against the Uncoupled Case, Study Case 2.

5.2.5.2 Water Production Rate

Fig. 5.26 illustrates the field water production rate, which is the same as the well water production rate since there is only one injector. This figure in particular might be the one that explains the behavior of all the previous figures.

The reservoir does not produce water up until 1825 days. This is the same for all uncoupled and coupled cases (just one line is observed). After this period, while oil production starts declining, water production starts increasing and keeps this way until the end of the simulation run. It can be seen that three coupled cases deviate from the Uncoupled Case during the transition period, and then converge again at day 3285 of the run. This behavior is seen, one way or the other, in the previous figures, indicating that water injection has a strong influence in the process.

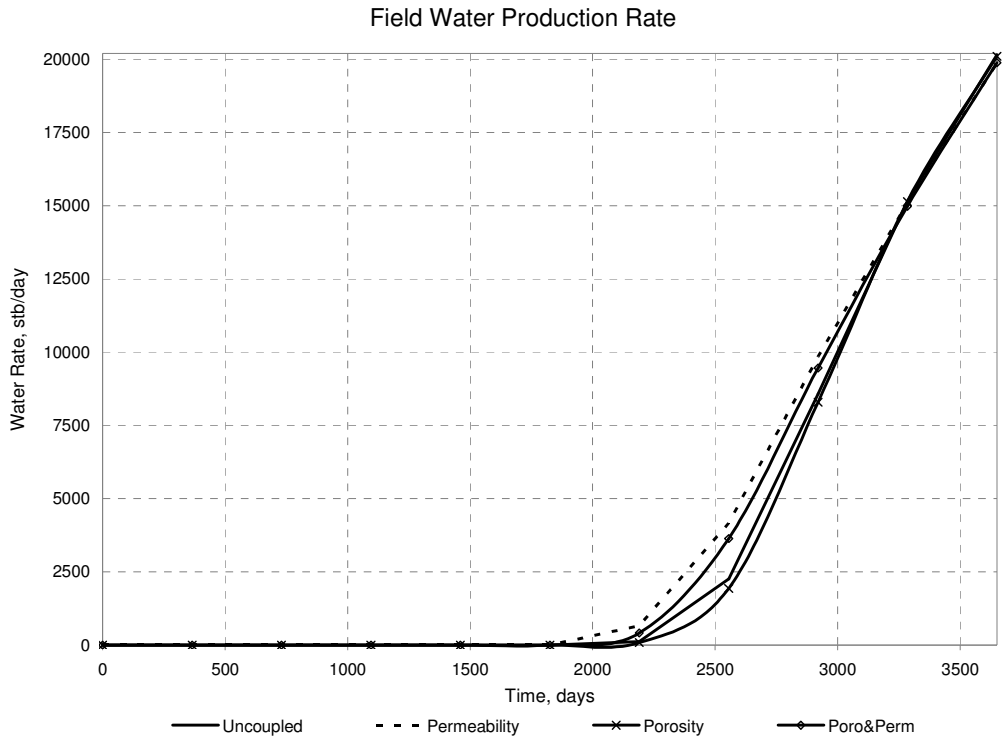

Fig. 5.26—Field water production rate, Study Case 2.

Fig. 2.27 presents the percentage relative difference, when comparing the Uncoupled Case with the coupled case.

It is observed that Permeability and Poro&Perm Cases predict a larger production rate, explaining why in predicts a smaller oil production. The scale of the y-axis should be qualitatively considered. The percentage is so high due to the small values that are handled. For example, it the original value is 0.15 STB/D, a new value of 2.205 STB/D has a relative difference of 1380%.

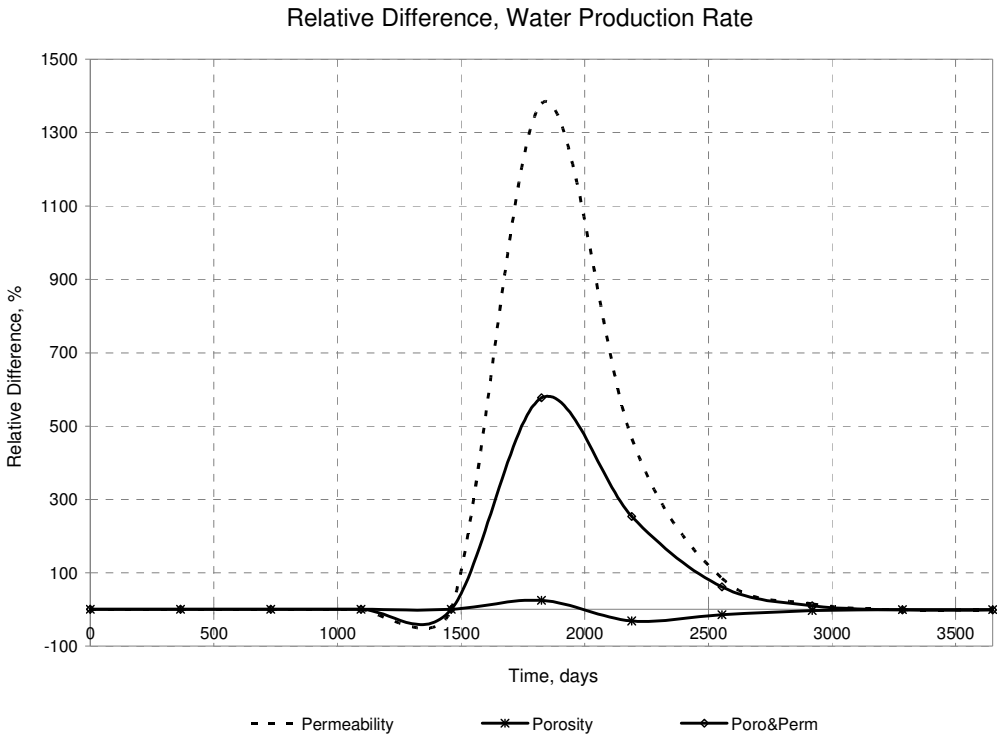

Fig. 5.27—Relative difference in water production rate when compared against the Uncoupled Case, Study Case 2.

5.2.6 Simulation Time

This subsection presents the simulation elapsed time run, **Table 5.4**, for the Uncoupled and coupled cases. It is corroborated that the geomechanical calculations consume much of the computational resources, taking most of the time of the simulation run.

Table 5.4—Comparison of total elapsed time runs among different simulations, in seconds, Study Case 2.

FrontSim (s)	FrontSim-FLAC^{3D} (s)
82.4920	1.1493e5

6
Conclusions

This research developed a two-way explicit approach for coupling streamline-based reservoir flow simulation and geomechanics with the objective of assessing the potential influence of geomechanics on porosity and permeability, two of the most important reservoir "static" parameters that affect reservoir pressure and recovery factor.

The strategy comprised testing the algorithm on two elastic, isothermal, synthetic three-dimensional models to determine the impact of volumetric strain variations on the average reservoir pressure and production rate profiles.

This approach consists of four major steps:

1) Establish equilibrium in the geomodel, prior to the coupling simulation.

2) Run the reservoir model, exclusively using the streamline reservoir, for the complete simulation time. This serves a double purpose; on one hand, it provides the results used to compare the performance of the coupled simulation, and on the other, it provides the pressures that are used as external loads for the geomechanical run.

3) Calculate the volumetric strains using the geomechanical code, and use these values to calculate porosity and permeability multipliers, which are passed (only their average) to the streamline simulator

4) Run the reservoir model once again, using these averages of the multipliers.

For each study case, four subcases were analyzed: one uncoupled case (no geomechanics are considered, and is used to compare the performance of the other

subcases), and three coupled cases. The coupled cases used either the permeability, porosity, or permeability and porosity as the coupling factors.

Overall, the approach is presented as a quick method to explore the potential of geomechanics on streamline simulations.

6.1 Accomplishments

Since a commercial streamline-based simulator with a built-in geomechanics package do not exist (at least to our knowledge), a coupling approach was developed to start exploring the influence of geomechanical response in pore pressure and production rates. This presented a quite challenge due to the limitations of both software (reservoir flow and geomechanical simulators).

Streamline simulators lack powerful keywords to account for changes in porosity and permeability with pressure, or to allow the introduction of lookup tables for rock compressibility, for example. This confirmed that streamline techniques are still at an early stage of evolution compared to conventional finite-difference reservoir flow simulators, and that much work still needs to be done.

On the other hand, the geomechanical program used in this research is not user-friendly, and is highly specialized. The user must have some level of expertise to be able to use it. This features obliged to develop two simple study cases to be analyzed.

Despite these limitations and technical problems, a conceptually simple method could still be developed. It is flexible and easy to implement, and was much faster to develop (compared to developing a new code). Despite its simplicity, it was still possible to observe and analyze the geomechanical response in streamline simulations.

Study Case 1 was obtained from a previous scientific study (Dean et al. 2006). The results of this scientific study were presented as a benchmark, without any in-

tention of trying to match them. The purpose was to observe if they resembled those of the coupled cases tested in this research.

Reservoir pressure and subsidence profiles could not be satisfactorily modeled. The results of the coupled cases neither followed a similar trend to that of the original case (Dean et al. 2006), nor deviated from the Uncoupled Case. However, these results were obtained not because of the failure of the two-way approach, but rather because of the simplicity of the model (elastic, homogeneous, one-phase, depletion, and one well). After the geomodel was run, considering the pore pressures obtained from the streamline simulator as external loads, it was observed that the changes in volumetric strains were not significant. The influence of these results was passed on to the rest of the results, and at the end, no significant changes were observed in the average reservoir pore pressure for the coupled cases.

It is more likely to have obtained a significant geomechanical response, if a more complex model was considered, e.g. considering failure criteria. However, it should be borne in mind that this is just a starting point in investigating the possibility of coupling geomechanics and streamline simulators. Most of the times, when starting a research of this nature, elastic models are used. Once it is proved that they work, more complex models are built.

Larger changes in the geomechanical response could have been also obtained by considering geomechanical response, not after a complete run of the reservoir simulator, but after each timestep. However, as previously explained, due to streamline simulator's limitations, this was hard to implement.

For all these reasons (and also because of time constraints), it was decided to continue with the testing of the approach using this study case.

Some general observations could be made. The method proved to be more useful in reproducing the average reservoir pressure than subsidence. For the former, there was a match at the beginning of the simulation run, revealing that geomechanical parameters do not have an immediate effect on flow response. For the latter, there was no change in subsidence (zero) for the whole simulation time.

Although the differences in the results of the coupled cases were rather insignificant compared to the Uncoupled Case, still some trends could be observed. The Porosity (considering porosity as the coupling term) and Poro&Perm cases (considering porosity and permeability as the coupling terms) predicted a larger value for the average reservoir pressure, following both of them the same trend.). Moreover, the Porosity Case presented a "larger" relative difference. In this sense, this behavior is similar to the one observed by Dean et al. (2006), who only considered the Porosity Case.

On the other hand, the Permeability Case (considering only permeability) had the closest results to the Uncoupled Case (the line was parallel to the Uncoupled Case), having even lower values. This was an unexpected result since it was observed that permeability was the parameter with the "largest" changes when considering the volumetric strains.

Despite these trends, it was not possible to conclude which coupling parameter or combination of them—porosity, permeability, or both—influenced the most during streamline-geomechanical simulations, since the differences in the results of the coupled cases were rather insignificant.

Smaller timesteps and more gridblocks were used in an attempt to improve the accuracy of the results. No improvement was observed; moreover, the simulation time increased considerably, especially when adding more gridblocks. It was observed that the relationship in computational time is not linear. The time simulation increases much more when incrementing the number of cells in the model than when incrementing the number of timesteps.

This confirms that it is not always justifiable to consider geomechanics on a frequent basis or using more gridblocks, as it is time consuming, and the results are comparable to those achieved under longer timesteps and fewer gridblocks.

Study Case 2 brought some light regarding the performance of the two-coupled approach, and also demonstrated that the results are problem-dependant. This is a two-phase, injection problem. Right before the production of water, the behavior is

the same as for Study Case 1, in the sense that there was no visible difference between the uncoupled and coupled cases. However, once water was starting to be produced, there was a deviation of the coupled cases from the coupled cases. Although the differences were still small, they were visible to the naked eye when analyzing the figures. This fact revealed that when more mechanisms enter to play (injection and production of a second fluid), this two-way approach can detect the geomechanical response, if not accurately, at least with some degree of confidence.

For this second study case, it was also observed that the Porosity Case predicted a larger value of average reservoir pressure, and oil production rate as well for the whole simulation time. On the other hand, the Permeability Case predicted a smaller value for these two parameters for most of simulation time; however, at the end of the simulation it even predicted a larger value for them. This indicates that Permeability coupling not always predicts smaller values. It depends on the problem, and the stage of the simulation. Poro&Perm Case, unlike in Study Case 1, it reproduced a behaviour similar to that one of the Permeability Case.

It seems that Poro&Perm Case reproduces the behavior of one of the other two coupled cases (Porosity or Permeability), depending on which one has the strongest influence. Study Case 1 was homogeneous (Poro&Perm was “parallel” to the Porosity Case), whereas Study Case 2 was heterogeneous (Poro&Perm “ran” parallel to the Permeability Case). Nevertheless, more study cases need to be considered before considering this as a general conclusion.

In summary, one of the main aspects of this study was the limitations of the simulators. When software and hardware capacities improve, so will the results of the coupling approach. Until then, more complex models should be tested, as well as more rigorous techniques, to improve the results presented here.

6.2 Future work

Numerous coupling studies have attempted to capture in a more realistic way the processes occurring in oil and gas fields. This is especially true for stress-sensitive reservoirs, which are more likely to be produced these days. This work is intended as another contribution to the combined effort. However, it only starts exploring the idea of streamline-geomechanical simulations, giving plenty of room for further work.

While the 3D model chosen for this research was a very simple one, it was still too ambitious for this initial exploration regarding the inclusion of geomechanics in streamline simulations. It is recommended to first develop a 2D model, including complex criteria (e.g. failure criteria) model for a further study. This is especially emphasized when the person is still learning the geomechanical software, which is not as friendly as the reservoir flow simulators. Great caution should be taken when introducing the data to avoid errors.

Once this is overcome, models should increase in complexity (3D), including non-pay region, and failure criteria. The ultimate goal is to conduct field-scale simulations.

At this stage, upgridding and downscaling techniques might be required since, to be able to pass the information from the models back and forth. As it was observed in this research, the geomechanical calculations consume most of the computational resources. Having more gridblocks for the non-pay region, automatically translates into higher computational costs.

More elaborated algorithms should also be developed alongside more complex models, taking into account convergence criteria. This is a complex task given that commercial streamline simulators are limited in handling rock deformations. However, it is still faster than writing a code from scratch.

Finally, at least for the two cases presented in this thesis, different values of rock compressibility should be used when testing this two-way approach. Different val-

ues of this parameter should be used in combination with this simple methodology, since it is likely that this approach needs equivalent rock compressibility to represent the problem more accurately.

7
References

Aadnoy, B.S. 1998. Geomechanical Analysis for Deep Water Drilling. Paper 39339 presented at the IADC/SPE Drilling Conference, Houston, Texas, 3–6 March.

Advani, S.H., Lee, J.K., Khattab, H.A., and Gurdogan, O. 1986. Fluid Flow and Structural Response Modeling Associated with the Mechanics of Hydraulic Fracturing. *SPEFE* **1** (3): 309–318, SPE-10846-PA.

Ammer, J.R., Covatch, G.L., Sames, G.P., Mroz, T.H., and Gwilliam, W.J. 2000. Technology for Increased Production from Low-Permeability Gas Reservoirs: An Overview of U. S. DOE's Program–Successes and Future Plans. Paper SPE 60310 presented at the SPE Rocky Mountain Regional/Low-Permeability Reservoirs Symposium and Exhibition, Denver, Colorado, 12–15 March.

Batycky, R.P., Blunt, M.J., and Thiele, M.R. 1997. A 3D Field-Scale Streamline-Based Reservoir Simulator. *SPERE* **12** (4): 246–254. SPE-36726-PA.

Berumen, S., Cipolla, C., Finkbeiner, T., Wolhart, S., and Rodriguez, F. 2000. Integrated Reservoir Geomechanics Techniques in Burgos Basin Mexico: An Improved Gas Reservoirs Management Stress. Paper SPE 59418 presented at the SPE Asia Pacific Conference on Integrated Modeling and Assess Management. Yokohama, Japan, 25–26 April.

Biot, M.A. 1941. General Theory of Three Dimensional Consolidation. *Journal of Applied Physics* **12**: 155–164.

Bogatkov, D. 2008. Integrated Modeling of Fracture Network System of the Midale Field. MSc thesis, University of Alberta, Edmonton, Alberta, Canada.

Bruno, M.S. 2002. Geomechanical and Decision Analyses for Mitigating Compaction-Related Casing Damage. *SPEDC* **17** (3): 179–188. SPE-79519-PA.

Chavez, J.C., McCurdy, P., and Morgan, L. 2004. Fracture Propagation in an Open Hole Horizontal Injector Well: An Applied Geomechanic Study. Paper SPE 88608 presented at the SPE Asia Pacific Oil and Gas Conference and Exhibition, Perth, Australia, 18–20 October.

Chen, H.Y., Teufel, L.W., and Lee, R.L. 1995. Coupled Fluid Flow and Geomechanics in Reservoir Study - I. Theory and Governing Equations. Paper SPE 30752, SPE Annual Technical Conference and Exhibition, Dallas, Texas, 22–25 October.

Cunha, L.B. 2006. *Reservoir Simulation Development*. Class Note for PET E 650, Dept. of Petroleum Engineering, University of Alberta, Edmonton, Alberta, Canada.

Datta-Gupta, A. 2000. Streamline Simulation. *JPT* **52** (12): 68–73,84.

Datta-Gupta, A. and King, M.J. 2007. *Streamline Simulation: Theory and Practice*. Textbook Series, SPE, Richardson, Texas **11**, p. 394.

Davies, J.P. and Davies, D.K. 1999. Stress–Dependent Permeability: Characterization and Modeling. Paper SPE 56813 presented at the SPE Annual Technical Conference and Exhibition. Houston, Texas, 3–6 October.

de Sá, A.N. and Soares, A.C. 1997. Coring Samples and Obtaining Geomechanical Properties for Wellbore Stability Analysis in Deepwater Brazilian Horizontal Wells. Paper SPE 39070 presented at the Fifth Latin American and Caribbean Petroleum Engineering Conference and Exhibition, Rio de Janeiro, Brazil, 30 August–3 September.

Dean, R.H., Gai, X., Stone, C.M. and Minkoff, S.E. 2006. A Comparison of Techniques for Coupling Porous Flow and Geomechanics. *SPEJ* **11** (1): 132–140. SPE-79709-PA.

Ertekin, T., Abou-Kassem, J.H. and King, G.R. 2001. *Basic Applied Reservoir Simulation*. Textbook Series, SPE, Richardson, Texas **7**: 406.

Fjaer, E., Holt, R.M., Horsrud, P., Raaen, A.M., and Risnes, R. 2008. *Petroleum Related Rock Mechanics*, second edition, Development in Petroleum Science, Elsevier, Hungary **53**, p. 491.

Fredrich, J.T., Arguello, J.G., Deitrick, G.L., and de Rouffignac, E.P. 2000. Geomechanical Modeling of Reservoir Compaction, Surface Subsidence, and Casing Damage at the Belridge Diatomite Field. *SPEREE* **3** (4): 348–359. SPE-65354-PA.

Geertsma, J. 1957. The Effect of Pressure Decline on Volumetric Changes of Porous Rocks. *Trans*. AIME **201**: 331–340.

Geertsma, J. 1973. Land subsidence above Compacting Oil and Gas Reservoirs. *JPT* **25** (6): 734–744. SPE-3730-PA.

GetData DigitizerTM, v. 2.24, http://getdata-graph-digitizer.com/download.php. Downloaded 22 October 2008.

Gu, F. and Chalaturnyk, R.J. 2005. Analysis of Coal Bed Methane Production by Reservoir and Geomechanical Coupling Simulation. *JCPT* **44** (10).

Gutierrez, M. and Lewis, R.W. 1996. The Role of Geomechanics in Reservoir Simulation. Paper SPE 47392 presented at the SPE/ISMR Rock Mechanics in Petroleum Engineering, Trondheim, Norway, 8–10 July.

Gutierrez, M., Lewis, R. W. and Masters, I. 2001. Petroleum Reservoir Simulation Coupling Fluid Flow and Geomechanics. *SPEREE* **4** (3): 164–172. SPE-72095-PA.

Hansen, K.S., Prats, M., and Chan, C.K. 1995. Modeling of Reservoir Compaction and Surface Subsidence at South Belridge. *SPEPF* **10** (3): 134–143. SPE-26074-PA

Heffer, K.J., Koutsabeloulis, N.C., and Wong, S.K. 1994. Coupled Geomechanical Thermal and Fluid Flow Modeling as an Aid to Improving Waterflood Sweep Efficiency. Paper SPE 28082 presented at the Eurock SPE/ISMR Rock Mechanics in Petroleum Engineering Conference. Delft, Netherlands, 29–31 August.

Heffer, K.J., Fox, R.J., McGill, C.A., and Koutsabeloulis, N.C., 1997. Novel Techniques Show Links between Reservoir Flow Directionality, Earth Stress, Fault Structure and Geomechanical Changes in Mature Waterfloods. *SPEJ* **2** (2): 91–98. SPE-30711-PA.

Ingebrigtsen, L., Bratvedt, F., and Berge, J. 1999. A Streamline Based Approach to Solution of Three-Phase Flow. Paper SPE 51904, SPE Reservoir Simulation Symposium, Houston, Texas, 14–17 February.

Itasca. 2006. *FLAC^{3D} 3.1*, *User Manual*.

Jha, B., and Juanes, R. 2006. A Locally Conservative Finite Element Framework of the Simulation of Coupled Flow and Reservoir Geomechanics. Paper SPE 102812 presented at the SPE Annual Technical Conference and Exhibition. San Antonio, Texas, USA, 24–27 September,

Ji, L., Settari, A., and Sullivan, R.B. 2007. A Novel Hydraulic Fracturing Model Fully Coupled with Geomechanics and Reservoir Simulator. Paper SPE 110845 presented at the SPE Annual Technical Conference and Exhibition, Anaheim, California, USA, 11–14 November.

Koutsabeloulis, N.C. and Hope, S.A. 1996. "Coupled" Stress/Fluid/Thermal Multi – Phase Reservoir Simulation Studies Incorporating Rock Mechanics. Paper SPE 47393 presented at the SPE/ISMR Rock Mechanics in Petroleum Engineering, Trondheim, Norway, 8–10 July.

Lolomari, T., Bratvedt, K., Crane, M., Milliken, W.J., and Tyrie, J.J. 2000. The Use of Streamline Simulation in Reservoir Management: Methodology and Case Studies". Paper SPE 63157, SPE Annual Technical Conference and Exhibition, Dallas, Texas, 1–4 October.

Minkoff, S.E., Stone, C.M., Arguello, J.G., Bryant, S., Eaton, J., Peszynska, M., and Wheeler, M. 1999. Staggered in Time Coupling of Reservoir Flow Simulation and Geomechanical Deformation: Step 1-One Way Coupling, Paper SPE 51920 presented at the SPE Reservoir Simulation Symposium. Houston, Texas, 14–17 February.

Nwaozo, J. 2006. Dynamic Optimization of a Water Flood Reservoir. MSc thesis, University of Oklahoma, Norman, Oklahoma, USA.

Pan, F., Sepehrnoori, K., and Chin, L.Y. 2007. Development of Coupled Geomechanics Model for a Parallel Compositional Reservoir Simulator. Paper 109867 presented at the SPE Annual Technical Conference and Exhibition, Anaheim, California, USA, 11–14 November.

Peaceman, D.W. 1977. *Fundamentals of Numerical Reservoir Simulation.* Developments in Petroleum Science, The Netherlands, Elsevier **6**: 176.

Ramos, G.G., Erwin, M.D., and Enderlin, M.B. 2002. Geomechanical Factors in the Successful Implementation of Barefoot Horizontal Completions Totaling 10,000 ft Long, Alpine Reservoir, Alaska. Paper SPE 78193 presented at the SPE/ISRM Rock Mechanics Conference, Irving, Texas, USA, 20–23 October.

Rodrigues, L.G., Cunha, L.B., and Chalaturnyk, R.J. 2007. Incorporating Geomechanics into Petroleum Reservoir Numerical Simulation. Paper SPE 107952 presented at the SPE Rocky Mountain Oil & Gas Technology Symposium, Denver, Colorado, 16–18 April.

Rodrigues, L.G. 2009. Flow Simulation in a Deepwater Reservoir: Fault Leakage Analysis. PhD Dissertation, University of Alberta, Edmonton, Alberta, Canada.

Samier, P., Onaisi, A., and Fontaine, G. 2006. Comparisons of Uncoupled and Various Coupling Techniques for Practical Field Examples. *SPEJ* **11** (1): 89–102. SPE-79698-PA.

Samier, P., Onaisi, A., and de Gennaro, S. 2008. A Practical Iterative Scheme for Coupling Geomechanics with Reservoir Simulation. *SPEREE*: 892–901.

Schlumberger. 2007. *FrontSim: Technical Description Manual*, version 2007.1.

Settari, A. 2002. Reservoir Compaction. *JPT* **54** (8): 62–69.

Settari, A. and Mourits, F.M. 1998. A Coupled Reservoir and Geomechanical Simulation System. *SPEJ* **3** (3): 219–226. SPE-50939-PA.

Settari, A. and Walters, D.A. 2001. Advances in Coupled Geomechanical and Reservoir Modeling with Applications to Reservoir Compaction. *SPEJ* **6** (3): 334–342. SPE-74142-PA.

Soares, A.C. and Ferreira, F.H. 2002. An Experimental Study for Mechanical Formation Damage. Paper SPE 73734, International Symposium and Exhibition on Formation Damage Control, Lafayette, Louisiana, USA, 20–21 February.

Soliman, M.Y., East, L., and Adams, D. 2008. Geomechanics Aspects of Multiple Fracturing of Horizontal and Vertical Wells. *SPEDC* **23** (3): 217–228, SPE-86992-PA.

Stone, T., Bowen, G., Papanastasiou, P., and Fuller, J. 2000. Fully Coupled Geomechanics in a Commercial Reservoir Simulator. Paper SPE 65107 presented at the SPE European Petroleum Conference, Paris, France, 24–25 October.

Stone, T.W., Xian, C., Fang, Z., Manalac, E., Marsden, R. and Fuller, J. 2003. Coupled Geomechanical Simulation of Stress Dependent Reservoirs. Paper SPE 79697 presented at the SPE Reservoir Simulation Symposium, Houston, Texas, 3-5 February.

Strenger–Proehl, T. 2002. Geomechanical Uncertainties and Exploratory Drilling Costs. Paper SPE 78230 presented at the SPE/ISRM Rock Mechanics Conference, Irving, Texas, USA, 20–23 October.

Terzaghi, K. 1925. *Erdbaummechanik auf Bodenphysikalicher Grundlage*, Vienna: Franz Deutike.

Tortike, W.S. and Farouk Ali, S.M. 1993. Reservoir Simulation Integrated with Geomechanics. *Journal of Canadian Petroleum Technology* **32**(5): 28-37.

Tran, D., Nghiem, L., and Buchanan, L. 2005a. An Overview of Iterative Coupling between Geomechanical Deformation and Reservoir Flow. Paper SPE 97879 presented at the SPE/PS-CIM/CHOA International Thermal Operations and Heavy Oil Symposium, Calgary, Alberta, Canada, 1–3 November.

Tran, D., Nghiem, L. and Buchanan, L. 2005b. Improved Iterative Coupling of Geomechanics with Reservoir Simulation. Paper SPE 93244 presented at the SPE Reservoir Simulation Symposium, The Woodlands, Texas, USA, 31 January–2 February.

Tran, D., Settari, A. and Nghiem, L. 2004. New Iterative Coupling Between a Reservoir Simulator and a Geomechanics Module. *SPEJ* **9** (3): 362–369. SPE-88989-PA.

Vidal-Gilbert, S. and Tisseau, E. 2006. Sensitivity Analysis of Geomechanical Behavior on Time-Lapse Seismic Velocity Modeling. Paper SPE 100142 presented at the SPE Europec/EAGE Annual Conference and Exhibition, Vienna, Austria, 12–15 June.

Wan, J., Durlofsky, L.J., Hughes, T.J.R., and Aziz, K. 2003. Stabilized Finite Element Methods for Coupled Geomechanics-Reservoir Flow Simulations. Paper 79694 presented at the SPE Reservoir Simulation Symposium, Houston, Texas, 3–5 February.

Williams, G.J.J., Mansfield, M., MacDonald, D.G. and Bush, M.D. 2004. Top-Down Reservoir Modelling, Paper SPE 89974, SPE Annual Technical Conference and Exhibition, Houston, Texas, 26–29 September.

Yale, D.P. 2002. Coupled Geomechanics-Fluid Flow Modeling: Effects of Plasticity and Permeability Alteration. Paper SPE 78202 presented at the SPE/ISMR Rock Mechanics Conference, Irving, Texas, USA, 20–23 October.

Appendix A
Matlab File (Main Program)

This appendix presents the code developed in Matlab that serve as the interface between FrontSim and FLAC3D.

```
% ================================================================
% Program to couple geomechanical and reservoir fluid flow simulators
% Application for SPE paper 79709, Problem No. 1

clear all  % Clear information in all windows
clear
clc   % Clear content of command window
tic;
m_path='C:/Dean1/poroperm'; %matlab codes's dir
fl_path='C:/Dean1/poroperm/flac_data'; %FLAC's
fr_path='C:/Dean1/poroperm/front_data'; %FRONTSIM's

cd(m_path); %Specify work dir containing data file

%
================================================================================
==
% INPUT DATA
%
================================================================================
==
% Declaring global input variables for functions; NO need to put them in
% input arguments
global pr nx ny nz ts fl_name

% FrontSim input data file.
fr_name1='fr_Dean1_1'; % name of 1st file to run. this is w/ the purpose of
   % having  <> names for resulting files (keep results of both runs)
fr_name2='fr_Dean1_2';

% FLAC3D input data file.
fl_name='fl_Dean1_0';


pr=0.3; % Poisson ratio
nx=int16(11); % Number of reservoir's cells in X dir
ny=int16(11); %                          Y dir
nz=int16(10); %                          Z dir
```

```
ncells=nx*ny*nz; % no. of cells in the model
ts=50;   %No. of timesteps in the simulation

head0=260; % It's an aux for headlines in .F0000
head1=670; %                          .F000n
head2=6; % Hearlines for .RSM (to obtain the average pressure

%
=========================================================================
==
% PRELIMINARY DATA PROCESS
%
=========================================================================
==

% -- Saving initial values and creating strings for data files

% -- Preallocating memory for arrays used in code to increase speed

% Static properties
new_poro=zeros(ncells,ts); % MULTIPLICADORES
multpv=zeros(ncells,ts);
multpmx=zeros(ncells,ts);

% Pressures
ppt1=zeros(ncells,ts+1); % 2 save RES press 4 e/timestep. 1st run
dpp=zeros(ncells,ts); % 2 save delta pressures 2 create the disturbance 2
% obtain the volumetric strains
ppt2=zeros(ncells,ts+1); % 2 save RES press 4 e/timestep. 1st run

% Strains
vs=zeros(ncells,ts); % vol. strain at each timestep, according to
% FrontSim numbering

% Files
TS_PRESFILE='';
TS_DSHFILE='';
TS_DSHRFILE='';
TS_VS='';

% Extras; auxiliary variables
SW = zeros(ny,1,nz);
SE = zeros(ny,1,nz);
SN = zeros(1,nx+2,nz);
SS = zeros(1,nx+2,nz);
SU = zeros(ny+2,nx+2,1);
SL = zeros(ny+2,nx+2,1);
F = zeros(ny+2,nx+2,nz+2);
ppi_flac=zeros(ny+1,nx+1,nz+1);
```

```
% -- Saving initial values and creating strings for data files

% Saving initial porosity and permeability into variables
phifile=[fr_path '\fr_D1_phi.txt']; % Initial porosity

kxfile=[fr_path '\fr_D1_permx.txt']; % Initial permeability

fid = fopen(phifile,'r');
fid1 = fopen(kxfile,'r');
aux01=textscan(fid,'%s',1,'delimiter','\n'); % skipping first line
aux01=textscan(fid1,'%s',1,'delimiter','\n');

% Reads WHOLE model
ini_poro=fscanf(fid,'%f',double(ncells)); %AUTOMATICALLY CONVERTS INTO
% COLUMN VECTOR
ini_kx=fscanf(fid1,'%f',double(ncells)); % ONLY X 'cause in Y is the same
                    % & in Z it's a multiple
status=fclose('all');

% - Creating file names used to store data (once per timestep)
TS_MULTPVFILE=[fr_path '\fr_Dean1_poro.txt']; % Creating files 4 pore vol
% multipliers
TS_MULTKXFILE=[fr_path '\fr_Dean1_permx.txt']; % Creating files 4 pore vol
% multipliers
TS_NODEFILE=[fl_path '\pres_node.txt']; % file containing pressure values in
% nodes with FLAC's order & in Pa
TS_DPRESFILE=[fl_path '\dpres.txt']; % Creating files for pressure
TS_FLAC=[fl_path '\' fl_name '_' num2str(1) '.txt']; % e/flac run has its own file

for j=1:ts
   TS_PRESFILE{j}=[fl_path '\pres' num2str(j) '.txt']; % Creating input file 4 flac (pres)
   TS_DSHFILE{j}=[fl_path '\dsh' num2str(j) '.txt']; % Delta horizontal
      % stress files which is used as a trick in order to obtain delta
      % volumetric strain, otherwise it'll be 0(equilibrium). %%%%STILL NEED TO VERIFY
   TS_DSHRFILE{j}=[fl_path '\dshr' num2str(j) '.txt']; % And reverse file
      % 2 reestablish equilibrium
   TS_VS{j}=['''vol_stra' num2str(j) '.txt''']; % volumetric strains 4 e/
% timestep
   TS_VS2{j}=[fl_path '\vol_stra' num2str(j) '.txt']; % volumetric strains 4 e/
% timestep
end

% Auxiliaries for creating and accommodating values in FLAC
nnz = nz+1; % layer nodes (nz+1)in res.
nnx = nx+1; % nodes per line in X
nny = ny+1; % nodes per line in Y

%
=========================================================================
==
```

```
% RUNS. Main Process
%
================================================================================
==
% FRONTSIM
% ------------------------------------------------------------------------
% -- Running FRONTSIM from MSDOS command
cd(fr_path);
aux02=['$frontsim -ver 2007.2 ' fr_name];
dos (aux02);
dos ('$convert');
cd(m_path);


% -- Extracting pressure data from FrontSim Files and “accommodating” then
% -- for future calculations & analysis

ppt1=zeros(ncells,ts+1);

for i=0:ts % Including original pressure for FLAc’s “trick”
   if i < 10
      res_pres=[fr_path '\' fr_name1 '.F000' int2str(i)];
   else
      res_pres=[fr_path '\' fr_name1 '.F00' int2str(i)];
   end
   fid=fopen(res_pres,'r'); % Open to read data
   if i==0 % skipping 1st info
      aux03=textscan(fid,'%s',head0,'delimiter','\n');
   else
      aux03=textscan(fid,'%s',head1,'delimiter','\n');
   end
   ppt1(:,i+1) = fscanf(fid,'%f\n',double(ncells)); % keeping values in matrix
   fclose(fid);
end

pp1_Pa=6894.76*ppt1(:,2:ts+1);% excluding original press & converting 2 Pa

% -- "Playing" with pressure values.
% Obtaining array 4 delta pressure used in calculations 2 obtain volumetric
% strains. In Pa 4 FLAC's compatibility
for ii=1:ts
   dpp(:,ii)=(ppt1(:,ii)-ppt1(:,ii+1))'*6894.76;
end

% -- Preparing press & stresses (in Pa) data for FLAC File

for i=1:ts %
   % Preallocating 4 e/timestep to avoid dimensional problems
   T=zeros(ncells,1);
   T2=zeros(ncells,1);
```

```
T(:,1)=pp1_Pa(:,i); % 4 dim compatibility; taking 1 timestep @ a
                    % time. In Pa
T2(:,1)=dpp(:,i);

% - Arranging in 3Dmatrix form (reservoir)
T=reshape(T,nx,ny,nz);
T=permute(T,[2 1 3]); % trick to obtain the right order

% -- Arranging values in matrix form & creating values 4 nodes (having
% -- the center pressures given by res. sim. as starting pt)

% - Creating extra values for nodes having the centered pressures (from res.
% - sim.) as starting pt. WHOLE MODEL(non pay+reservoir)

% Creating mirrors in 4 sides of e/ layer (just 1st and last rows/cols) 2 b
% able 2 interpolate in corners
SW = T(:,1,:); % west side of model
SE = T(:, nx,:); % east side
T = [SW,T,SE]; % concatenation in WE dir
SN = T(1,:,:); % north side
SS = T(ny,:,:); % south side
T = [SN;T;SS]; % concatenation in NS dir

SU = T(:,:,1); % creating "upper sandwich" of model
SL = T(:,:,nz); % creating "lower sandwich" of model

F = cat(3, SU, T, SL); %concatenates arrays along dimension

[XX, YY, ZZ] = meshgrid(1:double(nx)+2,1:double(ny)+2,1:double(nz)+2);
% always + 2 to include the "extended" model
% Produces a dimensional array used to evaluate functions of 3 variables & 3D
% volumetric plots. Rows of output array X are copies of vector x; cols. of
% output array Y are copies of vector y.

[X1,Y1,Z1] = meshgrid(1.5:double(nx)+1.5,1.5:double(ny)+1.5,...
1.5:double(nz)+1.5); % generate "inner mesh" (actual model nodes)

ppi_flac = interp3(XX,YY,ZZ,F,X1,Y1,Z1,'linear'); % Interpolates to find
% ppi_flac, the values of the underlying 3D function F @ the pts in arrays
% X1,Y1,Z1. X,Y,Z specify the pts @ which data ppi_flac is given. Methods
% available: nearest,linear,spline,cubic

% -- Dividing node- & block-centered pressure matrices in subgroups 4 FLAC
% -- numbering & changing order according to FLAC's IDs

% - Renumbering nodes to agree w/FLAC numbering
aux50=nnx;
aux51=nny;
```

```
aux52=nnz;
presnode_rev=mf_divmatrix(ppi_flac,TS_NODEFILE,aux50,aux51,aux52);

% - Dividing block centered-pressured matrix in subgroups for calculations
% - (the trick) of volumetric strains
% Preparing order of pressure to be compatible with FLAC's mesh, but using
% centered pressure values in order to calculate stresses (which are zone
% values, not node values as pore pressure
% Probably it's not even necessary, 'cause this is only a trick just to
% obtain the volumetric strains

T2=reshape(T2,nx,ny,nz);
T2=permute(T2,[2 1 3]); % trick to obtain the right order



% Auxiliaries
aux50=nx;
aux51=ny;
aux52=nz;
dpp_rev_Pa=mf_divmatrix(T2,TS_DPRESFILE,aux50,aux51,aux52);

% -- Printing the values of pressures in nodes in file for FLAC's reading
fid5=fopen(TS_NODEFILE,'rt+'); % to read interpolated pressure values as calculated by
matlab
frewind(fid5); % to guarantee it's in first line
fid6=fopen(TS_PRESFILE{i},'wt+'); % file prepared for FLAC as input

% Setting counters
nline = 1; % counter for no. if line read in input file
line = fgetl(fid5); % variable to make matlab read the line for pressure in input data
kk=1;

% Setting auxiliary variables
%c#: closure of logical expressions

while feof(fid5) == 0 %c0
  if isempty(line), break, end; % finish the program
  if kk == (nnz+1), break, end; % reinforcement to finish program
  if kk ==1 % Layer 1  c1
    for ii=1:nnx  % row 1  c2
      if ii<3   %c3
        id=nline;
        fprintf (fid6, 'ini pp %s range id %s \n', line,num2str(id));
        line = fgetl(fid5);
        nline = nline + 1;
      elseif ii==3
        id=id+7;
        fprintf (fid6, 'ini pp %s range id %s \n', line,num2str(id));
        line = fgetl(fid5);
        nline = nline + 1;
```

```
   else
      id=id+4;
      fprintf (fid6, 'ini pp %s range id %s \n', line,num2str(id));
      line = fgetl(fid5);
      nline = nline + 1;
   end %c3 - if ii<3
end %c2 - for ii=1:nnx
for ii=nnx+1:2*nnx  % row 2  c4
   if ii==nnx+1 %c5
      id=3;
      fprintf (fid6, 'ini pp %s range id %s \n', line,num2str(id));
      line = fgetl(fid5);
      nline = nline + 1;
   elseif ii== nnx+2
      id=id+2;
      fprintf (fid6, 'ini pp %s range id %s \n', line,num2str(id));
      line = fgetl(fid5);
      nline = nline + 1;
   elseif ii== nnx+3
      id=id+5;
      fprintf (fid6, 'ini pp %s range id %s \n', line,num2str(id));
      line = fgetl(fid5);
      nline = nline + 1;
   else
      id=id+4;
      fprintf (fid6, 'ini pp %s range id %s \n', line,num2str(id));
      line = fgetl(fid5);
      nline = nline + 1;
   end %c5 - if ii==nnx+1
end %c4 - for ii=nnx+1:2*nnx
for jj=3:nny % rows 3 – 12  c6
   for ii=1:nnx %c7
      if ii==1 && jj==3  %c8
         aux1=4;
         aux2=1;
         id=aux1*nnx+aux2;
         fprintf (fid6, 'ini pp %s range id %s \n', line,num2str(id));
         line = fgetl(fid5);
         nline = nline + 1;
      elseif ii==2
         id=id+1;
         fprintf (fid6, 'ini pp %s range id %s \n', line,num2str(id));
         line = fgetl(fid5);
         nline = nline + 1;
      elseif ii==3
         id=id+3;
         fprintf (fid6, 'ini pp %s range id %s \n', line,num2str(id));
         line = fgetl(fid5);
         nline = nline + 1;
      else
         id=id+2;
         fprintf (fid6, 'ini pp %s range id %s \n', line,num2str(id));
```

```
            line = fgetl(fid5);
            nline = nline + 1;
          end %c8 - if ii==1 && jj==3
        end %c7 - for ii=1:nnx
      end %c6 - for jj=3:nny
    end %c1 - if kk ==1
    if kk ==2 % Layer 2 c9
      for ii=nnx*nny+1: nnx*nny+nnx  % row 1  c10
        if ii== nnx*nny+1  %c11
          id=4;
          fprintf (fid6, 'ini pp %s range id %s \n', line,num2str(id));
          line = fgetl(fid5);
          nline = nline + 1;
        elseif ii== nnx*nny+2
          id=id+3;
          fprintf (fid6, 'ini pp %s range id %s \n', line,num2str(id));
          line = fgetl(fid5);
          nline = nline + 1;
        else
          id=id+4;
          fprintf (fid6, 'ini pp %s range id %s \n', line,num2str(id));
          line = fgetl(fid5);
          nline = nline + 1;
        end %c11 - if ii== nnx*nny+1
      end %c10 - for ii=nnx*nny+1: nnx*nny+nnx
      for ii=nnx*nny+nnx+1: nnx*nny+2*nnx % row 2  c12
        if ii== nnx*nny+nnx+1  %c13
          id=6;
          fprintf (fid6, 'ini pp %s range id %s \n', line,num2str(id));
          line = fgetl(fid5);
          nline = nline + 1;
        elseif ii== nnx*nny+nnx +2
          id=id+2;
          fprintf (fid6, 'ini pp %s range id %s \n', line,num2str(id));
          line = fgetl(fid5);
          nline = nline + 1;
        else
          id=id+4;
          fprintf (fid6, 'ini pp %s range id %s \n', line,num2str(id));
          line = fgetl(fid5);
          nline = nline + 1;
        end %c13 - ii== nnx*nny+nnx+1
      end %c12 - for ii=nnx*nny+nnx+1: nnx*nny+2*nnx
      for jj=3:nny % rows 3 – 12 %c14
        for ii=1:nnx %c15
          if ii==1 %c16
            if jj==3 %c17
              aux2=aux2+2;
              id=aux1*nnx+aux2;
            else
              id=id+3;
            end %c17 - if jj==3
```

```
            fprintf (fid6, 'ini pp %s range id %s \n', line,num2str(id));
            line = fgetl(fid5);
            nline = nline + 1;
          elseif ii==2
            id=id+1;
            fprintf (fid6, 'ini pp %s range id %s \n', line,num2str(id));
            line = fgetl(fid5);
            nline = nline + 1;
          else
            id=id+2;
            fprintf (fid6, 'ini pp %s range id %s \n', line,num2str(id));
            line = fgetl(fid5);
            nline = nline + 1;
          end %c16 - if ii==1
        end %c15 - for ii=1:nnx
      end %c14 for jj=3:nny
    end %c9 kk ==2
    if kk>2 % layers 3 – nnz  c18
      for jj=1:nny %c19
        if jj < 3 %c20
          for ii=1:nnx %c21
            if ii==1 && jj==1 %c22
              id=nline;
              fprintf (fid6, 'ini pp %s range id %s \n', line,num2str(id));
              line = fgetl(fid5);
              nline = nline + 1;
              aux3=id+1;
            elseif ii==1 && jj==2
              id=aux3;
              fprintf (fid6, 'ini pp %s range id %s \n', line,num2str(id));
              line = fgetl(fid5);
              nline = nline + 1;
            else
              id=id+2;
              fprintf (fid6, 'ini pp %s range id %s \n', line,num2str(id));
              line = fgetl(fid5);
              nline = nline + 1;
            end %c22 - if ii==1 && jj==1
          end %c21 - for ii=1:nnx
        else
          for ii=1:nnx %c23
            id=nline;
            fprintf (fid6, 'ini pp %s range id %s \n', line,num2str(id));
            line = fgetl(fid5);
            nline = nline + 1;
          end %c23 - for ii=1:nnx
        end %c20 - if jj < 3
      end %c19 - for jj=1:nny
    end %c18 - if kk>2
    kk=kk+1; % advance layers
  end %c0 - while feof(fid5) == 0
  status = fclose('all');
```

```
   % -- Preparing stresses (in Pa) data for FLAC File
   % Trick to be able to calculate vol. strain (assuming cte vertical strain,
   % affecting only horizontal stress).
   dsh_rev_Pa=((pr/(1-pr))-1)*dpp_rev_Pa;  % assuming alpha=1 (i.e.
   % incompressible grains)
   dshr_rev_Pa=-dsh_rev_Pa;  % same value but opposite sign

   fid1=fopen(TS_DSHFILE{i},'wt+'); % creating file 4 printing delta hor.
   % stress at current ts. A file per timestep
   fid2=fopen(TS_DSHRFILE{i},'wt+'); % Opening file for printing (-) delta
   % horizontal stress at current ts

   for j=1:ncells;
      fprintf(fid1,'ini sxx add %5.8f range id %s\n',dsh_rev_Pa(j),num2str(j));
      fprintf(fid1,'ini syy add %5.8f range id %s\n',dsh_rev_Pa(j),num2str(j));
      fprintf(fid1,'ini szz add 0.0 range id %s\n',num2str(j));
      fprintf(fid2,'ini sxx add %5.8f range id %s\n',dshr_rev_Pa(j),num2str(j));
      fprintf(fid2,'ini syy add %5.8f range id %s\n',dshr_rev_Pa(j),num2str(j));
      fprintf(fid2,'ini szz add 0.0 range id %s\n',num2str(j));
   end
   status = fclose('all');

   % -- Creating file from zeros 4 each flac run (there was problem with FISH functions and I
need to keep
   % -- changing names)
   % Writing the flac file
   fid1=fopen(TS_FLAC,'a+');
   if i==1
      fprintf(fid1,'new\n');
      fprintf(fid1,'restore %s_%s\n',fl_name,num2str(i-1));% Indicating to obtain data from
previous run
   end
   fprintf(fid1,'call pres%s.txt\n',num2str(i));
   fprintf(fid1,'call dsh%s.txt\n',num2str(i));
   fprintf(fid1,'solve\n');
   fprintf(fid1,'call dshr%s.txt\n',num2str(i));
   fprintf(fid1,'solve\n');
   fprintf(fid1,'def _writeev%s\n',num2str(i));% fish function to write vol strains
   fprintf(fid1,'array _%s(1)\n',num2str(i));
   fprintf(fid1,'_status = open(%s,1,1)\n', TS_VS{i});
   fprintf(fid1,'_p = zone_head\n');
   fprintf(fid1,'loop while _p # null\n');
   fprintf(fid1,'_%s(1) = string(z_vsi(_p))\n',num2str(i));
   fprintf(fid1,'_status = write(_%s,1)\n',num2str(i));
   fprintf(fid1,'_p = z_next(_p)\n');
   fprintf(fid1,'endloop\n');
   fprintf(fid1,'_status = close\n');
   fprintf(fid1,'end\n');
   fprintf(fid1,'_writeev%s\n',num2str(i));
   fclose(fid1);
```

```
end
% Giving the command to save the SAV file, in case I need to review the
% results w/o the need of the dongle.
fid1=fopen(TS_FLAC,'a+'); % Writing the flac file
fprintf(fid1,'save %s_1\n',fl_name);
fclose(fid1);

% FLAC3D
% ------------------------------------------------------------------------
% -- Running FLAC3D from MSDOS command
% Not need to be done everytime. I just need .sav file
cd(fl_path);
aux04=['"C:\Program Files\Itasca\Flac3d310_32\exe32\f3310_32.exe" ' ...
   TS_FLAC ' quit'];
dos (aux04);
cd(m_path);

% -- Preparing order of vol. strains to be compatible with FrontSim's mesh
for j=1:ts
   % Obtaining incremental volumetric strains
   fid = fopen(TS_VS2{j},'r');
   vs_revi = fscanf(fid,'%f',double(ncells)); % order given by FLAC3D
   fclose(fid);
  TT=vs_revi;

   % -- Arranging in matrix form
   TT=reshape(TT,nx,ny,nz); % RESERVOIR

   % -- Transposing layers
   TT=permute(TT,[2 1 3]);

   % -- Change order of delta pore pressure according to FLAC's IDs (block-
   % centered)

   % changing rows
   TT=flipdim(TT,1);

   % changing layers
   TT=flipdim(TT,3);

   % Tricks to convert it into column vector
   TT=permute(TT,[2 1 3]); % transpose 2 have the right order in column vector
   TT=reshape(TT,numel(TT),1);
   vs(:,j)= TT;
end

% -- Calculating AVERAGE poro & perm multipliers for FrontSim's File

for ii=1:ts
   for j=1:ncells
```

```
      new_poro(j,ii) = (ini_poro(j,1)+vs(j,ii))/(1+vs(j,ii));
      multpv(j,ii) = new_poro(j,ii)/ini_poro(j,1);
      multpmx(j,ii) = (1+vs(j,ii)/ini_poro(j,1))^3/(1+vs(j,ii));
   end
end

% - Obtaining the average of multiplier & poro for next run in FrontSim
new_poro=new_poro'; % trick to obtain the average of rows. Porosity
new_poro_ave=mean(new_poro); % average of rows
multpv=multpv'; % Pore vol. mult
multpv_ave=mean(multpv);
multpmx=multpmx'; % perm. X mult.
multpmx_ave=mean(multpmx);

% Changing to column vector
new_poro_ave=new_poro_ave';
multpv_ave=multpv_ave';
multpmx_ave=multpmx_ave';

% -- Front: Writing poro & perm multipliers
fid=fopen(TS_MULTPVFILE,'wt+');
fid1=fopen(TS_MULTKXFILE,'wt+');
fprintf(fid,'MULTIPLY\n');
fprintf(fid1,'MULTIPLY\n');
c=1; % counter for multpv
for l=1:nz;
   for j=1:ny;
      for m=1:nx;
fprintf(fid,'PORO %2.10f %s %s %s %s %s %s /\n',multpv_ave(c),...
num2str(m),num2str(m),num2str(j),num2str(j),num2str(l),num2str(l));
fprintf(fid1,'PERMX %2.10f %s %s %s %s %s %s /\n',multpmx_ave(c),...
num2str(m),num2str(m),num2str(j),num2str(j),num2str(l),num2str(l));
         c=c+1;
      end
   end
end
fprintf(fid,'/\n');
fprintf(fid1,'/\n');
status=fclose('all');

% -- Run FrontSim & extract pressure values
ppt2=mf_front(fr_path,fr_name2,m_path,head0,head1,ncells);


% -- Running FRONTSIM from MSDOS command
cd(fr_path);
aux02=['$frontsim -ver 2007.2 ' fr_name];
dos (aux02);
dos ('$convert');
cd(m_path);
```

```
% -- Extracting pressure data from FrontSim Files and “accommodating” then
% -- for future calculations & analysis
for i=0:ts % Including original pressure for FLAc’s “trick”
   if i < 10
      res_pres=[fr_path '\' fr_name2 '.F000' int2str(i)];
   else
      res_pres=[fr_path '\' fr_name2 '.F00' int2str(i)];
   end
   fid=fopen(res_pres,'r'); % Open to read data
   if i==0 % skipping 1st info
      aux03=textscan(fid,'%s',head0,'delimiter','\n');
   else
      aux03=textscan(fid,'%s',head1,'delimiter','\n');
   end
   ppt2(:,i+1) = fscanf(fid,'%f\n',double(ncells)); % keeping values in matrix
   fclose(fid);
end


t=toc;
```

Appendix B
Study Case 1. FrontSim File

This appendix shows the input file used to run FrontSim.

```
-- ================================================================
RUNSPEC
TITLE
 DEAN ET AL. 2006, PROBLEM NO. 1

DIMENS
  11   11    10  /

WATER

GAS

FIELD

SATOPTS
                      'HYSTER'   /

TABDIMS
   2   1  20   20   1   20 /

WELLDIMS
   1   10   1   2 /

START
  1 'OCT' 2008  /

--UNIFIN
--UNIFOUT

GRID    ============================================================

DXV
 11*200 /

DYV
 11*200 /

DZV
 10*20.0 /
```

```
TOPS
 121*6000.0 121*6020.0 121*6040.0 121*6060.0 121*6080.0
 121*6100.0 121*6120.0 121*6140.0 121*6160.0 121*6180.0/

INCLUDE
fr_Dean1_poro.txt /

INCLUDE
fr_Dean1_permx.txt /

COPY
 'PERMX' 'PERMY' /
 'PERMX' 'PERMZ' /
/
MULTIPLY
 'PERMZ' 0.1 /
/


PROPS    ================================================================

RVCONST
 0.01 /

SWFN
   .25   .0   0.0
   1.0   1.0   0.0
/

SGFN
   .3    .0   0.0
   .75   1.0   0.0
/
PVTW
 .0  1.0  3E-06  1.0  0.0 /

PVDG
 .0    1.0    2.0
 8000.0  .92   2.0
/

ROCK
 3000.0       3.71E-04 /

DENSITY
 1*  62.4000  .04400 /

RPTPROPS
   2*0 /

REGIONS   ================================================================
```

```
SOLUTION  ============================================================

SWAT
 1210*1.0 /

SGAS
 1210*0.0 /

PRESSURE
 121*3004.33 121*3012.99 121*3021.65 121*3030.31 121*3038.97
 121*3047.63 121*3056.29 121*3064.95 121*3073.61 121*3082.27 /

RPTSOL
 RESTART=1 /

SUMMARY  ============================================================
RUNSUM
EXCEL
FPR --- For average field pressure

SCHEDULE  ============================================================

RPTRST
 BASIC=3 SAVE=1 FREQ=1 PRESSURE STREAM=0 /
-- BASIC=1/
RPTSCHED
1 0 1 0 0  0 2 0 0 0
0 0 0 0 0  0 1 1 0 0
0 0 0 0 0  0 0 0 0 0
0 0 0 0 0  0 0 0 0 0
0 0 0 0 0  0 0 0 1 0
0 1 0 0 0  0 0 0 0 0
0 0 0 0 0  0 0 0 0 0
0 0 1 0 0  0 0 0 0 0/

WELSPECS
'P'  'G'  6 6  1*  'WAT'  /
/

WELDEBUG
'P' 2211 /
/

COMPDAT
'P'  6  6   1   10 'OPEN'   0  .0   0.5 /
/

WCONPROD
'P' 'OPEN' 'WRAT' 1* 15000.0 /
/

TSTEP
```

```
50*10 /

END
```

Appendix C
Study Case 1. FLAC3D File

This appendix shows FLAC3D input file used to establish equilibrium in the geo-model. The subsequent input file used to obtain the volumetric strains generated by the Matlab code, which can be consulted in Appendix A.

```
; ================================================================
new
set logfile = 'run0' ;
set log on

 ****************************************************************
; --- geometrical model ---
****************************************************************
gen zone brick size 50 50 10 p0 0,0,0 p1 670.56,0,0 p2 0,670.56,0 p3 0,0,60.96


****************************************************************
; --- mechanical model --- ********************************************************************
model elas
prop bulk 5.8e7 shear 2.65e7


****************************************************************
; --- setting ---
****************************************************************
set grav 0,0,-9.81 ; m/s2
prop den =2356.67; kg/m3


****************************************************************
; --- boundary conditions ---
****************************************************************
apply szz -41.37e6 range z 60.95 60.97 ;    6000 psi

fix x y z range z -0.1 0.1 ; z=0 bottom
fix x y range x -0.1 0.1 ;
fix x y range x 670.56;
fix x y range y 0 ;
fix x y range y 670.56;


****************************************************************
```

```
; --- initial conditions ---
**********************************************************************
ini pp 21.28e6 grad 0,0,-9.79e3

ini szz -42.78e6 grad 0,0,2.31e4 ;
ini syy -27.58e6                                ; 4000 psi
ini sxx -27.58e6


**********************************************************************
; --- run ---
**********************************************************************

solve

save fl_Dean11_0.sav ;
```

Appendix D
Study Case 2. FrontSim File

This appendix shows the input file used to run FrontSim.

```
-- ================================================================
RUNSPEC

FRONTSIM

TITLE
random geology test, modified

DIMENS
 50 50 25 /

FIELD

OIL

WATER

START
 1 JAN 1992 /

TABDIMS
 1 1 /

WELLDIMS
 2 50 2 2 /

GRID   ================================================================
GRIDFILE
-- Grid file is produced
2 /

INIT

NTRNSAVE
-- Turns off saving transmissibilities in memory

DXV
50*65.6168 / --ft

DYV
```

```
50*65.6168 / --ft

DEPTHZ
2601*6561.6798 /  --ft


DZV
25*13.1234/

INCLUDE
fr_pblm2_poro.txt /

INCLUDE
fr_pblm2_permx.txt /

COPY
 'PERMX' 'PERMY' / --OK
 'PERMX' 'PERMZ' /
/

MULTIPLY
 'PERMZ' 0.1 / --OK
/

PROPS
================================================================
PVDO
  4409.1472    1       1  /


PVTW
4409.1472   1       3E-6       1  / -- psi


RSCONSTT
0 0 /

DENSITY
48.6938   63.302    0.0624/ -- lbm/ft3


SWOF
     0      0      1      0
     1      1      0      0  /

ROCK
4409.1472    3.71E-04 /


REGIONS
================================================================
```

```
SOLUTION
=====================================================================

EQUIL
6561.6798  4409.1472 /

RPTSOL
 RESTART=1 /

SUMMARY
=====================================================================
RUNSUM
EXCEL
FPR

SCHEDULE
=====================================================================

TUNEFSSA
 1* 0.700000 1* 1* NO NO 1* 1* /

RPTRST
BASIC=3 SAVE=1 FREQ=1 PRESSURE  12*  1*  1  9*  300 /


RPTPRINT
 1 12* 1 1 0 /

WELSPECS
P1      A   50   50          1*        LIQ  3* 1* 3* /
 I1     B    1    1          1*        LIQ  3* 1* 3* /
/

COMPDAT
P1       2*    1   25 1* 1*  1*  1*  1*  1*  1*  Z  /
 I1      2*    1   25 1* 1*  1*  1*  1*  1*  1*  Z  /
/

WCONPROD
P1   1* LRAT 3* 34464.7049 1*  / --stb/day; 1m3=6.289811 bbl
/

WCONINJ
I1     WATER 1*    RESV   2*     1             FVDG /
/

WECON
 P1      1* 1* 1 /
/

TSTEP
 10*365 / -- 10 years
```

Appendix E
Study Case 2. FLAC3D File

```
; ===================================================================
new
set logfile = 'run0' ;
set log on

 ****************************************************************
; --- geometrical model ---
****************************************************************
gen zone brick size 50 50 25 p0 0,0,0 p1 1000.0,0,0 p2 0,1000.0,0 p3 0,0,100.0

 ****************************************************************
; --- mechanical model ---
****************************************************************
model elas
prop bulk 5.8e7 shear 2.65e7


 ****************************************************************
; --- setting ---
****************************************************************
set grav 0,0,-9.81 ; m/s2
prop den =2356.67; kg/m3


 ****************************************************************
; --- boundary conditions ---
****************************************************************
apply szz -41.37e6 range z 99.99 100.01 ;    6000 psi

fix x y z range z -0.1 0.1 ; z=0 bottom
fix x y range x -0.1 0.1 ; 1 lado
fix x y range x 1000.0; 2 lado
fix x y range y 0 ; 3 lado
fix x y range y 1000.0; 4 lado

 ****************************************************************
; --- initial conditions ---
****************************************************************
ini pp 31.2e6 grad 0,0,-7.6e3

ini szz -42.78e6 grad 0,0,2.31e4 ;
ini syy -27.58e6                                ; 4000 psi
ini sxx -27.58e6
```

```
 ***************************************************************
; --- run ---
***************************************************************
solve

save fl_Pblm2_0.sav ;
```

Appendix F
Study Case 2. Pore Pressure Profiles

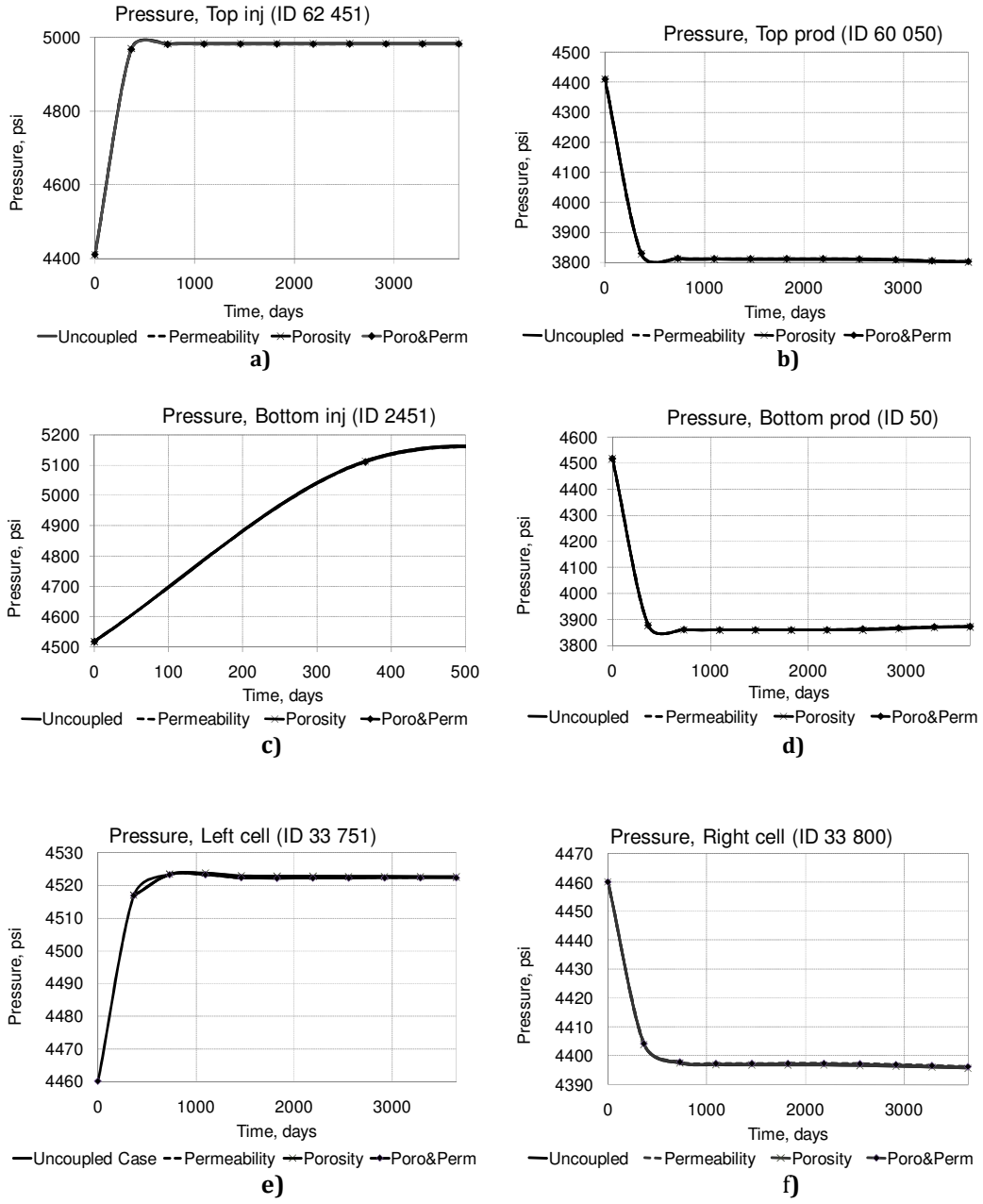

Fig. F.1—Pore pressure profile for cells a) 62 451 (top cell at injector location); b) 60 050 (top at producer location); c) 2451 (bottom at injector location); d) 50 (bottom at producer location); e) 33 751 (left boundary); and f) 33 800 (right boundary).